Structural Response of Precast Concrete Segmental Tunnel Linings

PhD DISSERTATION

Doctoral Thesis by
Oriol Arnau Delgado

Supervised by:
Climent Molins i Borrell

Barcelona, January 2012

Universitat Politècnica de Catalunya
Departament d´Enginyeria de la Construcció

AGRAÏMENTS

Si bé es cert que la realització d'aquesta tesi m'ha comportat un increment significatiu dels meus coneixements tècnics, el creixement personal ha estat 10 vegades superior. Tirar endavant les múltiples dificultats i traves a les quals un s'ha d'enfrontar al llarg d'aquest camí requereix d'un caliu i suport humà molt importat. Es per això que des d'aquestes línies vull mostrar el meu agraïment a totes aquelles persones que, conscient o inconscientment, han contribuït a que aquesta tesi hagi pogut arribar a bon port.

Primerament vull mostrar el més profund agraïment als imprescindibles d'aquesta història, sense els quals no s'hagués pogut ni començar. D'una banda als meus pares, per la seva tenacitat i persistència en inculcar-me la importància de l'educació i la formació, així com per la confiança mostrada en la tasca que he estat realitzant a pesar de la desinformació generalitzada a la que sovint els he sotmès. Gràcies per recolzar-me en tot allò que m'il·lusiona i la fe que dipositeu en mi. D'altra banda al meu tutor, Climent Molins, per oferir-me l'oportunitat de realitzar aquesta tesi, confiant exclusivament en les meves possibilitats i deixant al marge les teòriques limitacions que algunes etiquetes imposen en aquest món. Agreixo profundament el compromís i dedicació aportat a la meva recerca, així com la confiança tècnica demostrada en tot allò que hem fet plegats. Espero haver estat a l'alçada.

Han estat més de 5 anys voltant per el Departament d'Enginyeria de la Construcció, convivint diàriament amb un conjunt de persones que han fet que aquí em sentís com a casa. Vull agrair al Prof. Toni Marí el seu apadrinament social, tractar-me com un més dels seus. Al Prof. Pere Roca per comptar amb mi per a les assignatures de la secció d'edificació i permetre'm fer les meves primeres classes. També vull agrair l'amigable tracte que sempre he rebut per part dels professors Bairan, Mirambell, Real, Oller i Chacon, així com per el personal del laboratori i d'administració. Gràcies també a tu, Lluís, per haver compartit amb mi multitud d'estones i obrir-me la teva fraternal amistat. Et trobem molt a faltar.

Molts son els companys de fatigues amb els que hem conviscut al llarg d'aquests anys, doctorants, tesinants, i becaris, als quals vull agrair el tracte amigable que sempre m'han ofert. De forma particular, agrair a tots els que han hagut de compartit espais amb mi d'alguna o altra manera, Juan Carlos, Cristina, Jaume, Albert, Filipe, Selma, Betty, Sergio, Cristian, Álvaro, Edison, Roser, Olga, Raúl, André, Pau, Juliana, Isaac, Francesc, i evidentment a en Bernat, la proximitat i confiança amb la que m'han tractat i el suport que d'ells sempre he rebut. Gràcies a tots companys.

I would like to thank Prof. Joost Walraven and Dr. Kees Blom for giving me the chance to collaborate with them and to experience the live in Holland for 6 months. Thanks to Luz Estrada, Bas Lottman, Yuguang Yang, Albert and all the staff of TU Delft for sharing with me such pleasant work times. Stay abroad is always difficult, but the permanent support and friendship that Casper, Ivo and Debbie offered me, definitely made it easier. Dank je wel.

També vull mostrar el meu agraïment a totes les persones que han format part d'uns moments imprescindibles en tota tasca absorbent com aquesta, la desconnexió. Gràcies amics meus per estar sempre allà, per la fidelitat incombustible dels meus *apòstols*, per compartir amb mi la passió per els *ral·lis*, per a intentar anar *un pas* + enllà, o bé per fer que una simple *junta* bimensual ens recordi que ens tenim els uns als altres. Gràcies amics.

Finalment, agrair profundament a qui, dia rere dia, ha compartit amb mi aquesta aventura, amb qui he rigut en els moments divertits i he plorat en les adversitats, les meves *nenes*. Anna, Denise i Noemí, la millor de les sorts d'aquests últims anys ha estat poder-vos veure cada dia.

Moltíssimes gràcies a tots.

Oriol Arnau

SUMMARY

The increasing use of the tunnel boring machines (TBMs) has entailed their own evolution and the improvement of the construction processes applied, allowing the construction of tunnels on more complex hydro-geological conditions. These new drilling facilities imply that higher ground and water pressures have to be resisted by the structural lining, turning its design into a key item in all current tunnel projects.

TBMs construction process is mainly associated to precast concrete segmental tunnel linings, which are consisted of concrete rings sequentially placed as the tunnel drilling advances. Despite segmental tunnel linings are widely used, their structural response presents significant uncertainties due to the particular configuration on multiple precast pieces and the evolutionary construction process applied. The improvement and optimization of segmental tunnel linings, necessary to obtain safer structures at a lower cost, requires a significant advance in the knowledge of their structural response and about the appropriate techniques to properly reproduce it.

This PhD thesis present the mechanisms and phenomena involved in the structural response of precast concrete segmental tunnel linings, detailing numerical modeling strategies to properly simulate them. The integration of all these techniques in a unique model allows the analysis of a real tunnel lining subjected to different scenarios, determining the influence and relevance of the main parameters defining a tunnel and its structural lining.

Present research departs from an innovative *in situ* test carried out at Line 9 subway tunnel in Barcelona. The treatment and analysis of the obtained data provides experimental evidences about the structural response of segmental tunnel linings and the main involved mechanisms and phenomena. Different numerical simulation strategies are developed in order to properly reproduce such mechanism and phenomena, achieving a reliable simulation of an isolated ring response. The longitudinal response of the segmental concrete linings is obtained through the detailed study of the construction process applied and the ground-structure interaction mechanisms. The knowledge of the longitudinal force present at a segmental tunnel lining is of paramount importance in order to determine the interaction degree between adjacent rings and the consequent three-dimensionality of the lining response. Finally, the numerical simulation of a real tunnel section subjected to different scenarios of load and boundary conditions determines the influence of the three-dimensional effects on segmental concrete linings response, concluding about its structural implications in respect to the isolated ring approach usually employed in design processes.

RESUM

La creixent utilització de les modernes màquines tuneladores (*Tunnel Boring Machines*, TBMs) ha comportat tant una millora de les mateixes com dels procediments constructius aplicats, permetent la realització de túnels en condicions geològiques més complexes. Aquestes noves condicions atorguen un paper cabdal al revestiment estructural, el qual ha de resistir unes majors pressions de terres i agua, convertint-se en un factor clau en els actuals projectes de túnels.

De forma majoritària, la perforació mitjançant TBMs va associada a la utilització de revestiments de dovelles prefabricades de formigó, consistents en una successió d'anells que es van muntant a l'empara de la tuneladora a mida que aquesta avança. A pesar que aquesta tipologia es àmpliament utilitzada, la seva resposta estructural presenta nombroses incerteses degut a la seva particular configuració en múltiples peces i al procediment de construcció evolutiva aplicat. La millora i optimització dels revestiments, fet que permetrà gaudir d'un major nivell de seguretat a un cost inferior, requereix aprofundir en el coneixement de la seva resposta real així com desenvolupar eines per a la seva predicció acurada.

Aquesta tesi doctoral presenta els mecanismes i els fenòmens que condicionen la resposta estructural dels revestiments de túnel realitzats a base de dovelles prefabricades, descrivint les tècniques de modelització numèrica a emprar per a la seva adequada simulació. La integració de totes aquestes tècniques en un únic model de simulació permet analitzar la resposta d'un revestiment real per a diferents escenaris, determinant la influència i significança dels principals paràmetres que defineixen un túnel i el seu revestiment.

La recerca parteix d'un innovador assaig *in situ* realitzat a la Línea 9 del metro de Barcelona. L'anàlisi de la instrumentació disposada s'empra per a obtenir evidencies experimentals de la resposta real d'un revestiment, així com dels principals fenòmens i mecanismes que la condicionen. En base a aquest coneixement, es desenvolupen estratègies de modelització adequades per a la simulació acurada d'aquests fenòmens i mecanismes, permetent la reproducció fidedigna de la resposta radial d'un anell. L'estudi del procés constructiu i dels mecanismes d'interacció terreny-estructura revelen el comportament longitudinal del revestiment, aportant formulacions per a la seva adequada predicció. Conèixer la força longitudinal en el revestiment resulta imprescindible per a determinar el grau d'interacció entre anells adjacents i, per tant, la conseqüent tridimensionalitat de la resposta estructural. Finalment, l'anàlisi numèrica d'un tram real de túnel sotmès a diferents escenaris de càrrega i condicions de contorn permet determinar la resposta tridimensional dels revestiments, analitzant les seves implicacions estructurals respecte a la consideració d'anell aïllat comunament utilitzada en disseny.

TABLE OF CONTENTS

Chapter 1

INTRODUCTION

1.1. BACKGROUND

The use of tunnel boring machines (TBMs) has increased significantly during the last decade due to the multiple advantages presented in tunnel construction process. Mechanized tunnelling provides an enhanced health and safety conditions for the workforce and allows a better industrialization of the tunnelling process, thus increasing the achieved boring ratios. Moreover, TBMs has allowed the construction of tunnels on more complex hydro-geological conditions, also providing a better control of the surface settlements, that significantly enhance the planning, design and construction of multiple urban tunnels.

These new drilling facilities imply higher load requirements for the structure that has to resist the ground and water pressures. Moreover, the current trend indicates an increase of the tunnels diameter and a reduction of the lining thickness according to exploitation and economical criteria, thus increasing the significance of the structural design of the lining and converting it into a key item in the design process of tunnels.

The construction process applied by TBMs is mainly associated to segmental concrete linings, which are consisted of concrete rings sequentially placed as the tunnel drilling advances (Fig. 1.1). Despite its usual and generalized utilization, the structural response of segmental tunnel linings presents significant uncertainties caused by their particular configuration and construction process. Each ring comprises a certain number of segments, creating a multiple-hinged 3D structure that present a complex behavior. On the other

hand, elementary methods and simplified models are still widely employed in their design process due to two main reasons: the unknown of certain phenomena involved in segmental linings response and the difficulty of accurately reproduce some of the known ones. As a consequence, the improvement and optimization of segmental tunnel linings requires a significant advance in the knowledge of their structural response and the appropriate techniques to properly reproduce it.

Figure 1.1. Segmental tunnel lining of Line 9 subway of Barcelona.

1.2. SCOPE AND LIMITATIONS

Present research aims to better understand the structural response of segmental concrete linings and to provide numerical strategies to properly simulate them.

The adequate achievement of the main goals is planed through the sequential accomplishment of the partial targets listed below:

- Study and analyze the data obtained in a real scale “in situ” test in order to determine the main phenomena involved in the structural response of segmental concrete linings and their significance.
- Study and determination of numerical modeling strategies that allow the correct simulation of the observed phenomena. Performance of 2D and 3D structural models of a ring through the integration of these modeling techniques.

- Reproduction of the real scale “in situ” test in order to validate the applied hypotheses and the developed modeling strategies. Assessment of the current precision available with numerical models on the prediction of segmental concrete linings response.
- Analysis of the sequential construction process applied on mechanized tunnelling and the longitudinal ground-structure interaction mechanisms. Determination of the longitudinal stress state of the lining.
- Analysis of the adjacent rings transference force mechanisms. Development of a 3D multiple ring numerical model which adequately considers the rings’ interaction.
- Detailed explanation of the three dimensional response of segmental concrete linings through the appliance of the developed numerical model to linings under common design loads and also, when subjected to localized loads.
- Determine the structural implications of do not considering the 3D effects on segmental linings design.

Almost each precast concrete segmental tunnel lining presents its own configuration (diameter, thickness, joints number and height, etc) according to the particular requirements that has to satisfy. As a consequence, present research intends to clearly expose the mechanisms that govern the structural response of the linings to allow a general application of the knowledge obtained. Logically, and to allow the adequate comparison, the numerical corroborations are tackled by means of a certain lining configuration subjected to multiple scenarios and conditions.

FE ground modeling is applied when surface settlements or an accurate prediction of tunnel loads are intended, but it presents some handicaps from the structural analysis point of view. For present research, it was decided to assume the usual engineering approach employed for ground response in structural analysis (springs based on Winkler hypothesis) according to the following reasons:

- Do not introduce complex ground responses that can distort and difficult the comprehension of the structural response of the segmental concrete lining.
- Contrast the validity and versatility of the common approach employed in current segmental linings design.

- The simulation of a 3D tunnel section considering the nonlinear response of the ground and the multiple nonlinear behaviors affecting the segmental lining requires very heavy computational efforts, almost disabling the possibility of perform sensitivity analyses.

Present research also aims to be a direct contribution to the analysis and design techniques employed by the structural engineers on the design of segmental tunnel linings. According to that, it was decided to develop modeling strategies on commercial FE software for structural analysis instead of programming a particular tool with limited diffusion and difficult utilization.

A specific technical procedure was systematically applied through the modeling process (Fig. 1.2). That procedure was based in three basic steps: 1- identification of the involved phenomena, 2- determination of numerical strategies to properly simulate them one by one and 3- integrate all these techniques in a unique model.

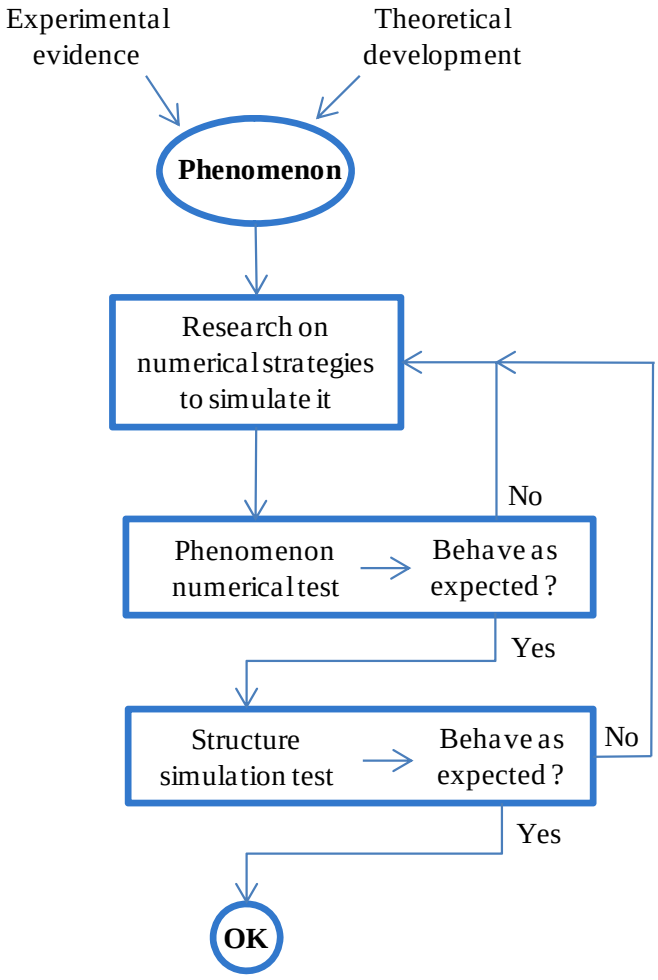

Figure 1.2. Procedure to develop numerical strategies for simulating segmental linings involved phenomena.

1.3. ORIGINAL FEATURES

To the best of the author's knowledge, the original features of the present work are:

- The results and the analysis of a real scale "in situ" test.
- Complete and deep description of the phenomena involved in the structural response of segmental concrete linings.
- Generation of numerical models that integrate accurately simulation procedures for main phenomena involved in the structural response of the lining.
- Description of the longitudinal time-dependent response of the linings and formulations to predict it.
- Determination of the three dimensional effects on segmental concrete linings response and their structural implications.

1.4. OUTLINE AND CONTENT

Present thesis is organized as a compilation of research papers. Each paper is properly edited according to the thesis format and presented as an individual chapter (view Fig. 1.3). The exception is only presented in chapter 6, which is currently presented as a usual thesis chapter. Details about the research publications are listed in the next section 1.5.

According to the continuous work performed on research departments, it is necessary to delimit the research work developed by the PhD candidate. The present thesis starts from the great opportunity that the real scale "in situ" test, previously performed on Line 9 tunnel, represents for the research on the structural response of segmental tunnel linings. This experimental work was designed and supervised by Prof. Climent Molins, whilst Ms. Roser Valls performed the test description, an exhaustive data treatment and an initial approximation to the test response as her graduate thesis[1]. The involvement of the PhD candidate began with the deep analysis of the data obtained in the test, its translation to structural behaviors and the identification and explanation of the structural response of the lining obtained on it (Fig. 1.3).

[1] Valls, R. *Seguiment i interpretació de l'assaig "in situ" del revestiment del túnel de la L9 del metro de Barcelona.* Graduate thesis. Universitat Politècnica de Catalunya. 2006.

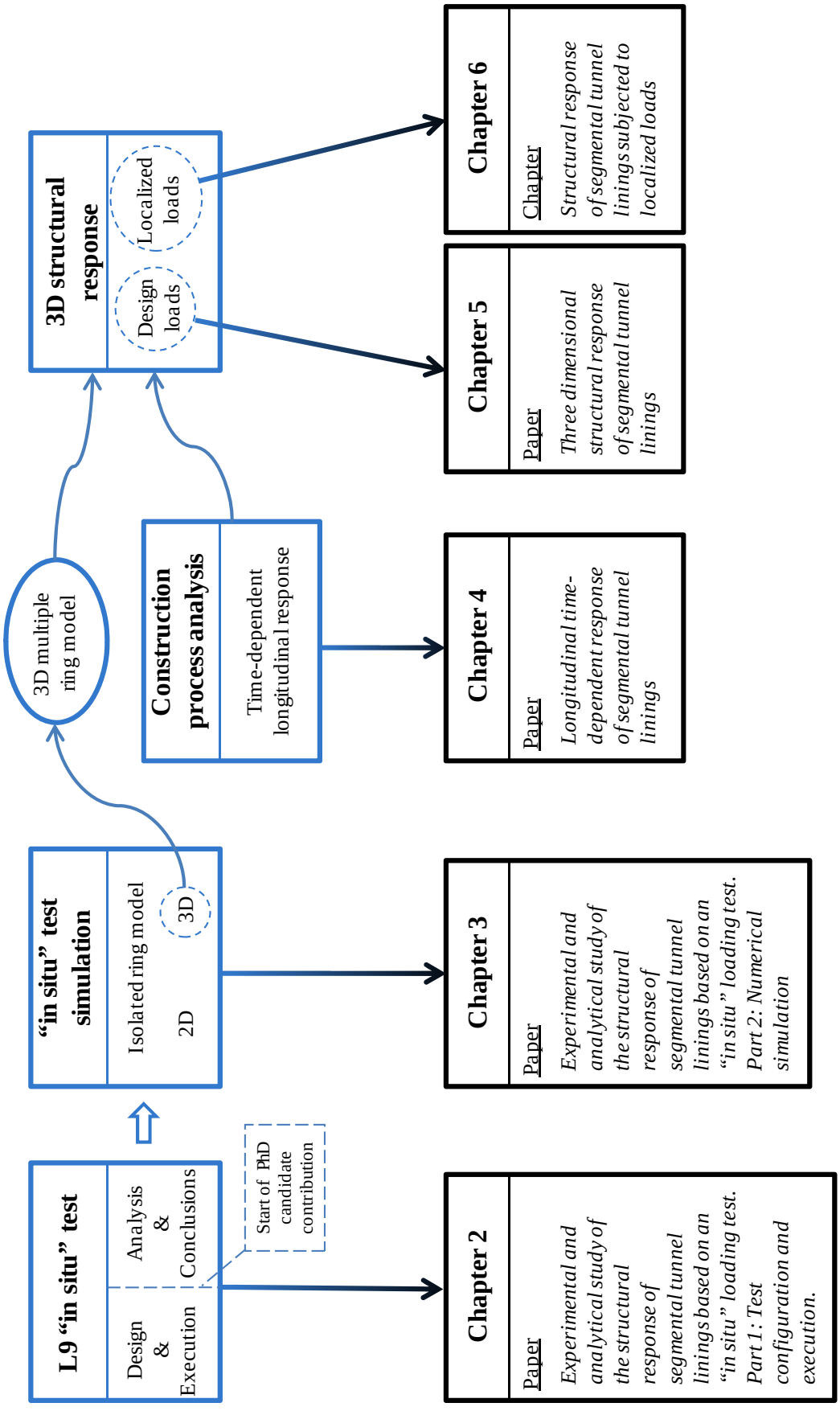

Figure 1.3. Schematization of the research work development and the associated thesis organization

The “in situ” loading test presented in **Chapter 2** was performed on a experimental section of the Line 9 subway of Barcelona, composed by 15 concrete rings exclusively reinforced with steel fibers. A maximum load of 3000kN was applied on the tunnel crown by means of hydraulic flat jacks. The lining response was registered by a complete set of external and internal instruments. The treatment and analysis of the obtained data allow the achievement of significant conclusions about the structural response of segmental concrete linings and the main involved phenomena.

Additionally, the data obtained in the “in situ” test represents an unbeatable chance to determine the accuracy achievable by numerical methods in the simulation of the structural response of segmental tunnel linings. **Chapter 3** deals with the numerical simulation of the “in situ” test. The main phenomena involved on the structural response of segmental tunnel linings are described, and modeling techniques to accurately simulate them are presented and discussed. 2D plane stress and 3D shell elements models of the loaded ring are employed to reproduce the test considering the ground structure interaction, the joints and packing materials’ behavior and the post-cracking response of the steel fiber reinforced concrete. The numerical results are compared with the experimental data in terms of general response, displacements, joints movements and crack patters. Significant conclusions about the potentiality of employing FE techniques on the simulation and prediction of segmental tunnel linings structural response are finally presented.

The target of properly analyze the three dimensional response of segmental tunnel linings required a previous research step. The construction process commonly applied on mechanized tunnelling introduce significant longitudinal forces that influence the interaction capacity between adjacent rings and, consequently, the three dimensional response of the lining. The analysis of the structural implication of the TBMs construction process was carried out in collaboration with Prof. J. Walraven and Dr. C.B.M. Blom during a 6 months stage performed by the PhD candidate at the department of concrete structures of the Delft University of Technology. The resultant **Chapter 4** initially presents a detailed study of the tunnel construction process and the ground-structure interaction mechanisms. As a consequence, it is pointed out that the longitudinal force, initially applied by the TBM, is progressively lost due to the lining creep. Analytical formulations to predict the remaining compression at certain time and the anchorage response of the linings are proposed and numerically contrasted. The long term response of plastic packing materials (packers) is experimentally determined and included on the global creep coefficient of the lining, revealing its significant influence on the remaining longitudinal compressive stress.

The three dimensional response of the segmental concrete linings subjected to design loads is tackled in **Chapter 5**. The adjacent rings interaction mechanisms are initially exposed and described. A 3D finite elements model is created based on a real section of Line 9 tunnel in Barcelona. Such purpose requires an adequate implementation of the circumferential joints response (between adjacent rings), which is combined with the knowledge previously obtained in individual rings modeling. Different tunnel scenarios subjected to design loads are analyzed, also considering the longitudinal compression presented at the lining. Conclusions about the conditions that produce significant coupling effects and their structural influence are presented. The comparison with the usual design methods and the study of the structural consequences of neglecting coupling effects provide significant recommendations for segmental linings design.

Segmental tunnel linings can be exposed to particular, transient or accidental loads that act over a certain part of the lining. The three dimensional model of Line 9 section is employed in **Chapter 6** of the present thesis to deeply analyze the structural interaction between adjacent rings and the consequent lining response in front of localized loads. The specific interaction mechanisms produced by localized loads or significant relative radial deformations between adjacent rings are initially presented. Different ground conditions and longitudinal force levels are applied to the Line 9 3D model in order to analyze the lining response in front of the same localized load. The analysis of the results provides significant conclusions about the interaction capacity between adjacent rings and the response and resistance of segmental concrete linings in front of localized loads.

Finally, **Chapter 7** presents the general conclusions achieved along the present PhD thesis and provides several recommendations for future research on the structural response of precast concrete segmental tunnel linings.

1.5. PUBLICATIONS

The details of the research papers presented as chapters of the present thesis are listed below:

Chapter 2:

Experimental and analytical study of the structural response of segmental tunnel linings based on an in situ loading test. Part 1: Test configuration and execution.

Authors: Climent Molins and Oriol Arnau.

Tunnelling and Underground Space Technology Nº26, pages 764-777. 2011.

Chapter 3:

Experimental and analytical study of the structural response of segmental tunnel linings based on an in situ loading test. Part 2: Numerical simulation.

Authors: Oriol Arnau and Climent Molins.

Tunnelling and Underground Space Technology Nº26, pages 778-788. 2011.

Chapter 4:

Longitudinal time-dependent response of segmental tunnel linings.

Authors: Oriol Arnau, Climent Molins, C.B.M Blom and Joost C. Walraven.

Tunnelling and Underground Space Technology Nº28, pages 98-108. 2012.

Chapter 5:

Three dimensional structural response of segmental tunnel linings.

Authors: Oriol Arnau and Climent Molins.

Engineering Structures. On review process.

Chapter 2

EXPERIMENTAL AND ANALYTICAL STUDY OF THE STRUCTURAL RESPONSE OF SEGMENTAL TUNNEL LININGS BASED ON AN *IN SITU* LOADING TEST

PART 1: TEST CONFIGURATION AND EXECUTION

ABSTRACT

During the last years the use of segmental linings in tunnels bored with tunnel boring machines (TBMs) have increased considerably. Despite this, uncertainties remain on the structural behavior of segmental tunnel linings. To overcome them, a new methodology for an *in situ* real scale test on this kind of tunnels was developed and applied on an experimental section placed at the new Line 9 (L9) of the metro of Barcelona. The main particularity of this test falls on its performance in the definitive placement of the rings and, therefore, in the real work conditions of the tunnel. The main advantage to previous real scale test experiences was the consideration of the real ground-structure interaction. The experimental section was composed by 15 rings built using steel fibers as a unique reinforcement. Significant loads were applied to the tunnel crown (max 3000 kN) by means of three hydraulic flat jacks embedded at the extrados of the loaded ring. A complete set of internal and external instrumentation was placed on the experimental section to obtain the necessary measurements to characterize the lining behavior. Such measurements were intensively treated and its main results are presented and analyzed in detail in this paper. This *in situ* test provides significant evidences of the structural response of SFRC segmental tunnel linings in hard ground conditions.

***Keywords*:** Segmental tunnel linings, SFRC, real scale structural testing.

2.1. INTRODUCTION

The evolution of the construction techniques and the development of the tunnel boring machines (TBMs) have allowed the construction of tunnels in almost all kinds of soils in difficult conditions such as low coverage or high ground and water pressures. These drilling advantages imply higher structural loads, both in construction stage to resist higher or more eccentric TBM thrust forces, and in the serviceability stage to resist higher ground and water pressures accomplishing the serviceability requirements.

The use of segmental tunnel linings allows an intensive industrialization of the construction process and, therefore, an accurate control of the segments quality. Moreover it also provides an important reduction of the time required to erect a complete structural member (ring) inside the TBM. This is one of the reasons for the construction speed provided by the TBMs that is turning them the most competitive drilling solution for the majority of modern tunnels.

Furthermore, the particularities of this construction method generate serious questions about its structural response that have to be progressively answered in order to optimize its design and to obtain the maximum safety at minimum cost. The influence of joints configuration, the ground-structure interaction or the real load redistribution capacity of the lining between adjacent rings have to be clarified in this particular structure.

Two different experiences in segmental tunnel linings real scale tests had been carried out at TUDelft (Blom, 2002) and in Germany by STUVAtec. Their focus was on the damages occurred during the construction process and the limit of the radial ovalisation experimented by rings under earth pressures in soft soils conditions. Additionally, these experiences also tried to study the load transferences between rings depending on the longitudinal axial stress remaining in the lining due to TBM jacks action. The load redistribution to adjacent rings should modify the response of the lining subjected to concentrated loads and, therefore, it is necessary to determine its influence in the actual structural capacity of the lining. These tests only considered the load transfer on a set of three rings due to the extreme difficulties to test more rings. Both tests were performed in labs, not having the possibility to take into account the actual soil-structure interaction and the behavior of more than three rings. Soil reaction was simulated by means of a complex system of radial hydraulic jacks.

A ring is composed by multiple segments defining a multiple-hinged structure and, consequently, the reaction of the ground is critical to keep the stability of the system. However, the bond existing between the lining and the ground constraints both the radial and the tangential deformations, which results in reaction stresses in the ground (Blom et

al, 1999). The load transference from the lining to the ground influences the stress state of the structure and, in consequence, its response.

To overcome the previous limitations, an experimental section of 15 rings was constructed inside the new L9 metro project in Barcelona using steel fibers as a unique reinforcement for concrete. The main objectives of this section were (1) to develop an *in situ* loading test that allows the characterization of the segmental tunnel linings behavior in hard ground conditions and (2) to determine the feasibility of using steel fibers as a unique reinforcement for concrete segments.

The use of steel fibers in segmental tunnel linings has significantly increased during last years with the aim of limiting the local spalling damage that often occurs in the corners of the segments. Nowadays, few authors have intended to determine the contribution of these fibers to the structural capacity of the segmental tunnel linings in order to reduce the amount of necessary conventional reinforcement (de Waal, 2000, Plizzari and Tiberti, 2006, Kasper et al., 2007, Tiberti et al., 2008). The *in situ* test of SFRC lining was an excellent opportunity to obtain significant information about it.

This paper describes the configuration and performance of the *in situ* test and analyzes the results obtained on it, involving a direct contribution to the knowledge of the structural response of segmental tunnel linings. The characteristics of the experimental section, the test set-up and its development are intensively explained. Finally, a selection of the most significant results is presented and analyzed in detail to highlight main conclusions.

2.2. EXPERIMENTAL SECTION

2.2.1 General aspects of the Line 9 project

Line 9 (L9) is an ambitious project for the construction of a new subway line in Barcelona. Designed as a bypass along the north part of the city and to link the most characteristic points of the neighboring towns, L9 comprises a total length of 47,8 km and 52 stations entailing an investment of more than 6.000 M€.

The line runs under a high density populated area that is often irregularly urbanized, making more difficult the surface works. Out of the deltas of the rivers that bound Barcelona, the uneven topography of the city provides high local tunnel overburdens, achieving a maximum close to 90m. In consequence, the majority of the tunnel linings were planned to be constructed by means of different TBM's, three of diameter (ø) equal to 12m and two of ø9.4m. The construction of one large diameter tunnel was selected in deep

sections instead of the twin tube option due to its best economical commitment tunnel-shaft to allow the allocation of the station inside the tunnel.

An experimental section of 15 rings was constructed inside the section 4a of Line 9. Section 4a is located between the city of Santa Coloma de Gramanet and the Besòs River and is characterized for its record in slenderness -ratio between the internal diameter ($ø_{int}$) of the lining and its thickness (t), $ø_{int}$ / t- of 31.1. The rings of this section are composed by seven segments (A1-A5, B and C) plus one key segment (K) defining a universal ring with a external diameter of 11.6m, 0.35m thickness,1.80m width and 0.57º conicity (Fig. 2.1).

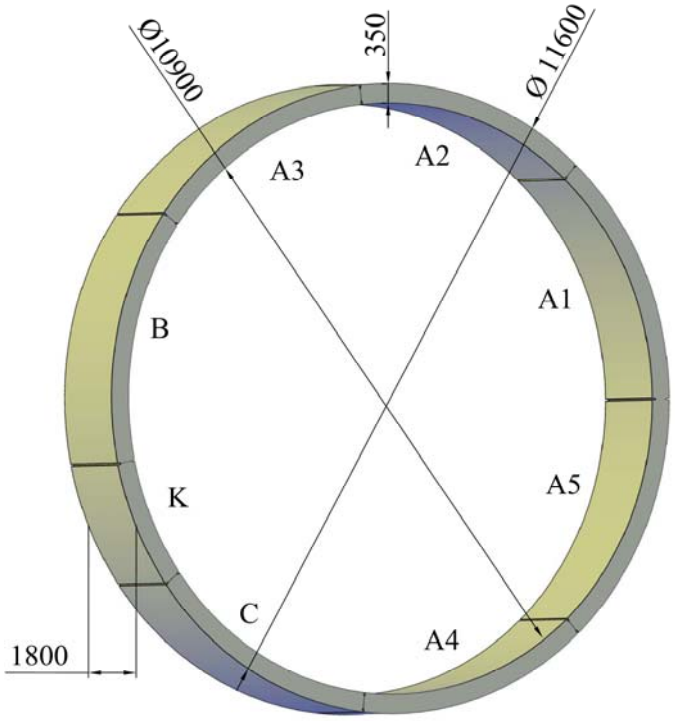

Figure 2.1. Ring Geometry. Dimensions in mm.

This record slenderness (Table 2.1) increase the interest to study its structural response in order to improve the design and the construction techniques employed for segmental tunnel linings.

Table 2.1. Most slender tunnels already constructed in the world.

Tunnel project	*$Ø_{int}$ (mm)*	*Thickness, e (mm)*	*Slenderness ($Ø_{int}$/e)*
Section 4a. L9 of Barcelona	10900	350	31.1
Dublin Port Tunnel	10840	350	31.0
Heathrow Baggage Handling	4500	150	30.0
Section 4b. L9 of Barcelona	10900	400	27.3
L8 and L9 of Madrid Subway	6700	250	26.8

The longitudinal joints (between segments of a same ring) present a packing material (packer) consisting of a bituminous sheet of 1750x204mm with 2mm thickness. The circumferential joints (between adjacent rings) present a set of 30 plastic packers of 785x204mm with 2mm thickness.

2.2.2 Material properties

The rings of the experimental section were constructed using 60 kg/m^3 of steel fibers as unique reinforcement instead of the 60 kg/m^3 of conventional rebars plus the 30 kg/m^3 of steel fibers that was the normal reinforcement of that lining. Only a slight amount of reinforcement bars were placed in some segments to hold the internal instruments necessary to monitor the test. Concrete mix to achieve the design strength (f_{ck}=50N/mm^2) and the main characteristics of the fibers are shown in Tables 2.2 and 2.3.

Table 2.2. Concrete mix.

Component	*Weight (kg/m^3)*
Cement CEM I 52.5R	410
Washed sand 0-5mm	580
Granitic sand 0-5mm	333
Gravel 5-12mm	410
Gravel 12-20mm	595
Water	115
Super plasticizer Glenium TC1332	3
Steel fibers	60

Table 2.3. Steel fibers characteristics.

Content	60 kg/m^3
Diameter ($Ø_f$)	1 mm
Aspect ratio (Fiber length / $Ø_f$)	50
Tensile strength	1,100 N/mm^2
Geometry	Hooked end

2.2.3 Ground properties

Section 4a runs inside a granodiorite rock formation that presents different alteration levels depending on the local tunnel depth. The experimental section is located 33.5m below the surface inside a low alteration granodiorite which presents a high modulus of elasticity

(11,225 N/mm^2). The groundwater table is located 18.6m over the tunnel axis, producing significant hydraulic pressures over the structure.

2.3. TEST SET-UP

2.3.1 Test configuration

As aforementioned, the main limitation presented by previous full scale test experiences was the realistic consideration of the ground response against the ring deformation. After the analysis of different laboratory options, it was concluded that the unique way to obtain the real segmental tunnel lings behavior was to perform an *in situ* test in the actual work conditions of the tunnel.

The conceptual definition of the test was based on applying radial loads close to the tunnel crown and the acquisition of the rings deformations and displacements by means of a complete set of instruments. The first difficulty of the *in situ* test was to decide how to generate external loads over a ring definitively placed inside the tunnel. Different options were analyzed selecting the use of hydraulic flat jacks that were previously embedded at the extrados of the tested ring (Fig. 2.2a) which apply the force against the surrounding hardened grout and ground (Fig. 2.2b). The employed jacks present a maximum nominal force of 1,700 kN and a maximum travel of 25mm. Their external diameter was $Ø_{ext}$=460mm and the pressure plate diameter was $Ø_{pres}$=365mm. All jacks were placed over Ø 700mm and 30mm thickness steel plate (Fig. 2.2b) in order to achieve a better distribution of the applied force into the segment. The selected configuration was based on three concentrated loads located in the tunnel crown and distributed symmetrically, encompassing a total sector of 48º (Fig. 2.3).

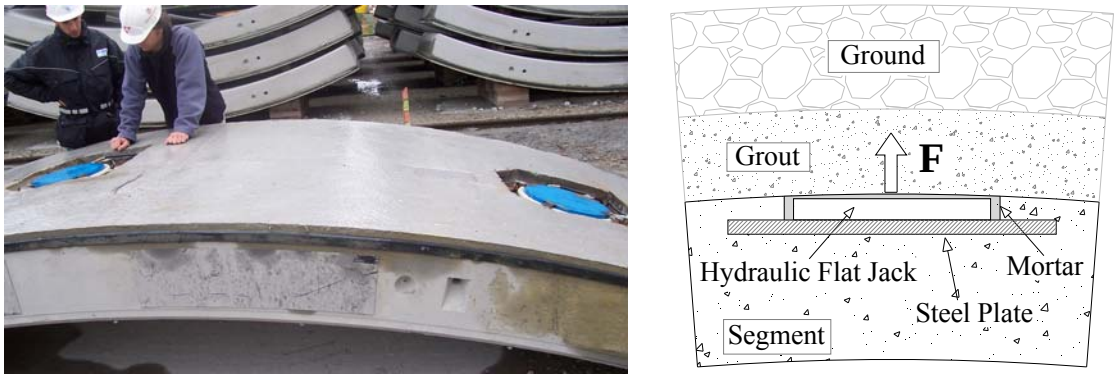

a) b)

Figure 2.2. Two hydraulic flat jacks on a segment (a) and its conceptual work scheme (b).

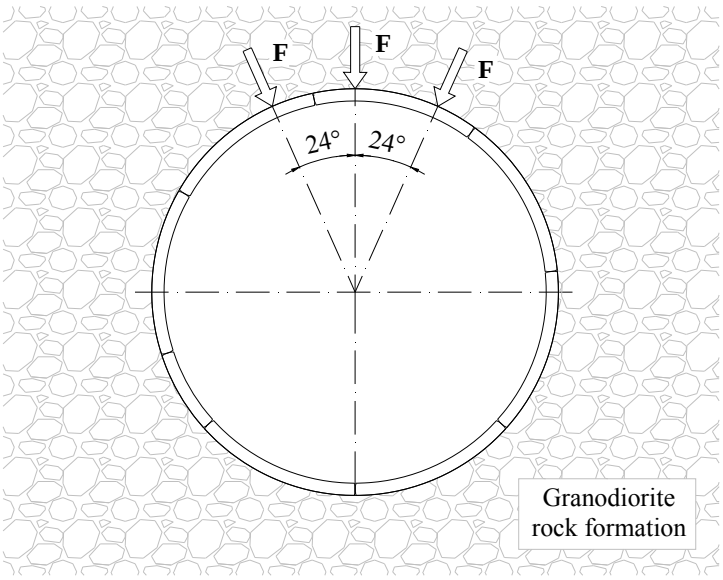

Figure 2.3. Selected configuration of the concentrated loads for the test.

2.3.2 Prediction of maximum loads

Two different numerical analyses were previously carried out to predict the behavior of the segmental lining during the test and to determine the maximum load per jack that should provide an advanced crack status without any risk: (1) individual ring model considering the non-linear behavior of concrete in both tension and compression and (2) a 3D shell elements model that considers the longitudinal load redistribution through the ring joints (Molins *et al.*, 2005). The maximum load per jack was fixed in 1,500kN.

2.3.3 Monitoring

Five of fifteen rings that compose the experimental section of SFRC were intensively instrumented internally and externally. The internal instruments of every segment of the loaded ring (numbered as 1838) was composed by fourteen extensometers (Fig. 2.4a), twelve measuring the circumferential strain (placed by pairs to allow the curvature measurement of different cross sections) and two measuring the longitudinal strain. Two load cells (Fig. 2.4b) were placed at ¼ and ¾ of the length of each segment.

a) b)

Figure 2.4. Extensometers (a) and load cells (b) employed in the *in situ* test.

Every one of the four rings adjacent to the loaded one (numbered as 1836, 1837, 1839 and 1840) contains one segment with twelve extensometers circumferentially placed (using the same configuration presented for the loaded ring segments) and one load cell centered at the segment extrados side. Table 2.4 summarizes the internal instrumentation placed in the experimental section and the dates of casting and placing.

Table 2.4. Description of the internal instruments placed in the experimental section.

Ring	*Position of K segment*	*Segment*	*Extensometers*	*load cells*	*Flat jacks*	*Casting date*	*Placing date*
1836	7	A2	12	1		14/04/2004	23/02/2005
1837	2	A4	12	1		30/03/2004	23/02/2005
1838	11	A1	14	2		01/04/2004	24/02/2005
		A2	14	2	2	07/04/2004	24/02/2005
		A3	14	2	1	01/04/2004	24/02/2005
		A4	14	2		02/04/2004	24/02/2005
		A5	14	2		05/04/2004	24/02/2005
		B	14	2		02/04/2004	24/02/2005
		C	14	2		02/04/2004	24/02/2005
		K	4	0		02/04/2004	24/02/2005
1839	1	A3	12	1		14/04/2004	24/02/2005
1840	8	A4	12	1		30/03/2004	24/02/2005

The external instruments consist of two different configurations of displacement transducers. In order to obtain the movements of the rings in the tunnel crown zone, displacement transducers were vertically placed across the tunnel section (Fig. 2.5a).

Eight sets of two transducers were placed in every longitudinal joint of the loaded ring to measure the circumferential joint movement at both sides. 4 transducers were also placed in the crown zone of the loaded ring to obtain, with the combination of the longitudinal joints transducers, 2D measurements of the rings movements (Fig. 2.5b).

The relative longitudinal displacements between adjacent rings were registered by means of 24 transducers placed in the circumferential joints of the instrumented rings.

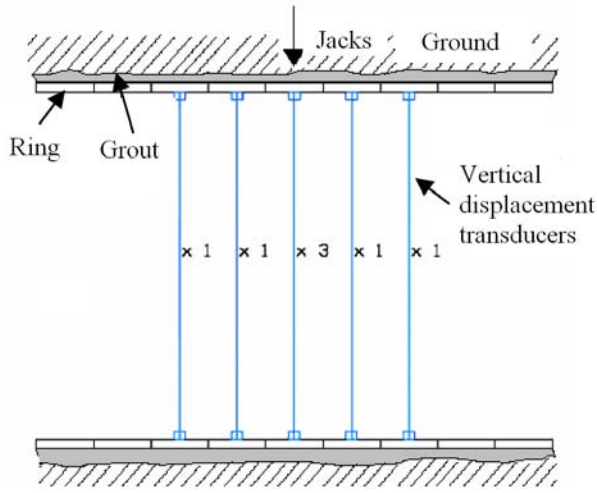

a)

b)

Figure 2.5. Vertical transducers in the tunnel cross section (a) and 2D transducers in joints (b).

2.3.4 Control and characterization of segments material

To control and characterize the mechanical properties of SFRC employed on the segments of the experimental section, four different tests were carried out:

(1) Compression test on cylindrical 300x150 mm specimens to control the compressive strength (results are presented in Table 2.5).

Table 2.5. SFRC compression test results.

Description	*Compression test*
Number of specimens	36
Average value	54.13
Typical deviation	2.90
Variance $()^2$	8.47
Minimum value	47.57
Maximum value	60.20
Coefficient of variation	5.37%

(2) Elasticity modulus test, with an average value of 38,700 N/mm^2.

(3) The characterization of the SFRC flexural response was carried out by means of a set of twelve 4-point beam tests that were performed according to NBN regulations (IBN,1992) (Fig. 2.6a). Tests were performed over prismatic specimens 600x150x150. The main average results are presented in Table 2.6 and the mean load-deflection diagram obtained is shown in Figure 2.6b.

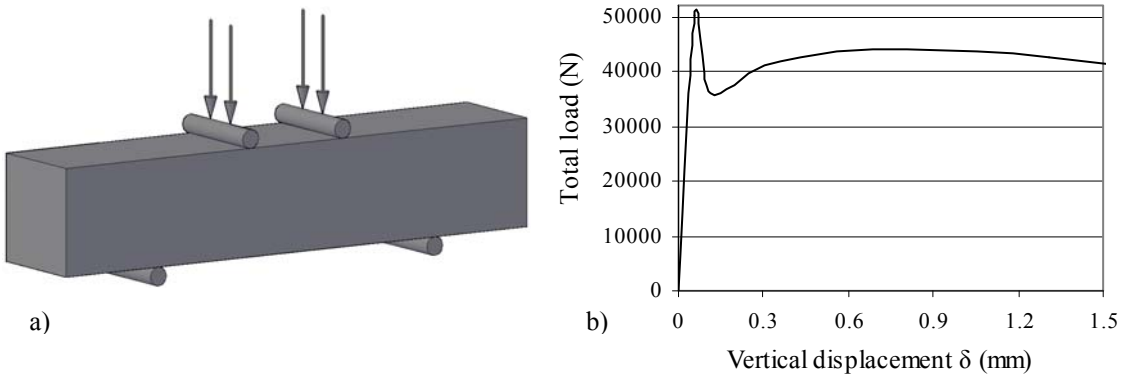

Figure 2.6. NBN flexural test scheme (a) and the average behavior obtained in L9 SFRC (b).

Table 2.6. Average results obtained in NBN SFRC test set.

$f_{f,300}$ (28 days)	5.62 N/mm^2
f_r	6.67 N/mm^2

(4) Additionally, the Barcelona test (Molins *et al.*, 2009) was employed to control the SFRC post cracking properties in real segments. For that purpose, several cores were directly drilled on segments that were never installed. This work allows the evaluation of the resistance differences presented by SFRC depending on the segments zones and bending plane caused by fiber distribution and orientation (Mora, 2008).

2.4. DEVELOPMENT

Previously to the test performance, it was necessary to establish the actual state of the experimental section. For that purpose, a complete check-out was carried out covering: (1) a topographic survey of the instrumented rings, (2) the measurement of the joints lags, (3) the determination of the final position of the hydraulic jacks and the instrumentation devices and (4) a complete description of the cracks on the segments caused by the manufacturing, transport and installation processes besides the initial groundwater and backfill grout pressures. Despite the accurate definition of the test carried out prior to segments manufacturing, some significant differences were observed in the hydraulic jacks position (Fig. 2.7), forcing new analyses to contrast the suitability of the maximum selected load per jack. Furthermore, the eccentricity of the jacks in reference to the middle axis in the width of the ring (located at 90cm of the ring edges) should produce an asymmetry in the ring behavior that had to be taken in consideration.

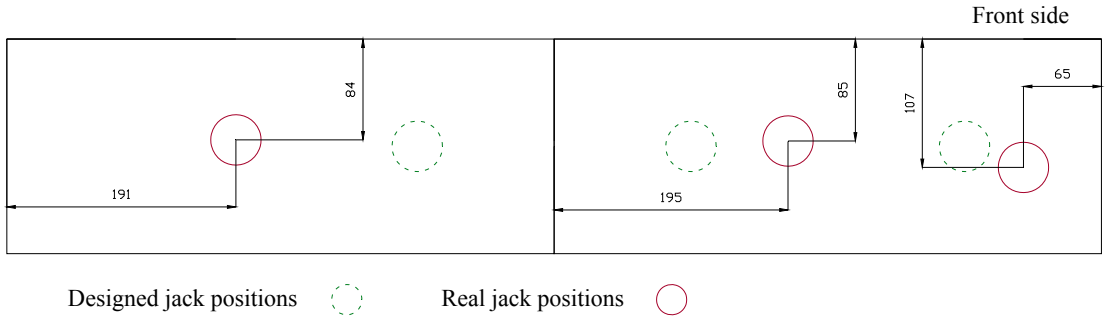

Figure 2.7. Designed and real positions of the hydraulic flat jacks (dimensions in mm).

2.4.1 Loading process

The test started on Tuesday 13th of December 2005 and finished on Friday 16th. In the initial phase (numbered as 0) a load of 100 kN per jack was applied to all jacks and maintained along 18 hours to compensate the relaxation experimented by the hydraulic pressure. The first stage of phase 1 consisted in the achievement of 500 kN per jack in all jacks, but when the pressure was close to 26 bar (260 kN), the jack number 3 suddenly failed, leaving two active jacks for the rest of the test. Therefore, phase 1 was reduced to 500kN per jack acting simultaneously in jacks 1 and 2 and maintaining it during 14 hours (Fig. 2.8). At that moment, it was necessary to quickly determine the suitability of continuing with the designed test plan. In consequence, a set of nonlinear analyses were carried out according to the new test configuration, concluding that the initially planned load procedure could go ahead without significant additional risks. Finally, the same load of 500kN was applied to every jack individually to conclude phase 1. The same procedure was employed for phase 2 but achieving a load of 1500 kN/jack and reducing the maintenance time of the simultaneous load. The load appliance was finally divided in 7 different stages that are detailed in Table 2.7. The failure of jack 3 produced reductions on the maximum applied force and in the planned loading scenarios. Despite that, the remaining load capacity was enough to produce in the lining significant movements, pressures, strains and damages (cracking) to adequately analyze the structural response of the lining.

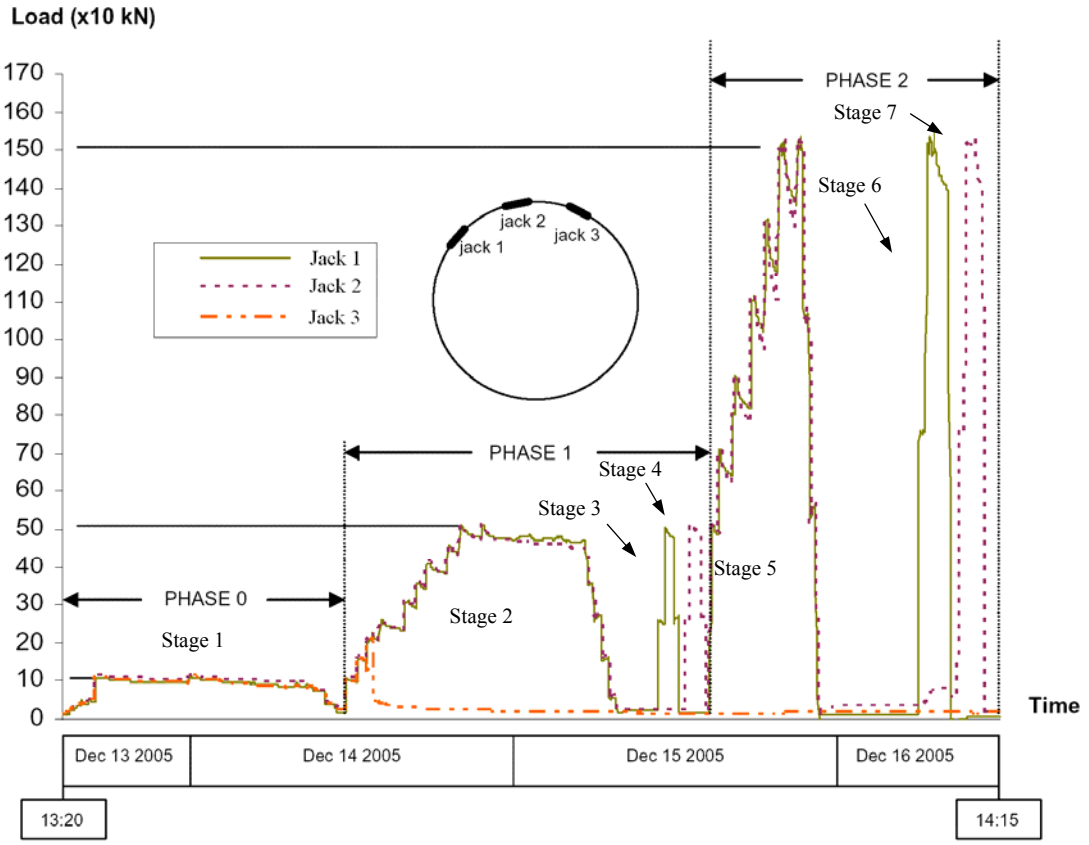

Figure 2.8. Load diagram performed in the *in situ* test.

Table 2.7. Load phases applied during the *in situ* test.

Phase	*Stage*	*Active Jacks*	*Load / Jack (kN)*
0	1	Jack 1 + Jack 2 + Jack 3	100
	2	Jack 1 + Jack 2	500
1	3	Jack 1	500
	4	Jack 2	500
	5	Jack 1 + Jack 2	1500
2	6	Jack 1	1500
	7	Jack 2	1500

2.5. RESULTS

The instrumentation placed in the experimental section provides a large amount of measurements that require an enormous work of selection and treatment to be presented in a clear and intelligible form. Figure 2.9 shows the schematic representation adopted for the ring movements and pressures for the loaded ring at stage 5, corresponding to the

maximum load applied on the ring (1,500 kN per jack). Load cells provide important information about the zone where the structure increase/decrease its pressure against the surrounding ground, thus supplying evidences of the ring resistance mechanisms and the ground-structure interaction. The joints movement measurements provide information about the joints behavior that can help to understand its involvement on the ring structural response. Schematic results of all stages are presented in the Appendix 2.

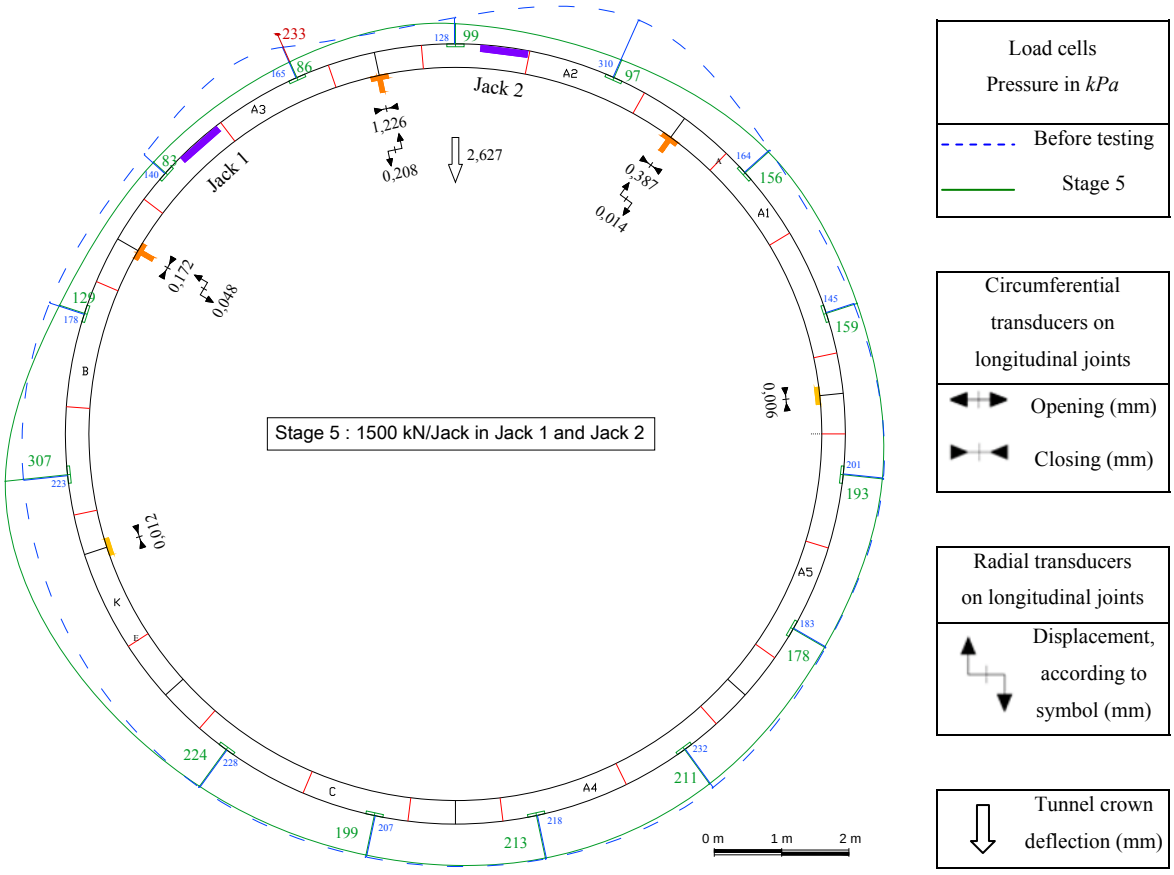

Figure 2.9. Schematic representation of the movements and external pressures at stage 5.

2.5.1 Pressure on the extrados

Pressure distribution in load cells after loading (Fig. 2.9) shows a reduction of pressure on the upper part of the loaded ring. This reduction results of the loose of contact between the lining and the ground due to jacks action. It is also possible to notice the increase of pressure where the ground provides reaction against the lining deformation. The extrados pressure did not experience any variation in the lower part of the ring showing that, for the particular conditions of this test, the load only affects the upper part of the structure.

These results show an arch behavior under a concentrated load (F_L) discharging the structure stresses to the ground. It is expected that the reaction zone (space where the ground presents forces F_{GR}) depends on the ground stiffness and the ring geometry due to the displacement concentration in joints (Fig. 2.10). A stiff ground should provide short arch lengths and small reactions zones whilst soft grounds should provide larger arch lengths and ground reaction zones.

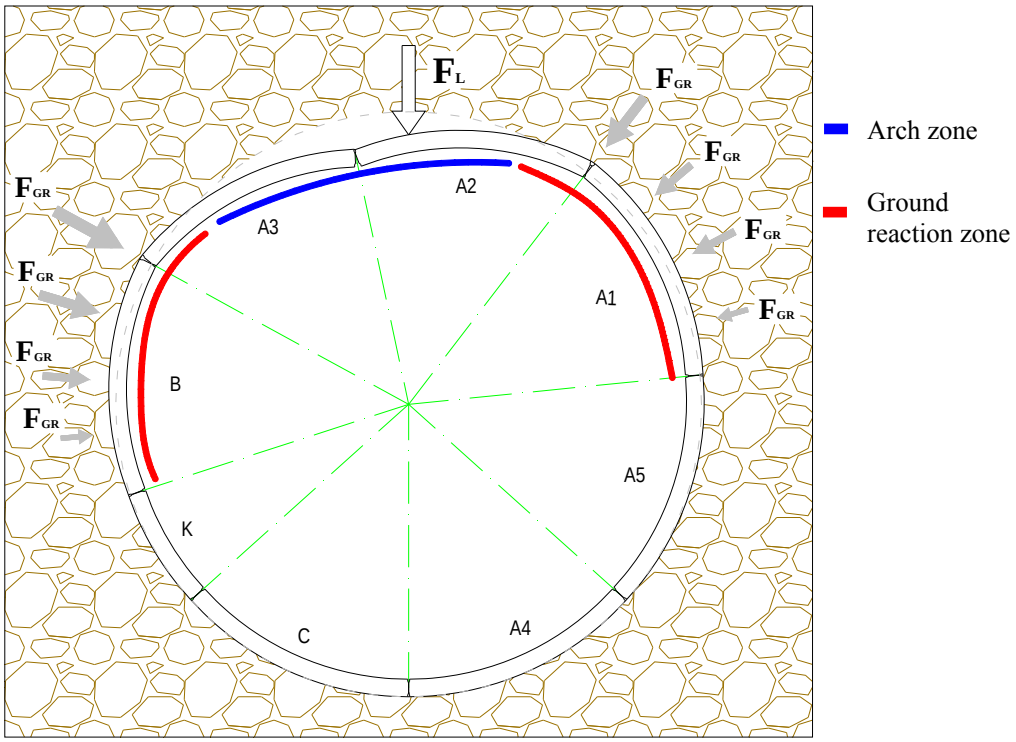

Figure 2.10. Local arch mechanism originated by the force applied by jack 2.

Additionally, for stiff grounds it is also discussed the significance of the lining-ground interaction through tangential mechanisms that transmit the forces directly to the ground (Fig. 2.11). This mechanism is based on the tangential adherence between the interface formed by the lining, the grout and the ground and affects directly the ring stress-distribution. Consequently, the structural response of the lining is also affected. The increase of radial pressure between the lining and the ground in the ground reaction zone should increase the tangential stress transmission capacity of the interface. This topic was analyzed using results provided by the extensometers embedded in the segments to monitor the circumferential strains.

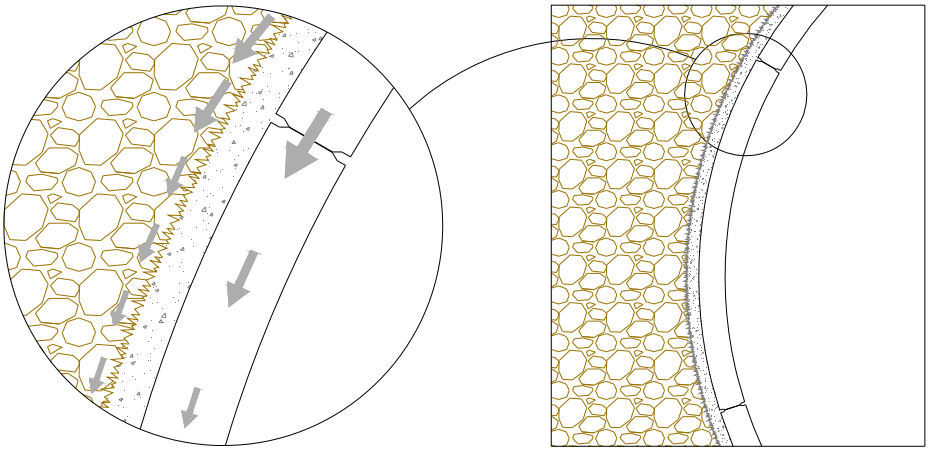

Figure 2.11. Lining-ground tangential force transmission mechanism.

2.5.2 Circumferential extensometry

Figure 2.12 shows the average values of the axial stress measured in the loaded ring during stage 5 (1500 kN in jacks 1 and 2), obtained after applying the value of the deformation modulus of concrete to the measured increments of strain produced by loading. The maximum increment of compression stress was reached in the tunnel crown and it was gradually lost in a short space out of the jacks zone (segments A1 and B), denoting the axial force transmission from the ring to the ground through tangential mechanisms. Extensometers data process was very demanding. Results had to be carefully analyzed and some of them were disregarded due to the low reliability of their signals. Some interference was proved to be caused by cracks across the instruments.

To assess the results provided by the extensometers, a bar elements structural model of the loaded ring was developed employing the software Robot office. The joints were reproduced by means of lineal hinges, which rotational stiffness (c_r) was estimated by means of the relation 2.1 (Blom, 2002), where b is the width of the segments, l_h is the height of the joint contact and E_c is the concrete modulus of elasticity. The parameters adopted for its determination are shown in table 2.8.

$$c_r = \frac{b l_h^{\,2} E_c}{12} \tag{2.1}$$

Table 2.8. Values of the parameters employed to calculate the rotational stiffness of joints.

Parameter	*Value*
Width of segments (b)	1800 mm
Height of joint (l_h)	204 mm
Concrete modulus of elasticity (E_c)	38,700 N/mm^2

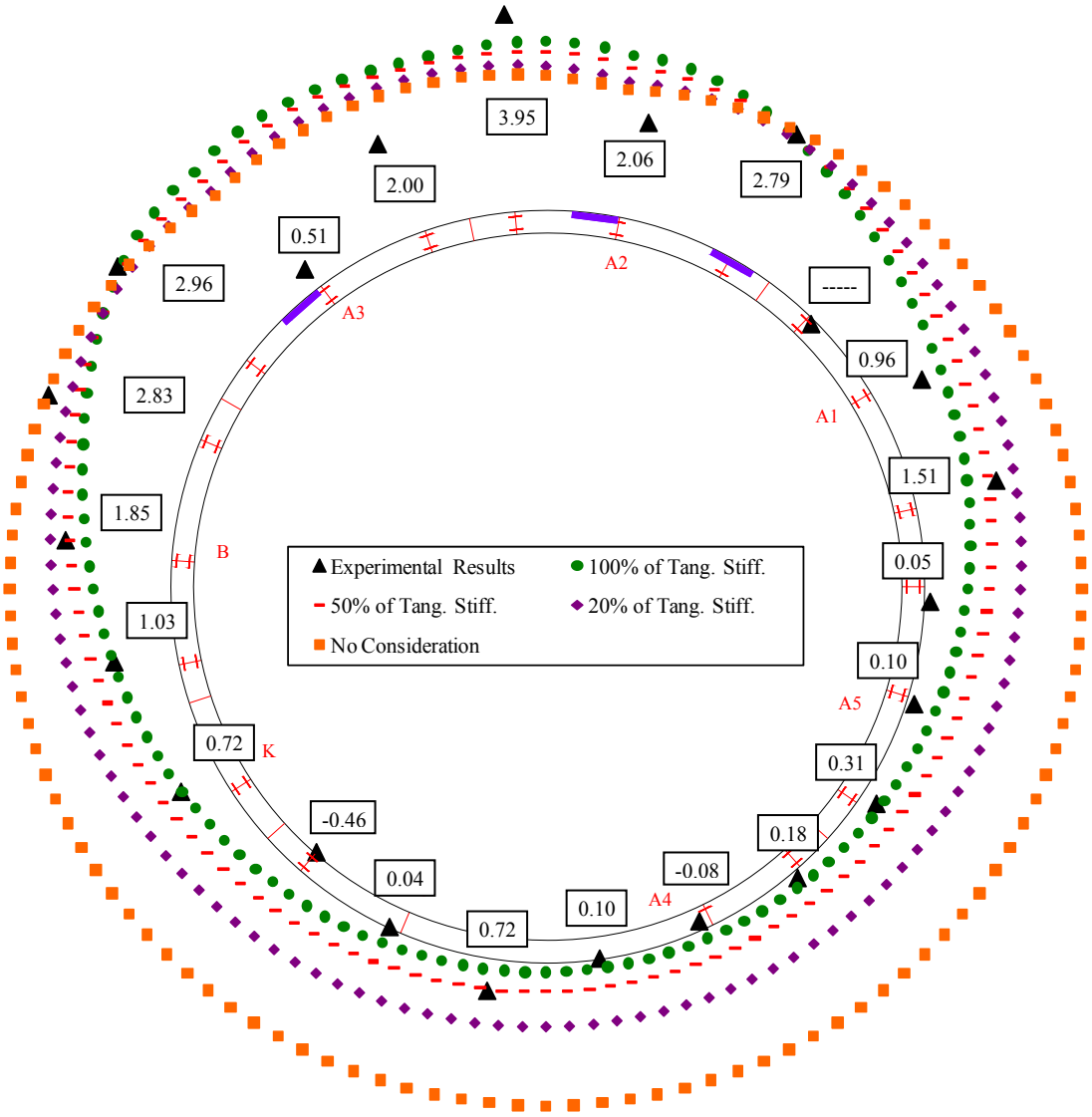

Figure 2.12. Experimental increments of axial stresses reached in loading stage 5 (in N/mm^2) and analytical distributions varying tangential stiffness.

Ground structure interaction was modeled according to Winkler hypothesis by means of radial and tangential springs. In order to consider the loose of contact in the loading zone, a non linear stiffness was assigned to the radial springs (K_r) according to relation (2.2), which corresponds to the analytical solution of a circular tunnel in elastic ground. A ground modulus of elasticity (E_s) of 11,225 N/mm^2 and a Poisson ratio (υ) of 0.24 were employed whilst R corresponds to the lining external radius. Initially, the tangential spring stiffness (K_t) was assumed according to the relation proposed by Plizzari and Tiberti (2006), fixing the tangential spring stiffness as 1/3 of the radial stiffness (eq. 2.3). Departing on this assumption, different analyses were carried out reducing the tangential stiffness at 50%, 20% and also disregarding it at all. Figure 2.12 shows the axial stress distribution assuming the different values of tangential stiffness.

$$K_r = \frac{E_S}{R \cdot (1+\upsilon)} \qquad (2.2)$$

$$K_t = \frac{K_r}{3} \qquad (2.3)$$

The full consideration of the tangential stiffness provided the best fitting of the experimental results in both, the maximum stresses reached in the tunnel crown and the stress transference length out of the jacks' zone. Lower values of tangential stiffness produced a reduction of peak axial stresses and a smoothing of the distribution, obtaining significant stresses at the bottom of the ring. Disregarding the tangential stiffness at all produces a uniform distribution of the axial stress. Therefore, in the experimental section conditions, the tangential force transmission plays a decisive role on the lining stress distribution. The adequate consideration of the tangential mechanisms presents a great importance in the determination of the segmental tunnel linings structural behavior in hard ground conditions.

Despite the significance of the applied loads, the high stiffness of the ground implies low deformations to provide the necessary reaction to equilibrate the loads. In consequence, low deflections were measured on the tunnel crown. Table 2.9 summarizes the most significant vertical deflections obtained at the tunnel crown during the *in situ* test. A maximum deflection of 3.1mm was obtained during stage 7, presenting a post-load remaining value of 1.2mm (39%). As can be observed, the remaining deflections measured in the initial phases are higher than in the last ones. This fact is caused by the nonlinear behavior with high remaining deformations presented by the bituminous packer placed at longitudinal joints, which is described on the part 2 of this paper (Arnau and Molins, 2011).

Table 2.9. Vertical deflections at the tunnel crown during the *in situ* test.

Phase	*Stage*	*Deflection (mm)*	*Remaining deflection (mm)*
1	2	0.537	0.231 (43%)
	4	0.543	0.267 (49%)
2	5	2.627	0.840 (32%)
	7	3.076	1.220 (39%)

As was previously explained, a ring is composed by various segments defining a multiple-hinged structure. Joints present a lower rotational stiffness than concrete segments caused by the softness of the packing material, the smaller height of the packer sheet (204 mm) and the incapability of the joint to transfer tensile stresses. Additionally, significant cracks appear under jacks positions, diminishing the rotational stiffness of the segment at the load

appliance zone and consequently reducing the length of the concrete segment without structural hinges. Therefore, it was expected that the ring displacements were based more on concentrated rotations at joints and cracked sections than in the elastic curvature of the concrete segments.

2.5.3 Longitudinal redistribution

The structural response of the segmental tunnel linings also depends on the load redistribution capacity from a loaded ring to its adjacent ones. A high redistribution means a response similar to a continuous pipe whilst a low redistribution capacity means a unique ring resistance and the consequent weakness in front of concentrated loads. The study carried out by Liao et al. (2008) concluded that the bending moment in tunnel cross section decreases with the shear stiffness and, therefore, structural measures should be taken to strengthen the shear resistance ability between rings.

The longitudinal redistribution is governed by the shear force transmission capacity between rings that mainly depends on the joint configuration, the deformability of the rings (it also implies the surrounding ground influence) and the construction process. The rings of the experimental section present a flat ring joint configuration using plastic packers to regularize the contact zone and to transmit forces. In consequence, the tangential transmission capacity will be determined by the maximum shear force resisted by the joint before its slipping, which depends of the remaining axial stress in the lining, originally caused by the TBM thrust force during the tunnel construction.

The external transducers placed at the ring joints of the tunnel crown provided significant data about the global structural behavior of the lining. Figure 2.13 shows the relative displacements between adjacent rings measured in the tunnel crown during the individual application of the maximum load in jacks 1 and 2 (stages 6 and 7). The action of jack 1 (stage 6) does not produce significant movements in the tunnel crown joints showing the localization of the experimented displacements. Moreover, the action of Jack 2, which is much closer to the tunnel crown (Fig. 2.9), is much more noticeable by the instruments placed at the crown. The measurements show that movements only occurred in the limiting joints of the loaded ring.

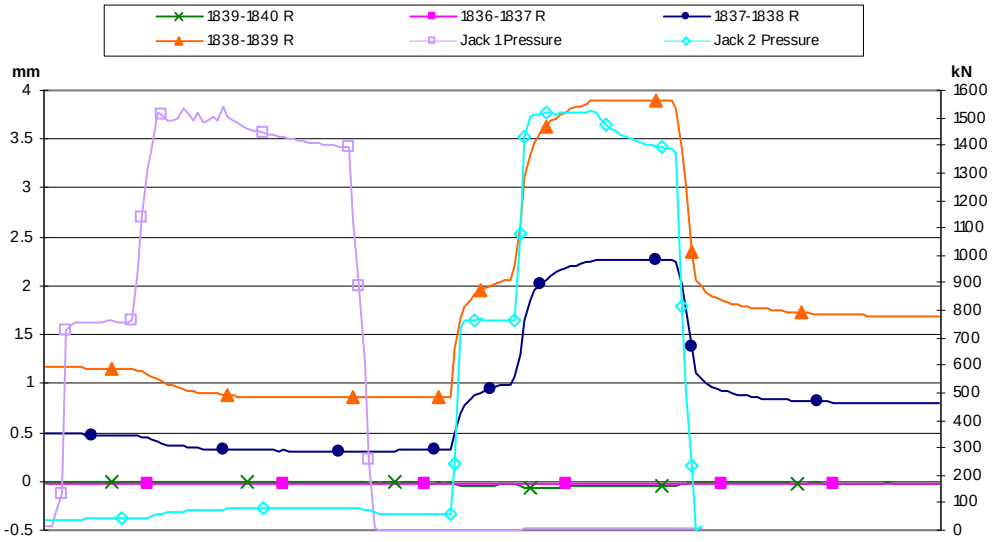

Figure 2.13. Temporal evolution of jack force and radial displacements between rings at the crown during stages 6 and 7.

The magnitude of the obtained relative displacements (max 3.1mm) clearly denotes the slipping of the 2mm packer placed at ring joints. An experimental campaign to determine the maximum tangential stress and displacement for different packers employed in Spanish tunnels was carried out by Cavalaro (2009) at the laboratory of the Universitat Politècnica de Catalunya (UPC). Results for Line 9 ring joint packer showed that for a high normal compressive stress (15 N/mm^2), the maximum displacement before slipping was close to 0.3mm (Fig. 2.14).

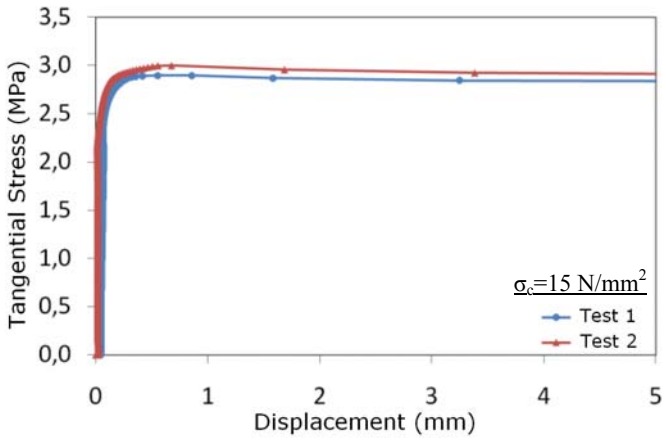

Figure 2.14. L9 ring joint packer tangential behavior subjected to a compressive stress (σ_c) of 15 N/mm^2 (Cavalaro, 2009)

The joint slipping means that their force transmission capacity is exhausted and therefore the load redistribution to the adjacent segments is clearly limited. Furthermore, the instruments placed in the adjacent rings did not present a significant response against the different loading stages, showing a quasi-individual response of the loaded ring. For the

particular conditions of the *in situ* test, it can be considered that no significant stress redistributions occurred from the loaded ring to the rest of the structure caused by the ring interaction.

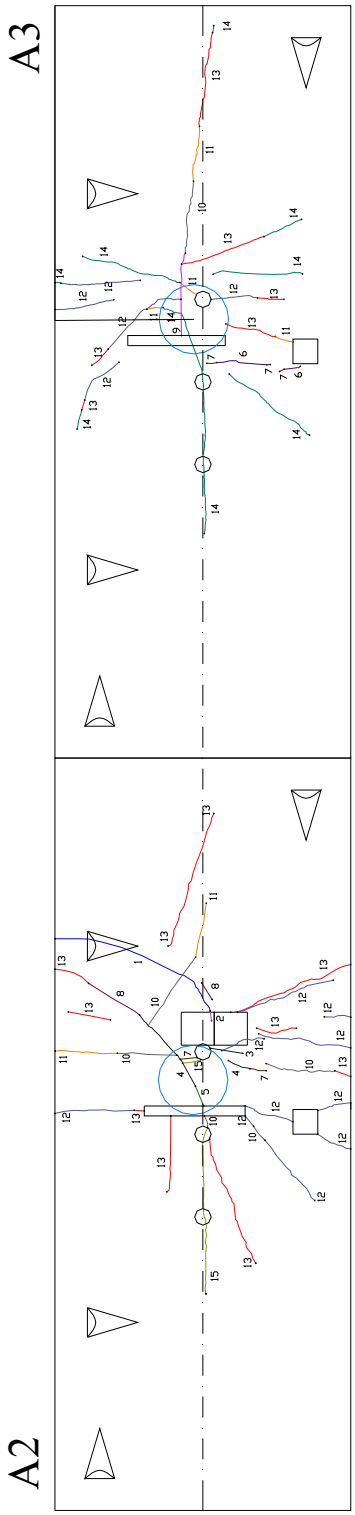

Figure 2.15. Crack patterns obtained at the end of stage 5. Numbers define the load per jack when the crack or certain part of it appraised (view Table 2.10).

2.5.4 Crack patterns.

Additionally to the all measurements obtained by the instrumentation, the crack patterns of the segments were meticulously registered as the load increased. Figure 2.15, shows the crack patterns of segments A2 and A3 of the loaded ring obtained along the test. The numbers close to cracks are indicators of the stage and load value when the crack (or a significant part of it) was recorded (view Table 2.10).

Table 2.10. Indicators for cracking advance employed in Fig. 2.15.

Stage	*Num*	*Load / Jack (kN)*
5	9	700
	10	900
	11	1,100
	12	1,300
	13	1,500
6	14	1,500
7	15	1,500

First significant cracks appeared in stage 5 for a load around 900 kN per jack (60% of the total loading). No cracks produced by loading were detected out of segments A2 and A3 where the jacks were located. Figure 2.15 neatly shows that cracks in the intrados of the ring were concentrated under jacks' positions. Most cracks are orientated in the longitudinal direction according to the ring arch mechanism, but radial cracks caused by the spreading of the concentrated loads across the section of the ring were also appraised. An advanced crack status was achieved during the test registering a maximum crack opening of 1.31mm in segment A2 during stage 7.

The obtained crack patterns provide significant information of great interest for the study and modeling of segmental linings constructed with steel fibers as a unique reinforcement for concrete.

2.6. CONCLUSIONS

An innovative technique to perform real scale tests on segmental tunnel linings has been successfully developed and carried out. The *in situ* test provides evidences of the lining behavior on its real work conditions and, therefore, considering all parameters involved in its structural response. This is, as far as known by the authors, the unique approach available up to the present to asses a realistic consideration of the ground-structure interaction. Additionally, the test performance over a lining constructed using steel fibers as unique concrete reinforcement supplies relevant information about the structural contribution of such material to this structural typology.

The study, performance and analysis of the *in situ* test carried out at L9 experimental section provided several conclusions about the structural response of SFRC segmental tunnel linings in hard ground conditions:

- The loaded ring presents a localized arch behavior under concentrated loads. It is assumed that the ground stiffness and the ring geometry mostly determine the length of the arch and the ground reaction zones.
- The tangential ground-structure interaction mechanism presents a decisive influence on the ring stress distribution and, in consequence, on the structural response of the lining. In this case, a tangential stiffness equal to 1/3 of the radial stiffness provides the best fitting approach.
- The deformation of the loaded ring should be mainly caused by concentrated rotations in the ring joints and in the cracked sections under the jacks.
- For the particular conditions of the section 4a of L9 it can be considered that no significant stress transmissions from the loaded ring to the adjacent ones exist.
- The crack patterns are fully consistent with an arch behavior of the loaded ring. Radial cracks were result of the spreading of the load across the section of the ring.

The *in situ* test carried out at the experimental section of L9 provides significant evidences about the structural behavior of this segmental tunnel lining in its particular hard ground conditions. The collected data allows the verification and calibration of the numerical models employed to understand and design segmental tunnel linings. Part 2 of the present

paper (Arnau and Molins, 2011) describes the numerical simulation of the in situ test. The main phenomena involved in the experimental section structural response and its modeling techniques are described. Analytical results are then compared with the experimental evidences in terms of general response, displacements, joints behavior and crack patterns.

ACKNOWLEDGEMENTS

The authors thank *Gestió d'Infraestructures, S.A.* (GISA), the public company responsible of the design and construction of the L9 of the Barcelona's subway, for the effort made to provide all the necessary staff and equipment to perform the test and also the construction company FCC Construcción S.A., for its promotion and collaboration in the investigation of the behavior of packers.

Chapter 3

EXPERIMENTAL AND ANALYTICAL STUDY OF THE STRUCTURAL RESPONSE OF SEGMENTAL TUNNEL LININGS BASED ON AN *IN SITU* LOADING TEST

PART 2: NUMERICAL SIMULATION

ABSTRACT

The numerical simulation of the *in situ* test described in the part 1 of the paper is performed by means of two different approaches: a 2D plane stress model and a 3D shell elements model. A consistent modeling of the tunnel behavior is achieved through the proper simulation of the main phenomena involved on the structural response of the lining: 1) the steel fiber reinforced concrete (SFRC) post-cracking behavior, 2) the detailed behavior of the joints between segments and 3) the ground-structure interaction. The origin and the effects of all these phenomena and the modeling techniques employed to simulate them are carefully described and discussed. Finally, the results obtained are compared with the experimental evidences, showing the excellent accuracy achieved in terms of displacements, joints closures and crack patterns.

Keywords: Segmental tunnel linings, structural analysis, numerical simulation, SFRC, ground-structure interaction, joints behavior.

3.1. INTRODUCTION

During last years, the evolution of the Tunnel Boring Machines (TBM) and the construction techniques associated to these drilling devices gave the opportunity to plan and construct tunnels under increasingly difficult scenarios. Nowadays, it is possible to construct tunnels under severe conditions and at any range of overburdens, with the possibility of achieving unsuspected drilling rates under high ground and water pressures. These unfavorable conditions imply higher structural requirements in order to resist the increments of ground pressures and the forces imposed by the advances of the TBM, conferring to the segmental tunnel lining a decisive role in the tunnel construction.

The optimization of segmental tunnel linings requires the utmost knowledge about the lining behavior and the structural forces that have to be resisted. Such like on the design practice of other structures, the prediction of linings behavior is commonly carried out by numerical models that simulate the conditions and phenomena imposed by the designers. Therefore, further to contrast the suitability of the adopted models it is also of paramount importance an appropriate selection and comprehension of the main phenomena involved in the structural response of the lining to achieve a better approach of the simulated situation. The behavior of segmental tunnel linings is affected by multiple phenomena that even individually present a complex behavior that significantly complicate the prediction of their structural response.

The *in situ* test performed on the experimental section of L9 tunnel of the subway of Barcelona (described in part 1 of this paper (Molins and Arnau, 2011)) represents, as far as known by the authors, a unique chance to determine the most important phenomena involved in segmental tunnel linings real behavior besides to allow the calibration and checking of the numerical models on the simulation of their structural response.

This paper deals with the numerical simulation of the *in situ* test and the comparison of the obtained results with the experimental evidences. In the first part, the main phenomena involved in the structural behavior of segmental tunnel linings are described and their modeling techniques are presented and discussed. These techniques are applied to the particular conditions of the experimental section of L9, defining both 2-D and 3D models to reproduce the test. The comparison of the experimental data with the numerical results in terms of general response, displacements, joints movements and crack patterns, allows the determination of the accuracy achieved with the proposed numerical models.

3.2. TUNNEL BEHAVIOR AND ASSOCIATED PHENOMENA

3.2.1 Phenomena common to all segmental tunnel linings

The models actually employed in the prediction of tunnel behavior are mostly created for design purposes. This fact allows the assumption of certain hypotheses that simplify the solution by providing safety results. On the other hand, the reproduction of the real response requires an adequate consideration of all parameters involved in that behavior. Therefore, it is necessary to clearly define them and develop numerical strategies for their accurate simulation.

Former approaches to predict the structural forces in tunnel linings were based on analytical solutions obtained from simplified models which considered the structure as a rigid pipe embedded on ground continuum model (Morgan, 1961, Muir Wood, 1975, Duddeck and Erdmann, 1985). The consideration of the ground-structure interaction was usually performed by means of the so-called bedded ring models, where the ground reaction is approached by means of discrete springs according to the Winkler's theory (e.g. Shulze and Duddeck, 1964). The analytical solution of these single models can neither take into account the complexities of the different phenomena involved in the structural behavior of segmental tunnel linings nor analyze complex situations suchlike a tunnel section crossing different ground layers. The use of the finite element method (FEM) allows the resolution of the bedded spring model for multiple load cases or support situations even including more advanced material properties or approximations to consider the effect of the joints between segments.

The adequate consideration of the joints behavior and its influence on the lining structural response have probably been the most discussed items in literatures regarding structural analysis of segmental tunnel linings. The first attempts to consider the influence of longitudinal joints were based on the increase of the lining flexibility. Muir Wood (1975) proposed a formulation to reduce the moment of inertia of a rigid pipe depending on the number of segments that composes the ring. Recent models consider the joints behavior by means of rotational springs located at joints places (JSCE, 1996, Blom, 2002 and Ding et al, 2004), presenting the advantage of being easily implemented in bedded beam models. As it was defined by Blom (2002), the longitudinal joints present a complex non linear behavior due to their incapacity to transfer tensile stresses. For a certain axial stress level and an increasing bending moment, a loose of contact occurs at one side of the joint (joint gapping) generating a non linear behavior that is dependent on the axial stress. For the same joint, different axial stress levels provide different rotational behaviors, thus increasing the complexity of its appropriate consideration on the analysis models. In consequence, the main drawbacks of the rotational springs are the need of previous

knowledge on the behavior of the implemented joint and the difficulty to take into account the influence of a certain axial stress level in the joint response.

More sophisticated approaches were used in shell elements models in order to achieve a better simulation of the real joint response. Vervuurt et al. (2002) modeled the joints between the shell elements segments by means of concrete beam elements which presented no tensile resistance whilst Van Empel and Kaalberg (2002) employed a combination of three springs to model their particular joint configuration. On approaches where the height of the structure is modeled by finite elements (plane stress models or 3D brick models) joints behavior is typically considered by means of interface elements placed at joints locations that do not allow the transmission of tensile stresses (Plizzari and Tiberti, 2006, Blom et al. 1999). This method represents the physical phenomenon occurring at the joint and, therefore, it is the most natural approximation to the real joint behavior.

Within the available bibliography it is assumed that a realistic simulation of segmental tunnel linings requires the consideration of the structural interaction between adjacent rings (coupled analysis) that is produced through the circumferential joints. The analyses performed by Klappers et al. (2006) show that the coupling of rings in segmental tunnel linings with staggered joints produce a stiffer structure respect of the aligned joints configuration. In consequence, higher bending moments are obtained with lower structure deformations. The coupling capacity of adjacent rings depends on multiple factors involving the joint configuration, the axial stress remaining in the lining due to the TBM ram forces and also the ground stiffness due to its influence on the rings displacements and deformations. The lateral ring interaction is commonly modeled by means of coupling springs or interface elements located at contact points between adjacent rings. According to Blom (2002) those springs describe the combined behavior of the dowel and socket system and the lateral friction through packing materials.

Apart from the joints behavior, there is another parameter that significantly influences the structural response of tunnel linings: the ground-structure interaction. A ring of a segmental lining is a multiple hinged structure and, consequently, its equilibrium in front of loads depends on the surrounding ground response. The ground-structure interaction defines the boundary conditions of the structure and therefore its variation modifies the structural response of the lining. There are two main techniques for its modeling: 1) discrete springs assuming the Winkler hypothesis and 2) directly modeling the ground with finite elements. The full modeling of the ground with finite elements is mainly applied for analyses where surface settlements or accurate tunnel loads predictions are intended (e.g. Broere and Brinkgreve, 2002, Kasper and Meschke, 2004) while spring models are commonly used on the analyses focused on the structural behavior of the segmental

concrete lining (e.g. Plizzari and Tiberti, 2006, Blom et al. 1999). Although the full modeling of surrounding ground should provide more accurate results (despite the fact that the interface conditions have also to be adequately selected), it requires heavy computational efforts when a detailed analysis with ground and structure non linear behaviors is intended. Additionally, the study of the lining structural response requires the evaluation of multiple structure, ground and load scenarios that suppose a tedious and difficult work to be created with the full ground modeling.

3.2.2 Particularities of the L9 experimental section

Besides the common phenomena associated to all segmental tunnel linings, the simulation of the *in situ* test requires the consideration of three particular phenomena occurring at the tested structure:(1) the use of steel fibers as unique reinforcement for concrete (only few small reinforcement bars were used to sustain the instrumentation of the test), (2) the use of bituminous packers in longitudinal joints (between segments of the same ring) which present a complex behavior and (3) the flat circumferential joints between rings.

Steel Fiber Reinforced Concrete (SFRC)

The use of steel fibers in segmental tunnel linings has considerably increased during last years. Their main contribution is traditionally related to the avoidance of concrete spalling. Spalling is used to occur in segment joints due to deficient segment allocation, inadequate segment construction tolerances or joints geometries when the TBM jack forces are applied. Steel fibers act as small links between the detached concrete and the segment avoiding the reparation of the superficial damage. But steel fibers are not only present at the edges or corners of the segments. Their presence inside the whole element may contribute to the structural resistance of the lining. Different works have been developed in order to quantify the contribution of steel fibers to the lining resistance (de Waal, 2000, Plizzari and Tiberti, 2006 and Kasper et al., 2007). The *in situ* test aimed to perform a step forward and directly prove the suitability of using it as unique reinforcement. Moreover, the multiple data and the crack patterns obtained are used in the present paper to calibrate and contrast the precision offered by tunnel numerical models when the consideration of the structural contribution of such complicate material is intended. An accurate numerical simulation will allow the study, comprehension and the design improvement of SFRC segmental tunnel linings.

Bituminous packer

The experimental section of L9 presents a singular joints configuration. Whilst the circumferential joints (between adjacent rings) present the usual plastic packers, the longitudinal joints (between segments of the same ring) present a 2mm thick bituminous sheet instead of the more common concrete-to-concrete contact. During the characterization test of the packers carried out at UPC by Cavalaro (2009), a plastic behavior with significant remaining deformations was observed for the bituminous sheet. The *in situ* test comprises various load-unload cycles and consequently, the accumulation of plastic deformations causes different initial joint rotations at the start of each load phase. Therefore, it is necessary to accurately consider the packer behavior to obtain a satisfactory movements and displacements prediction.

An experimental campaign was carried out in order to determine the behavior of the L9 longitudinal joints packer. The test consists of 5 load-unload cycles with three different compression stresses (20, 40 and 60 N/mm^2), repeating three times the maximum stress cycle. Figure 3.1 shows the stress-strain relation obtained in the performed test.

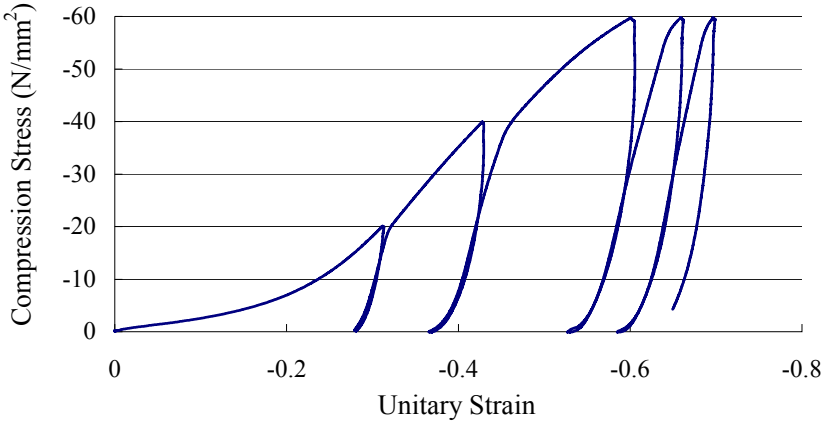

Figure 3.1. Stress-Strain relation for L9 bituminous packer under cyclic loading.

As can be clearly observed in Figure 3.1, the bituminous packer presents a non linear stress-strain diagram showing a soft behavior for low stresses and a hardening process close to 10 N/mm^2. A significant deformation remains in the packer after the unloading, presenting similar slopes for the unloading branches at different stress levels. The three consecutives cycles at 60 N/mm^2 denote a small additional remaining deformation despite the previous achievement of the stress level.

Flat circumferential joints

The circumferential joints do not present any dowel and socket system. In consequence, the transference of tangential forces is limited by the lateral friction between the concrete

surface and the packers. Additionally, the experimental section was located inside a hard rock formation which severally limits the deformation of the loaded ring and consequently diminishing the coupling effect of the adjacent rings. Moreover, the results obtained in the *in situ* test showed that no significant stress redistributions occur from the loaded ring to the rest of the structure (Molins and Arnau, 2011). For this reason, it was decided to perform unique ring models to simulate the *in situ* test.

3.3. MODELIZATION STRATEGIES

As previously mentioned, this work intends to evaluate the precision that can be achieved with the numerical models on the simulation of the structural behavior of segmental tunnel linings from a practical engineering point of view. In this way, the most reasonable modeling philosophy goes through the simulation "one by one" of the main phenomena involved on the lining structural response and their subsequent integration in tunnel models. This section shows the numerical strategies followed to reproduce the material and physical behaviors that particularly affect the structural response of the test.

3.3.1 Steel Fiber Reinforced Concrete (SFRC)

The experimental campaign carried out to characterize the SFRC of the segments is described in the part 1 of this paper (Molins and Arnau, 2011). The results of the 4 point beam tests (IBN, 1992) were used to determine the tensile behavior of the SFRC. This test provides the flexural post-cracking response of the SFRC by means of a load-deflection diagram, but the adequate material definition requires the tensile *versus* crack-opening response. The conversion factor that provides the crack-opening from the deflection was obtained through the geometrical analysis of the test configuration.

Steel fibers present a random distribution inside the concrete suck like aggregates and, therefore, can present multiple orientations. For this reason, the easiest and most common way to consider steel fibers contribution goes through the improvement of the post-cracking behavior of concrete.

In order to obtain the SFRC tensile behavior from the flexural response measured at 4 point beam tests, a simplified inverse analysis (Roelfstra and Wittmann, 1986) was applied. The SFRC sectional behavior described in the guidelines provided by Rilem (TC-162-TDF, 2003) was employed to determine the best-fitting post-cracking law according to a predefined function shape. Among the multiple possibilities of shapes that can be used to characterize SFRC post-cracking behavior (Antunes and Gettu, 2006), a sloped-constant diagram was selected (Fig. 3.2). The value of the load at first crack obtained in the NBN

test was used to calculate the maximum flexural tensile stress of concrete (f_r = 6.67 N/mm^2) and was converted to the maximum elastic tensile stress (f_{ct} = 5.67 N/mm^2) by means of the formulation proposed in the Model Code 1990 (CEB-FIP, 1993). Figure 3.2 shows the results obtained on the inverse analysis to adjust the sloped-constant post-cracking diagram for the tested SFRC.

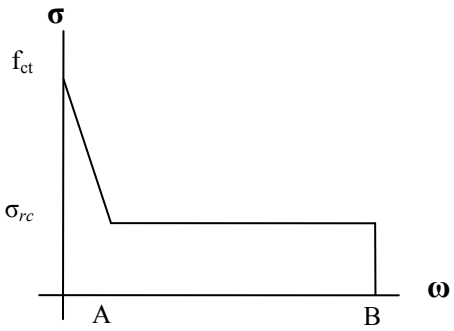

f_{ct}	5.67 N/mm^2
σ_{rc}	2.08 N/mm^2
A	0.025 mm
B	12.5 mm

Figure 3.2. Adopted sloped-constant diagram employed in the inverse analysis and its best fitting parameters to reproduce the experimental section SFRC behavior.

With the aim of test and calibrate the numerical model of SFRC behavior, two different simulations of the 4-point beam test were carried out by means of plane stress and shell elements models. Both analyses were performed by means of the Multi-Directional Fixed Crack Model. This material model is based on the decomposition of the total strain into an elastic strain ε_{el} and a crack strain ε_{ck}, being necessary to define the stress-crack strain relation (σ-ε_{ck}) for concrete tensile behavior. The conversion factor between crack-opening (ω) and crack strain (ε_{ck}) is the so-called crack bandwidth (h_{ck}) and corresponds to a numerical criterion based on the formulation of the finite elements (Bazant and Oh, 1983). In these analyses, it was assumed a crack bandwidth equal to the square root of the elements area ($h_{ck} = \sqrt{A_{el}}$). Additionally, for shell elements models, a geometrical equality between the side length of the element and the represented height was assumed.

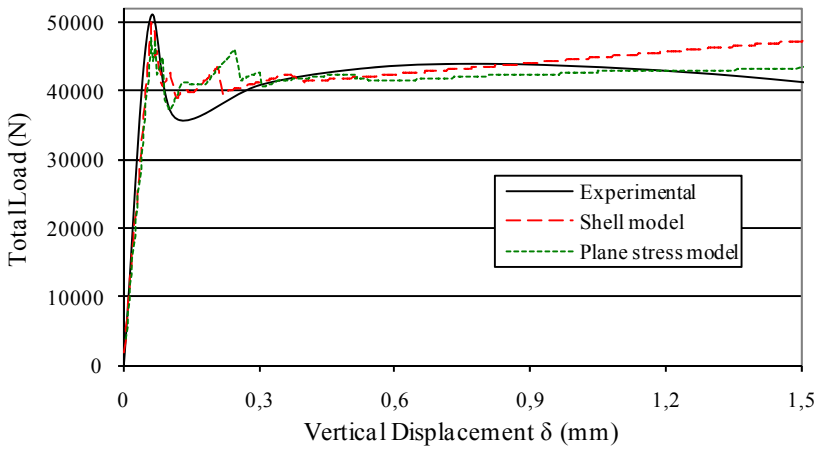

Figure 3.3. Results obtained in the 4-point beam test simulations.

As can be observed in figure 3.3, the results obtained from both type of models present a very good agreement to the experimental ones, thus validating the assumptions and modeling techniques used to define the SFRC post-cracking behavior.

3.3.2 Packer behavior

The modeling of the complex bituminous packer response (described at section 2.2) was performed by means of a Von Mises plasticity model. The behavior presented in unloading and re-loading process is assumed to determine the elasticity modulus of the packer (670 N/mm^2). A hardening diagram is employed to modify the selected elasticity modulus in order to reproduce the initial load response of the bituminous packer. The simulation of the packer test was performed in order to contrast the suitability of the adopted model. The results are shown in figure 3.4.

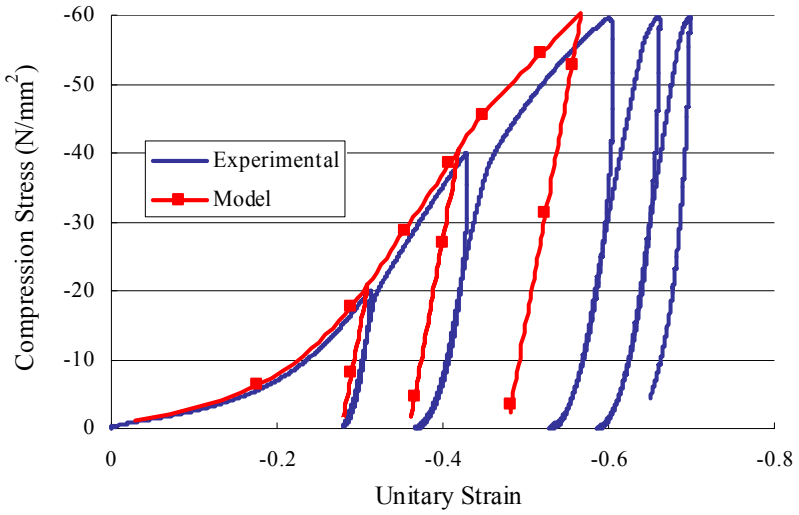

Figure 3.4. Results of the simulation of the bituminous packer test.

The implemented model uses the same branch for the unloading and reloading processes presenting a small inaccuracy because it does not reproduce the additional plastic deformation occurred at every reloading, providing a slight underestimation of the total remaining deformation (Fig. 3.4) that should not affect the overall response of the ring.

3.3.3 Longitudinal Joints

The simulation of the loose of contact in longitudinal joints was performed by means of unilateral interface elements located at one side of the plastic packer elements (Fig. 3.5). Nonlinear stiffness was assigned to them, defining a rigid behavior in compression whilst gapping is produced in tension. For shell elements model, a specific interface element with integration points along its height was used -CL24I, Diana 9 Manual (2005)-. The main

limitation of this shell configuration in front of plane stress models is the incapacity to consider the local deformation of the concrete behind the packer (Figure 3.6a). Despite this, no significant stress differences along the joint occur when comparing with results of the plane stress model, as can be seen in the example of Figure 3.6b. The loose of contact on the upper part of the joint (around 200mm in height) can also be observed in figure 3.6b, in which stress transmission zone is absent. This fact is particularly crucial because it allows the modeling of joints in an accurate way when using 3D shell elements models.

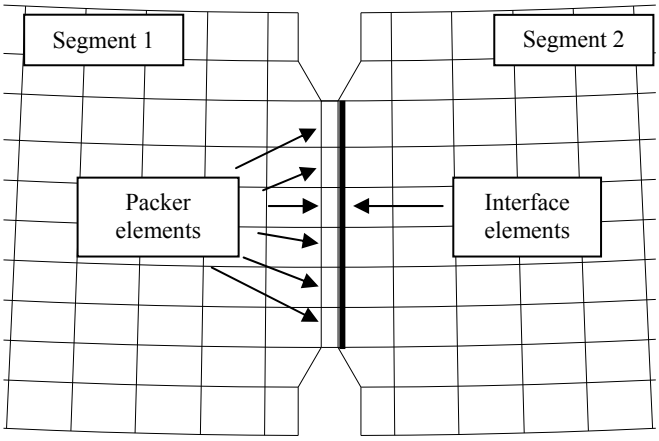

Figure 3.5. Layout of joints configuration in plane stress finite elements model.

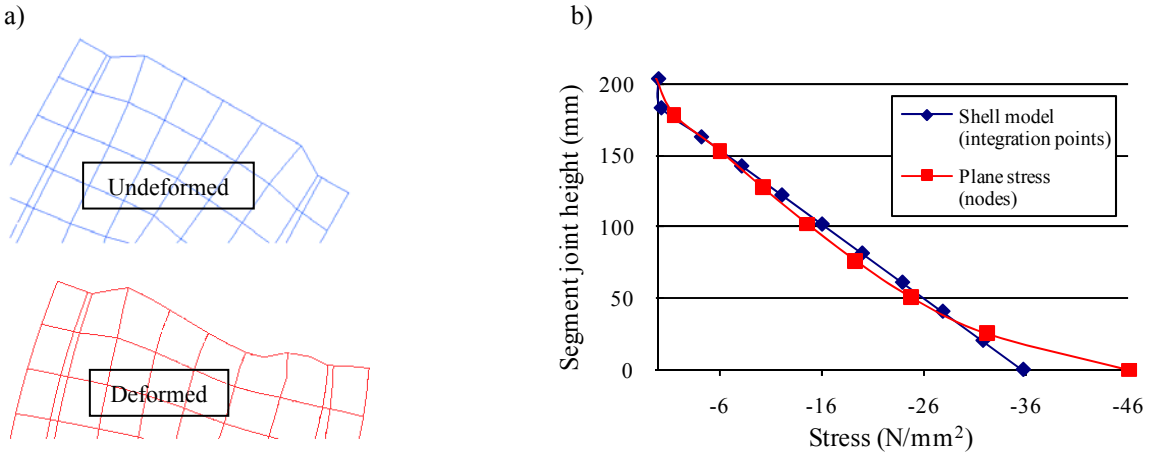

Figure 3.6. Image of local concrete deformation at joints (a) and an example of its effect on the joint stress distribution (b).

The combination of the packer behavior and the gapping phenomenon provides the nonlinear response of the joint that can be observed in figure 3.7. It shows the evolution of the rotational stiffness of L9 longitudinal joint for two different axial forces of 525 kN/m and 1050 kN/m, corresponding to a concrete compressive stresses of 1.5 N/mm^2 and 3 N/mm^2 respectively.

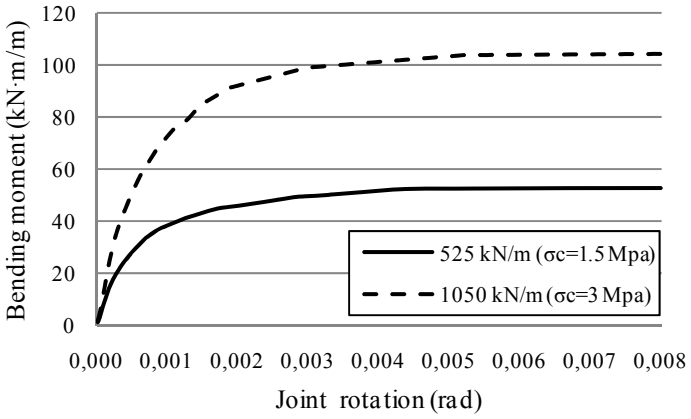

Figure 3.7. Evolution of the rotational stiffness of L9 longitudinal joint for two different axial forces.

3.3.4 Ground-structure interaction

As previously discussed, the adequate consideration of the ground-structure interaction plays a decisive role on the structural simulation of segmental tunnel linings response. There exist two different elements that play a structural role beyond the segmental concrete lining: the hardened backfill grout and the surrounding ground (Fig. 3.8a). A bedded spring model was selected for the analysis of the *in situ* test, placing spring elements in radial (K_r) and tangential (K_t) directions (Fig. 3.8). The grout was simulated by means of interface elements placed between the structure and the ground spring elements. Figure 3.8b shows the conceptual scheme for a plane stress configuration whilst figure 3.8c is related to the shell elements configuration.

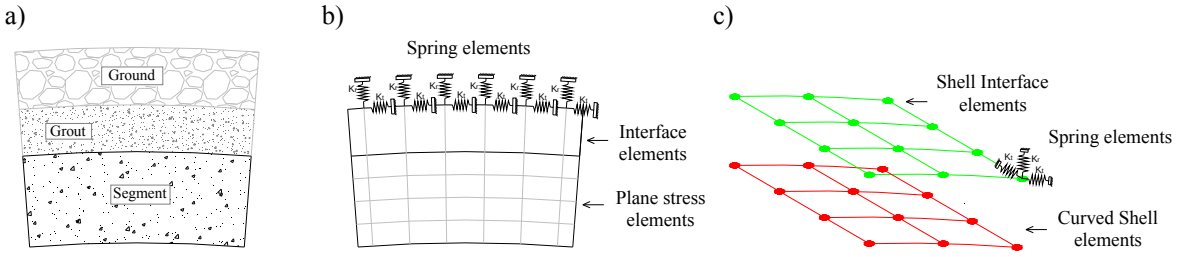

Figure 3.8. Tunnel cross section scheme (a). Plane stress modeling (b) and shell elements modeling (c).

To consider the loose of contact between the lining and the grout a Mohr-Coulomb material model with tensile gap is applied to the interface elements. In consequence, when an interface element is subjected to a radial tension the gap arises, avoiding the transference of forces to the radial or tangential ground springs related to it. The compression stiffness of the interface elements is related to the gap size (175mm in L9) and the grout elasticity modulus. For the latter, a value of 1000 MPa was estimated from

the grout mix proportion, which is in accordance with the experimental results obtained at the district heating tunnel of Copenhagen described by Kasper et al. (2007).

The radial spring stiffness was assumed according to relation (3.1), corresponding to the analytical solution of a circular tunnel in elastic ground. Tangential stiffness (eq. 3.2), was assumed as 1/3 of the radial (Molins and Arnau, 2011). According to the geotechnical information, the parameters assumed to characterize the granodiorite rock formation surrounding the tunnel were an elastic deformation modulus of E_s=11225 N/mm^2 and a Poisson ratio of ν=0.24.

$$K_r = \frac{E_s}{R \cdot (1+\nu)} \qquad (3.1)$$

$$K_t = \frac{K_r}{3} \qquad (3.2)$$

3.4. REAL SCALE TEST: NUMERICAL MODELS AND ANALYSES

The previous modeling techniques of the different phenomena involved on the structural behavior of the L9 experimental section were applied on two different approaches: a 3D shell elements model and a 2D plane stress model. Both models only considered a unique ring regarding the quasi-individual response observed during the test (Molins and Arnau, 2011). Plane stress model should provide a more accurate sectional response due to the modeling of the segments height whereas the shell elements model can consider the effects of loads out of the middle plane. The latter is necessary in this case because the final position of the jacks was out of the middle plane of the ring. Table 3.1 shows the description and the amount of finite elements employed in each member of both models: 2D plane stress and 3D shell.

The reinforcement elements were used to simulate the small amount of reinforcement bars placed in the loaded ring to sustain the internal instruments. The steel plates located under the jacks were considered through the modification of the material properties of the affected elements.

Before the test simulation it was necessary to reproduce the previous state of the ring for three main reasons: (1) previous stress states play a decisive role on cracking formation and development, (2) the joints behavior depend on the real axial stress level and (3) the non linear behavior of bituminous packer, which presents high plastic deformation and a soft stiffness for low stress levels, determinates the ring displacements.

Table 3.1. Main characteristics of the *in situ* test performed models.

	Shell model		*Plane Stress model*	
	Description	Quantity	Description	Quantity
Nodes		3882		18464
Segments Elements	Quadrilateral 8 nodes curved shell elements (CQ40S)	525	Quadrilateral elements, 8 nodes (CQ16M)	5104
Plastic Packer Elements	Quadrilateral 8 nodes curved shell elements (CQ40S)	40	Quadrilateral elements, 8 nodes (CQ16M)	32
Segment joints elements	Line interface shell elements, 3+3 nodes (CL24I)	40	Line interface elements, 3+3 nodes (CL12I)	32
Grout interface elements	Plane quadrilateral interface shell elements, 8+8 nodes (CQ48I)	525	Line interface elements, 3+3 nodes (CL12I)	735
Reinforcement elements	Reinforcement bar elements (Reinforcement)	844	Reinforcement bar elements (Reinforcement)	1458
Spring elements	Translation spring element, 1 node (SP1TR)	3746	Translation spring element, 1 node (SP1TR)	2956

Note: Diana 9 codification for each kind of element is specified in brackets.

The experimental section was located inside a hard granodiorite rock formation that was resistant enough to generate a self-stable excavation and, hence the ground almost did not generate external pressures over the lining, as proved the measurements of the instruments. Consequently, it was supposed that the initial load over the lining was caused by the hydraulic pressure of the ground water. This pressure was obtained from the load cells placed at the extrados of the experimental ring and was applied to the numerical models to perform the initial situation analysis. In order to correctly simulate the tunnel construction process, the ground-structure interaction was remained inactive in this initial phase. Water pressure acts prior to the backfill grout hardening which fix the lining to the ground and marks the start of the transmission of forces between the lining and the ground. After the analysis of the initial state, the same load procedure followed during the "in situ" test was reproduced. The load stages described in table 3.2 were sequentially applied, considering that every stage is defined by a loading and unloading cycle (Molins and Arnau, 2011). The jack forces were applied by means of distributed loads according to the real placement and surface of the jacks.

Table 3.2. Load stages performed in the *in situ* test (Molins and Arnau, 2010).

Phase	*Stage*	*Active Jacks*	*Load / Jack (kN)*	*Tunnel crown vertical Deflection (mm)*
0	1	Jack 1 + Jack 2 + Jack 3	100	-
1	2	Jack 1 + Jack 2	500	0.531
	3	Jack 1	500	0.022
	4	Jack 2	500	0.543
2	5	Jack 1 + Jack 2	1500	2.627
	6	Jack 1	1500	0.198
	7	Jack 2	1500	3.076

3.5. ANALYSIS OF THE RESULTS

The results obtained in the numerical simulation of the test, which are presented along this section, are compared with the experimental measurements to analyze their validity and precision. The comparison is carried out in terms of general behavior, displacements, joints movements and crack patterns.

3.5.1. General behavior

Figure 3.9 shows the circumferential stresses predicted by the plane stress model on the tunnel crown zone and the finite elements affected by cracking at stage 5 (Table 3.2), corresponding to a load of 1500 kN per jack. Joint non linear behavior can be clearly appraised through the absence of tensile stresses at the extrados side of the joint at 102º and the concentration of compressions at the intrados side. Equally as observed during the test, cracking is only present at the intrados of the locations of the jacks. At these points, compression stresses are observed at the extrados, including a concentration at the steel plate.

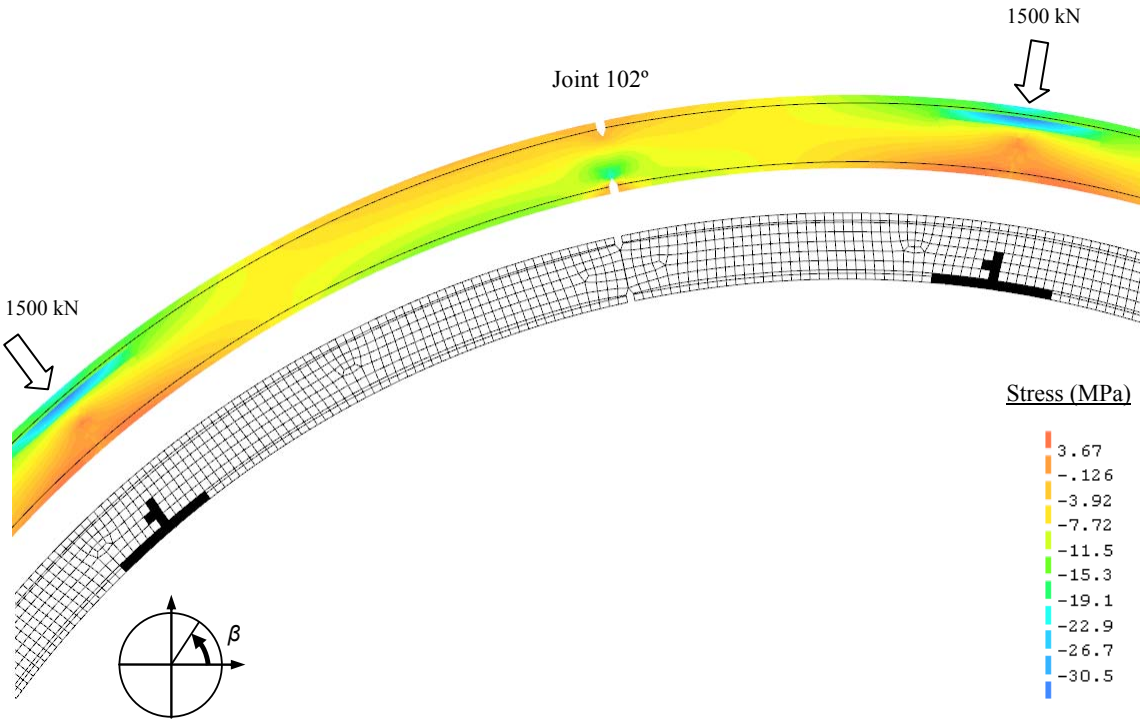

Figure 3.9. Circumferential stress during stage 5 (MPa) and cracked elements (in black).

The numerical simulations reproduce the same mechanism governing the displacements of the loaded ring observed experimentally. As can be seen in Figure 3.10 where the plane stress model deformed shape for stage 5 is shown, ring movements are mainly caused by concentrated rotations in longitudinal joints and in the cracked sections under the jacks.

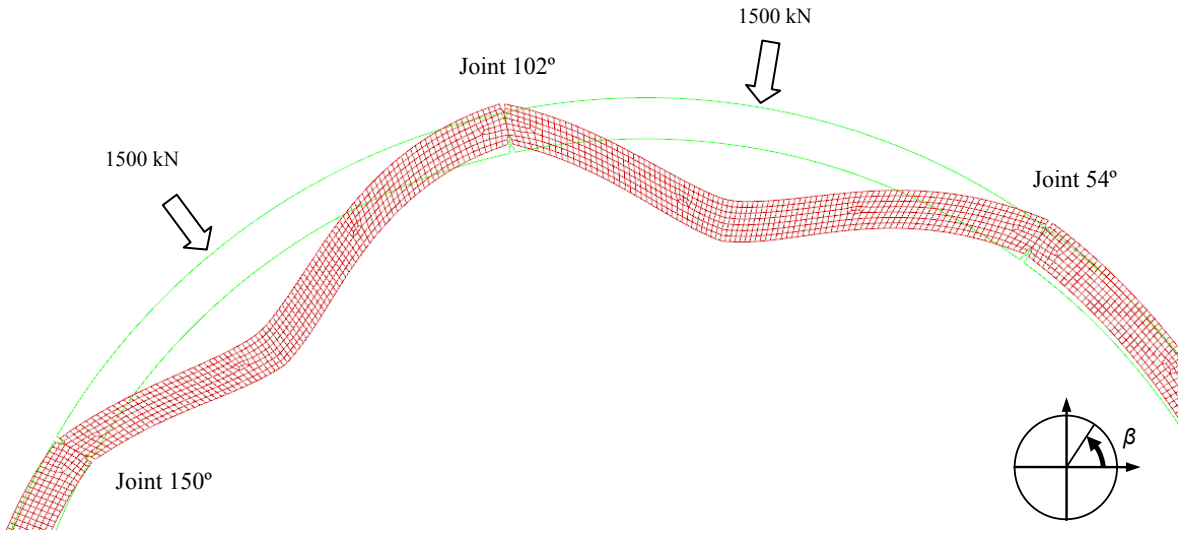

Figure 3.10. Tunnel crown deformed shape during stage 5 (amplification factor = 300).

One of the most important conclusions from the *in situ* test (Molins and Arnau, 2011) was that, for hard ground conditions, the ring response under concentrated loads is related to an arch behavior that directly discharge the load to the ground. This fact produces a resisting mechanism which is concentrated nearby the zone where the loads are applied. Figures 3.11(a) and 3.11(b) show the numerically obtained radial ground response for stages 5 and 7 and the associated deformed shape of the ring respectively.

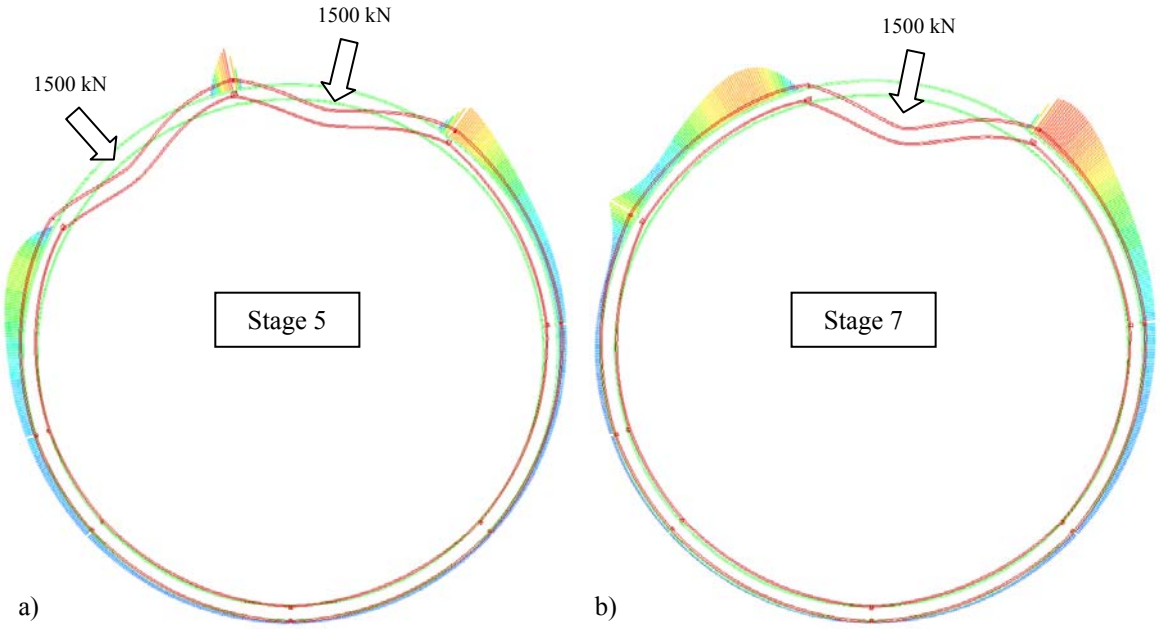

Figure 3.11. Radial ground response in stages 5 (a) and 7 (b) and associated deformed shapes (in red).

In both cases, the radial response clearly denotes the zone where the arch is pressuring the ground and how the rest of the ring does not present any significant interaction. Consequently, the structural response of the ring under concentrated loads in hard ground conditions is limited to the behavior of the zone close to the loads appliance points.

3.5.2. Displacements

The radial displacement obtained by both models for stages 2, 4, 5 and 7 and the experimental measurements are presented in Figures 3.12, 3.13, 3.14 and 3.15. For the shell model, the displacements of the two segment edges are presented. Jack 1 was located far from the tunnel crown and, in consequence, its isolated action (stages 3 and 6) did not generate significant movements on the instruments placement (Table 3.2). For this reason, the numerical results obtained for these stages are not presented.

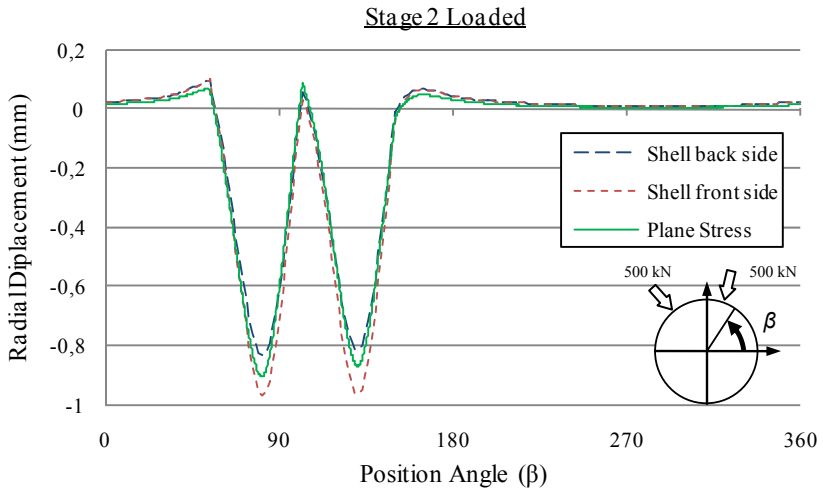

Figure 3.12. Comparison of results of radial displacement at stage 2.

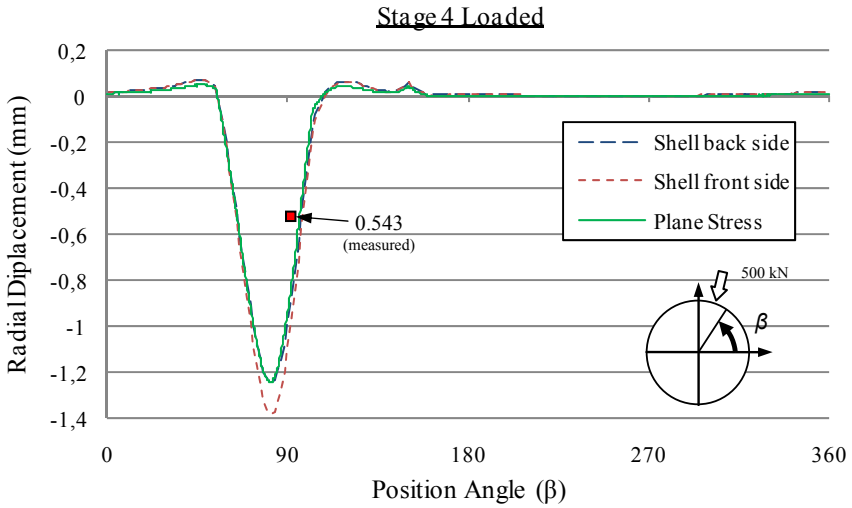

Figure 3.13. Comparison of results of radial displacement at stage 4.

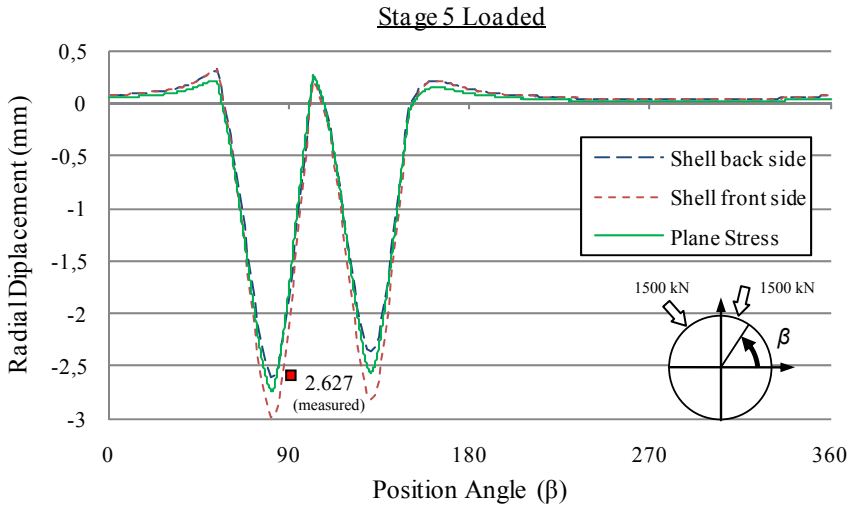

Figure 3.14. Comparison of results of radial displacement at stage 5.

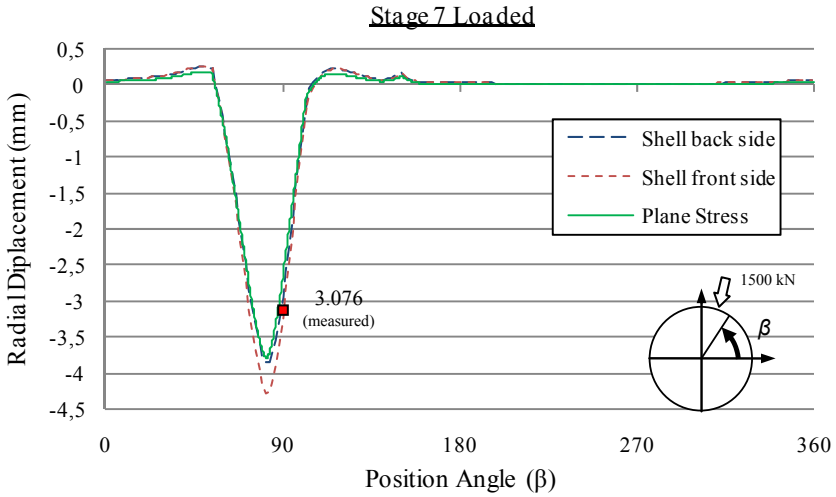

Figure 3.15. Comparison of results of radial displacement at stage 7.

The vertical displacement of the tunnel crown obtained in the numerical models (radial displacement at β=90º) shows a very good agreement with the experimental results (Table 3.2, and square point in figures). Plane stress and shell models present very similar results for all loading stages. The vertical displacement obtained for stages 2 and 7 presents an excellent accuracy whilst the analysis of stage 5 shows a slight underestimation in front of the experimental data. A small overestimation of the measured movement is obtained for stage 4. In fact, the measured result is not in concordance with the tendency of each load configuration because the isolated action of jack 2 (stages 4 and 7) should provide higher crown displacements that the simultaneous action of jacks 1 and 2 (stages 2 and 5). It is also important to notice that displacements are mainly concentrated under the jacks and, in consequence, present a high variation in a short distance. In consequence, some small variations in the test instruments positions can provide differences like the obtained between the experimental and the numerical results.

The effects of the final eccentricity of the jacks caused by its deficient allocation can be observed in shell elements model results. The displacements obtained in the ring front side are always higher that the ones obtained in the back side, thus showing the non-uniform deflection of the ring.

Figure 3.16 shows the comparison of the radial displacements obtained for the configurations where jacks 1 and 2 acts simultaneously (stages 2 and 5). The load increase does not entail a widest descent zone, maintaining it between the joints. In consequence, the increase of the radial displacement is originated by higher rotations in joints and in the cracked sections under the jacks. In fact, both analytical and experimental results coincide that no cracking is produced during stage 2.

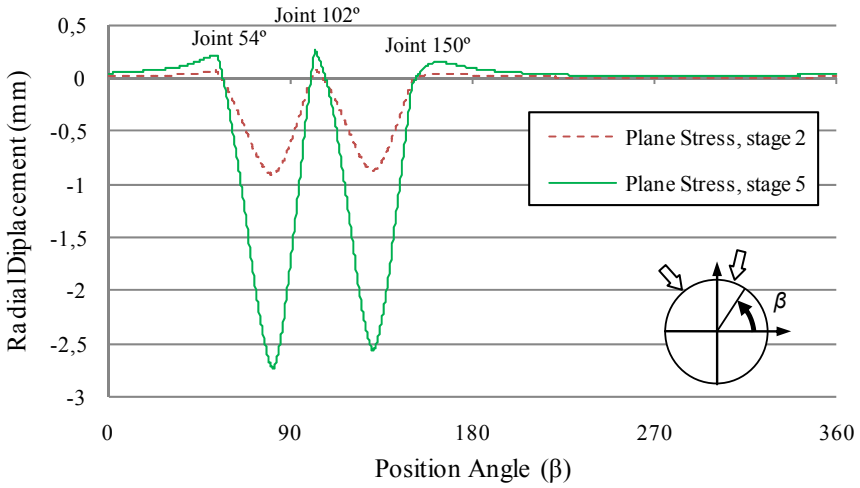

Figure 3.16. Radial displacement obtained in plane stress model at stages 2 and 5.

3.5.3. Joints movements

The comparison of the evolution of joints closures obtained experimentally and analytically during the stages 5 and 6 of the test are presented in Figures 3.17 and 3.18. Experimental results in joints were measured by displacement transducers (T1, tunnel side, and T2, excavation side) placed at the intrados of the loaded ring between segments A1-A2 (54º), A2-A3 (102º) and A3-B (150º).

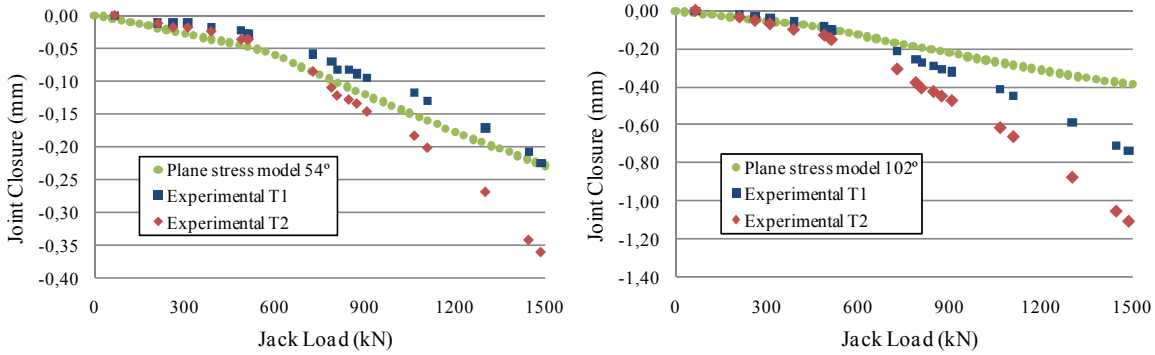

Figure 3.17. Evolution of joints closure (intrados side) at 54º and 102º during stage 5.

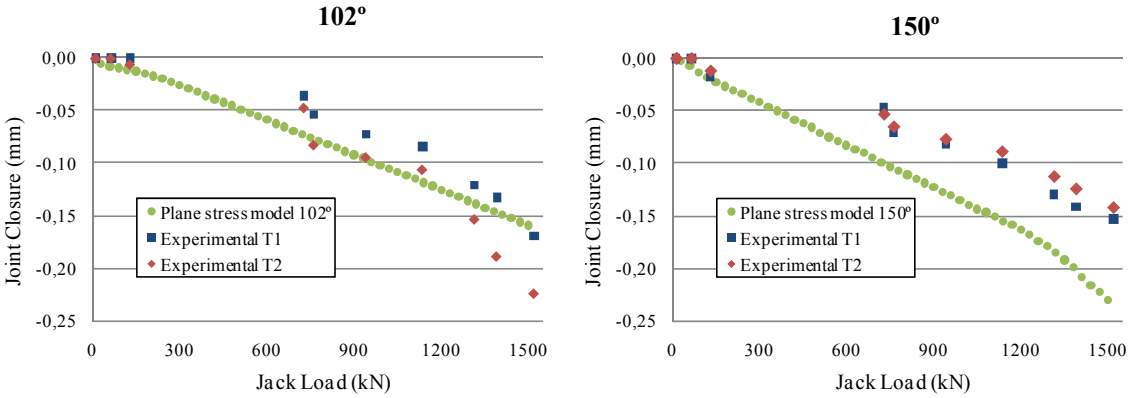

Figure 3.18. Evolution of joints closure (intrados side) at 102º and 150º during stage 6.

As can be clearly observed in both graphs of figure 3.17, the evolution of joints closure perform a sudden variation for a jack load close to 600 kN which is caused by the start of joint gaping due to the loose of contact at the extrados side. The evolution of closure at 54º joint presents a very good fitting to the experimental results, whereas the results at joint 102º present some differences for high load values. On the other hand, the evolution of 102º joint closure during stage 6 perfectly fits with the numerical prediction (Fig. 3.18) whilst the 150º joint is the one that present some differences. This fact means that the small inaccuracy of the numerical model should be caused by the imprecision of some input parameters more than the strategies used to model the different phenomena involved on the structural response of the ring. The agreement obtained in the radial displacements shows that these differences might be caused by small variations on the distribution of the concentrated rotations between the joints and the cracked sections. If the radial ground stiffness is slightly overestimated the flexibility of the arch mechanism is reduced, diminishing the rotations experimented at joints. Consequently, to obtain the same ring deformation, higher rotations have to be concentrated on the cracked sections.

3.5.4. Crack patterns

The experimental crack pattern observed at stage 5 and the one obtained using the shell model are presented in Figure 3.19. The numerical model fits very well the general tendency of ring cracking. As was previously described, cracks appear exclusively under the jacks (this fact was also confirmed by the plane stress model, Fig. 3.9), but the 3D features of the shell model provide improved information about the cracking prediction skills of the presented numerical models. The main cracks that appear in the longitudinal tunnel direction have the expectable orientation due to the bending moments produced in the ring by the load. Furthermore, the shell model is capable to reproduce the circumferential cracks (horizontal in figure 3.19) and, in minor extent, the cracks that

appear on radial orientation from the jacks positions. Both cracks are caused by local bending stresses derived from the spreading of the jacks loads across the segment. Finally, it is worth noting that the analytical results fit the widest damage zone (with more longitudinal cracks) that was recorded in the experiment for the segment A2.

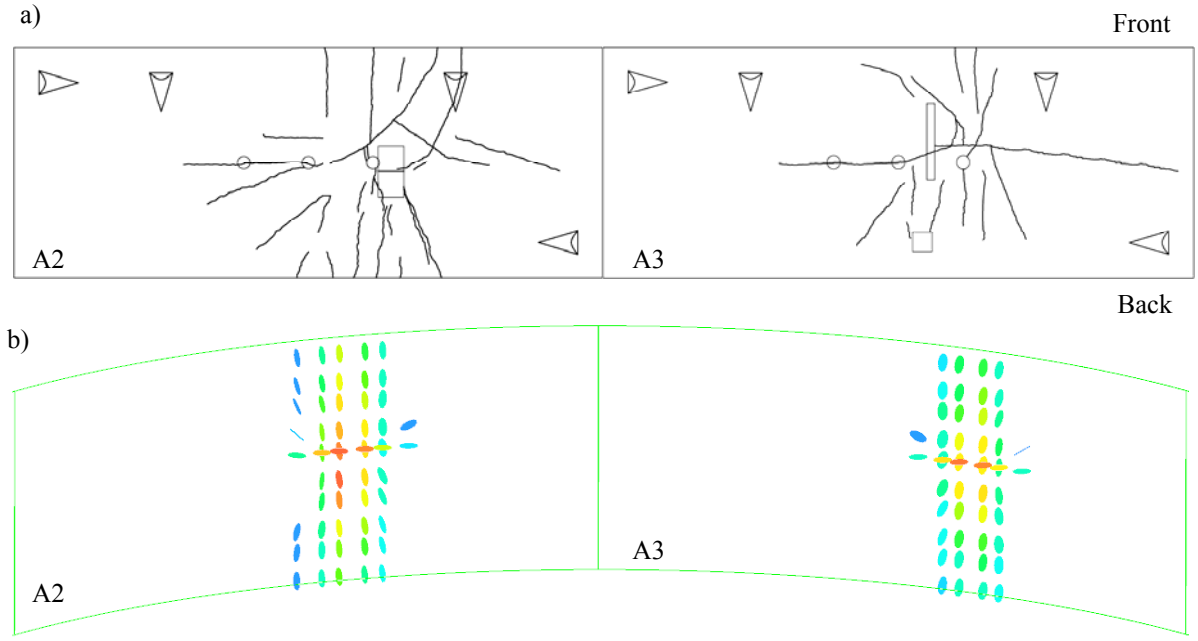

Figure 3.19. Crack patterns obtained by the in situ test (a) and by the shell numerical model (b).

3.6. CONCLUSIONS

The simulation of the complex *in situ* test carried out in its definitive position inside a real tunnel is presented in this paper. The test presents the advantage of providing the real structural response of a certain tunnel section by taking into account all the parameters that affect it, from the most important to the less relevant. The knowledge about the real segmental tunnel lining behavior gives the insights of which are the main phenomena affecting its response and, consequently, the most affecting on numerical simulations. Within this process there are a lot of secondary parameters, mainly caused by the tunnel construction process (backfill grout influence, irregular segments connections, etc), that can affect the precision of the analytical results but should not be determinant on the behavior of the segmental tunnel lining. Additionally, the exactitude of some parameters assumed in the model is questionable (for example, the ground elastic modulus and its homogeneous distribution around the whole tunnel) and this may also affect the precision of the model. Despite these facts, the analysis of the results obtained in the simulation of the *in situ* test performed by the aforementioned numerical models and its comparison with the experimental evidences showed that:

- The lining behavior obtained by the numerical model perfectly fits to the real one deduced from the test measurements. The local arch behavior and the rings displacements caused by joints and cracked sections rotations were clearly appraised.
- The accuracy shown in the displacements predictions through all the loading process confirms the validity of the adopted modeling philosophy, hypothesis and techniques.
- The similarities obtained between the real and the numerical crack patterns corroborate the suitability of the adopted model on taking into account the steel fibers contribution to the structural response of the lining.
- The obtaining of the real structural response of segmental tunnel linings requires the realistic simulation of: (1) the unilateral behavior of joints, including the packing material response if it exists, (2) the ground-structure interaction, considering the tangential effects and the loose of contact, and (3) the cracking of concrete for high load scenarios such as applied to L9 tunnel during the *in situ* test.

For these reasons, it can be concluded that the structural behavior of SFRC segmental tunnel linings can be accurately simulated by adopting the appropriate hypothesis and modeling techniques.

ACKNOWLEDGEMENTS

This research was possible thanks to the support provided by GISA, the public company of the Generalitat de Catalunya responsible of the design and construction of L9 and by FCC Construcción, S.A. The first author also wants to thank the support of the University and Research Commissioner of the DIUE of the Generalitat de Catalunya and also the European Social Fund (ESF).

Chapter 4

LONGITUDINAL TIME-DEPENDENT RESPONSE OF SEGMENTAL TUNNEL LININGS

ABSTRACT

The longitudinal forces introduced by tunnel boring machines (TBMs) to the segmental tunnel linings influence their structural response. The analyses of the linings construction process and the ground-structure interaction mechanisms have shown the influence of the lining creep on the progressive loss of the initial longitudinal force. An analytical formulation to predict the remaining compression of the linings as a function of time is proposed, supported by means of a complete numerical model, which considers the effect of creep during the sequential construction process. An experimental program to determine the creep of plastic packers was developed, revealing its significant influence on the global lining creep factor and the evolution of the remaining compressive stresses.

***Keywords*:** Segmental tunnel lining, longitudinal response, packers, lining creep.

4.1. INTRODUCTION

The application of modern tunnel boring machines (TBMs) allows the construction of tunnels of larger dimensions at increasing depths under complex ground conditions. Its use is mostly associated with segmental concrete linings which provide the structural resistance to the ground and water pressure, further to provide the necessary reaction to generate the progress of the TBM. The improvement of the knowledge and comprehension of the structural response of segmental tunnel linings will entail the optimization of their design, providing economical, efficient and safer structures.

A segmental concrete lining is composed of multiple concrete rings that are sequentially placed as tunnel boring advances (Fig. 4.1). There exist different types of linings depending on the shape of the segments and the ring (JSCE, 2006; Guglielmetti et al., 2008). Concrete segments have to be designed in order to individually resist the casting and storage process and the forces coming from the TBM. The whole ring design is focused on the adequate resistance of all foreseeable ground loads, which can be determined by means of advanced numerical models that simulate the influence of the boring process into the ground stresses (Broere and Brinkgreve, 2002; Kasper and Meschke, 2004). The analysis of the lining internal forces is nowadays performed by means of finite element models that allow the consideration of the structural particularities presented in segmental linings (Plizzari and Tiberti, 2006; Blom et al., 1999). The joints existing between segments create a multiple-hinged structure that presents a complex structural behavior (Muir Wood, 1975; Blom, 2002; Teachavorasinskun and Chub-uppakarn, 2010). Research programs have been developed recently in order to determine, explain and model the different phenomena involved in segmental linings radial response (Molins and Arnau, 2011; Arnau and Molins, 2011), to optimize its structural resistance by means of steel fiber additions (de Waal, 2000; Kasper et al., 2007; Tiberti et al., 2008) or directly increase the structural resistance by applying composite sections (Zhang and Koizumi, 2010).

TBM's apply a large longitudinal force to segmental tunnel linings by means of multiple hydraulic jacks in order to produce their movement and to resist the excavation face pressure. Packing materials are commonly placed in circumferential joints (between adjacent rings) in order to regularize the contact surfaces and to center the TBM force into the segments height (Fig. 4.1). As a consequence, the structural collaboration between adjacent rings is governed by a packer-concrete friction mechanism that directly depends on the normal force applied on. A few tunnel projects include a dowel and socket system on their circumferential joints in order to confine the differences in deformation between adjacent rings (Blom, 2002). In these cases, the frictional mechanism only acts until the

dimensional tolerance of the dowel and socket system is exhausted. Therefore, the structural analysis of segmental tunnel linings should include the longitudinal forces applied on the lining if its real three-dimensional behavior needs to be adequately considered (Blom et al., 1999, Mo and Chen, 2008).

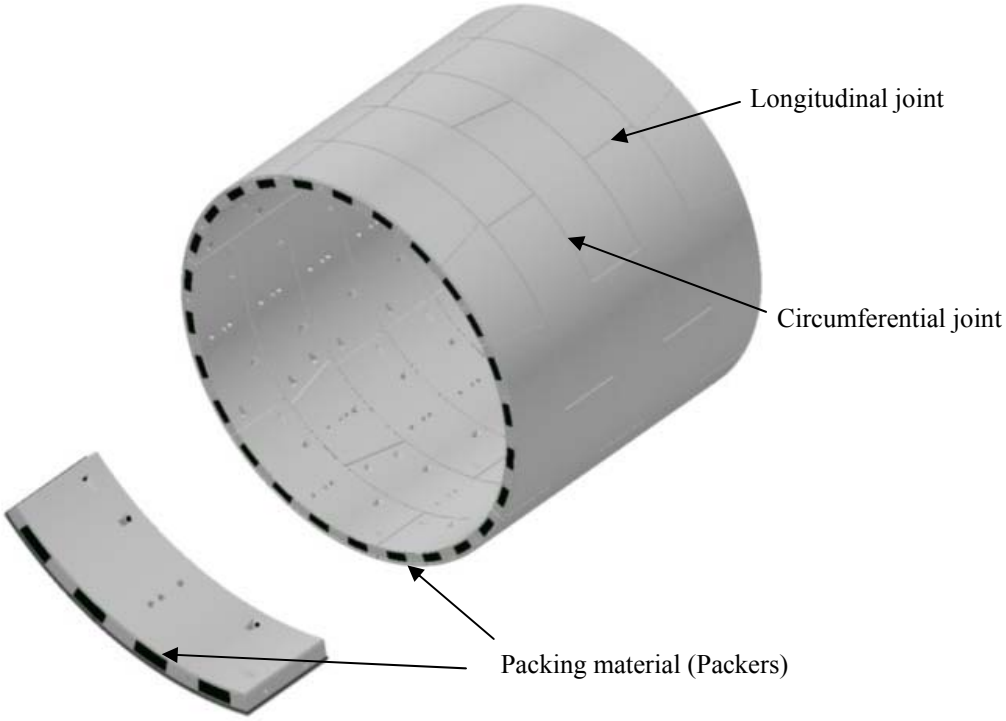

Figure 4.1. Segmental tunnel linings most common configuration.

Recent research programs employed advanced 3D structural models that consider the longitudinal force to analyze different scenarios during construction or in service (Blom, 1999; Klappers et al., 2006; Mo and Chen, 2008). In these cases, the force applied to the lining by the TBM is adopted, assuming that the long term ring forces remain close to their initial value. As this hypothesis entails the maximum structural interaction between adjacent rings, it is necessary to ensure its validity during the full tunnel service life. Additionally, a possible loss of the longitudinal compressive stresses involves a reduction of the closing pressure in the sealing devices (gaskets) placed in the circumferential joints, causing a reduction of the watertightness of the lining.

Koek (2004) performed a study, which focused on the influences of the lining and ground stiffness on the tunnel's longitudinal response in front of TBM force variations. This work includes a brief analysis assuming that the lining is subjected to a pure relaxation process, which implies that longitudinal stress losses can occur. As a consequence, it was shown that is necessary to carry out a thorough study and analysis of the ground-structure interaction mechanism, which can cause a transfer of forces from the lining to the ground, as well as of the influence of the segmental construction process. The knowledge of the

force transfer mechanism will enable the determination of the stress development in segmental tunnel linings.

The conicity and the thickness of the TBM shield and the overcut produced by its cutting wheel produce an annular gap between the external radius of the lining and the ground, which width ranges between 13 and 18cm (Thewes and Budach, 2009). The complete and fast fulfilling of the annular gap presents a paramount importance in order to minimize the surface settlements (Pelizza et al., 2010) and to lock the segmental lining into its definitive placement (Fig. 4.2). It is usually performed by means of cementitious mixes or two component grouts (Peila et al., 2011) which conforms a stiff material between the lining and the ground. As a consequence, the adequate study of the ground-structure interaction requires the consideration of the backfill grouting process.

This paper deals with the determination of the longitudinal force that remains in segmental tunnel linings during their service lives. In the first part, the construction process and the ground-structure interaction mechanism are thoroughly analyzed, showing the dependence of the longitudinal force on the long term deformations of the lining. A formulation is proposed to predict the remaining compressing force on the lining at a certain time, based on its longitudinal creep coefficient (Remaining Compression Factor approach, RCF). A Finite Elements Model is used to simulate the construction process of a tunnel and its time-dependent response in order to verify the suitability of the proposed formulation and to study the particular influence of lining creep during the construction stage. The influence of the creep of the packers is also studied, presenting the results of a particular experimental program. Finally, a formulation for a global longitudinal creep coefficient of the lining (φ_G) which includes both the concrete and the packers creep is proposed.

4.2. GROUND-STRUCTURE LONGITUDINAL INTERACTION MECHANISM AND THE REMAINING COMPRESSION FACTOR (RCF) APPROACH

As a consequence of the construction process of segmental tunnel linings, the TBM is constantly applying a minimum longitudinal axial force in order to compensate the excavation face pressure, which mainly depends on the TBM face support method and the ground conditions (Maidl et al., 1996). At structural level, this is achieved by means of a sequential loading process based on the individual loading of each segment, generating a permanent longitudinal compression state of the lining.

In this section, the influence of the construction process on the stress state of the lining is analyzed. Firstly, the ground-structure interaction mechanisms are studied in order to determine the longitudinal force transfer that can cause the loss of the initial compression

state of the lining. As a result, a formulation to predict the evolution of the remaining compressive stress of the lining is proposed based on its longitudinal creep (RCF approach).

4.2.1 Ground-structure interaction mechanisms

In order to present in a simple and understandable way the effect of the construction process on the longitudinal response of the lining, an ideal case is firstly analyzed. The increase of the longitudinal force that can be caused by the radial loading of the rings (produced by the existing confinement in the longitudinal direction) is neglected due to its usual minor influence on the longitudinal stress of the lining. Despite that, it can be easily contemplated by superposing it to the initial applied force. Concrete is assumed as a linear elastic material without time dependent deformations whilst packing materials are not yet contemplated.

Usually, the TBM first reaction point is a steel frame installed in the field or in the shaft where the tunnel starts as it is schematically shown in figure 4.2. The loading process of ring 1 is completed once it leaves the TBM shield and becomes surrounded by the liquid backshield grout or mortar. No constraints affect its longitudinal strain ε_c, being determined as $F_{TBM} / E_c \cdot A_c$, where F_{TBM} is the longitudinal force applied by the TBM, E_c is the concrete deformation modulus and A_c is the concrete cross area. Assuming that F_{TBM} remain constant during the different construction stages, when a new ring is placed (2), it is also subjected to the same initial strain ε_c. At this time, the grout over ring 1 becomes stiffer, relating its initial zero strain ($\varepsilon_g = 0$) to the segments deformed shape ($\varepsilon_c = F_{TBM} / E_c \cdot A_c$). Whilst the TBM force remains constant and permanently applied, the situation will be the same for all rings. Therefore, under the assumption of the ideal conditions described, the ground does not contribute to the equilibrium of longitudinal forces of the lining. The activation of the ground-structure interaction requires longitudinal lining movements after grout hardening. Two main different circumstances can cause displacements of the lining: (1) changes in the applied forces (F_{TBM} or the reaction at the initial frame, F_{RF}) and (2) long-term deformations of the concrete segments.

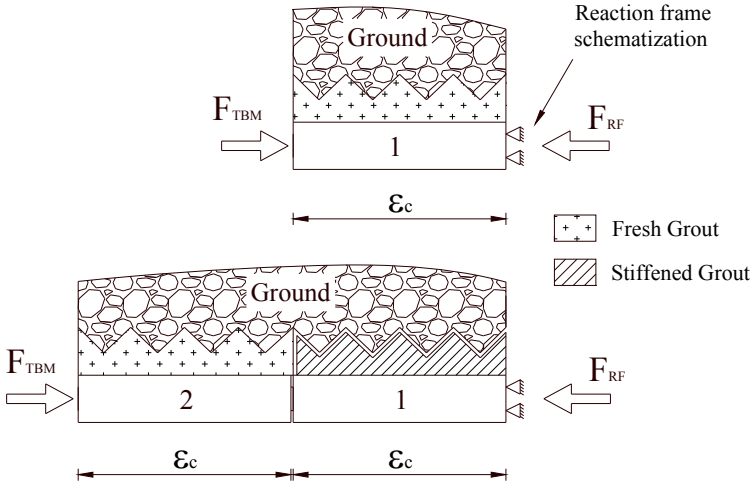

Figure 4.2. Forces and constraints of an ideal construction case.

The removal of the initial frame produces the disappearance of the reaction force (F_{RF}). In consequence, the lining starts its displacement, activating the transfer of forces from the lining to the ground until the lining is fully anchored. Severe changes in TBM forces generate a similar process, producing lining displacements until the force difference is fully transmitted to the ground. Both transfer mechanisms are local, only affecting a certain lining section depending on the necessary length to complete the transmission of forces.

As long as the lining and the ground properties remain linear elastic, the transfer of forces between them is governed by the problem of a bar embedded in an elastic media (Fig. 4.3). The differential equation that defines the equilibrium of forces is obtained from the scheme presented in figure 4.3 (Eq. 4.1), where x is the variable of position, u is the longitudinal displacement, K_l is the longitudinal stiffness of the ground (N/mm^3) and P_e is the external perimeter of the tunnel (mm).

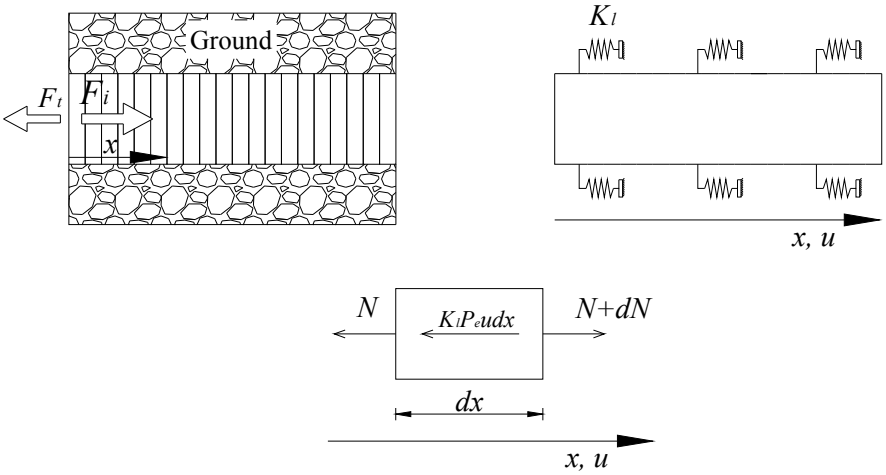

Figure 4.3. Schematization of the development of the force in the lining based on differential analysis.

$$E_c A_c \frac{d^2u}{dx^2} - K_l P_e u = 0 \qquad \text{(Eq. 4.1)}$$

$$\frac{d^2u}{dx^2} - \alpha^2 u = 0 \qquad \text{where:} \quad \alpha^2 = \frac{K_l P_e}{E_c A_c} \qquad \text{(Eq. 4.2)}$$

Equation 4.1 corresponds to a second order differential equation (Eq. 4.2). The mathematical solution of equation 4.2 can be found in some publications (i.e. Bouma, 1989), providing the expression of the transferred force F_t (Eq. 4.3). Assuming that a force F_i is initially applied to the tunnel, the evolution of the tunnel longitudinal force (N) corresponds to equation 4.4.

$$F_t(x) = F_t e^{-\alpha x} \qquad \text{where:} \quad \alpha = \sqrt{\frac{K_l P_e}{E_c A_c}} \qquad \text{(Eq. 4.3)}$$

$$N(x) = F_i - F_t \qquad N(x) = F_i - F_i e^{-\alpha x} \qquad \text{(Eq. 4.4)}$$

$$L_{an} = \frac{\ln(0.05)}{-\sqrt{\frac{K_l P_e}{E_c A_c}}} \qquad \text{(Eq. 4.5)}$$

The force transmission zone (anchorage length) ends when the lining force $N(x)$ is equal to the initial applied force F_i. Eq. 4.4 presents an asymptotic behavior to F_i, and therefore, if it is solved assuming that F_t is equal to F_i, the value of x is infinite (∞). As a consequence, it is necessary to assume a tolerance value of the initial force F_i which determines that the lining is fully anchored. Assuming a tolerance of 5% in the force (F_i-$N(x)$=0.05·F_i), the resolution of Eq. 4.4 provides the expression for the anchorage length (L_{an}) shown in Eq. 4.5.

According to Eq. 4.5, for certain lining conditions (fixed E_c, A_c and P_e) the anchorage length only depends on the ground stiffness K_l. Therefore, as long as the ground (or the ground-structure interface) presents a linearly elastic behavior, the anchorage length (L_{an}) is independent of the initial force (F).

4.2.2 Effect of long-term deformations (RCF approach)

Creep and shrinkage are the essential time dependent deformations experienced by the structural concrete. In tunnel linings construction, concrete segments are precast in an industrial plant and subsequently stocked until their assembly. As a consequence, creep is the only time dependant deformation that significantly affects the behavior, because shrinkage is almost fully developed when the segments are placed.

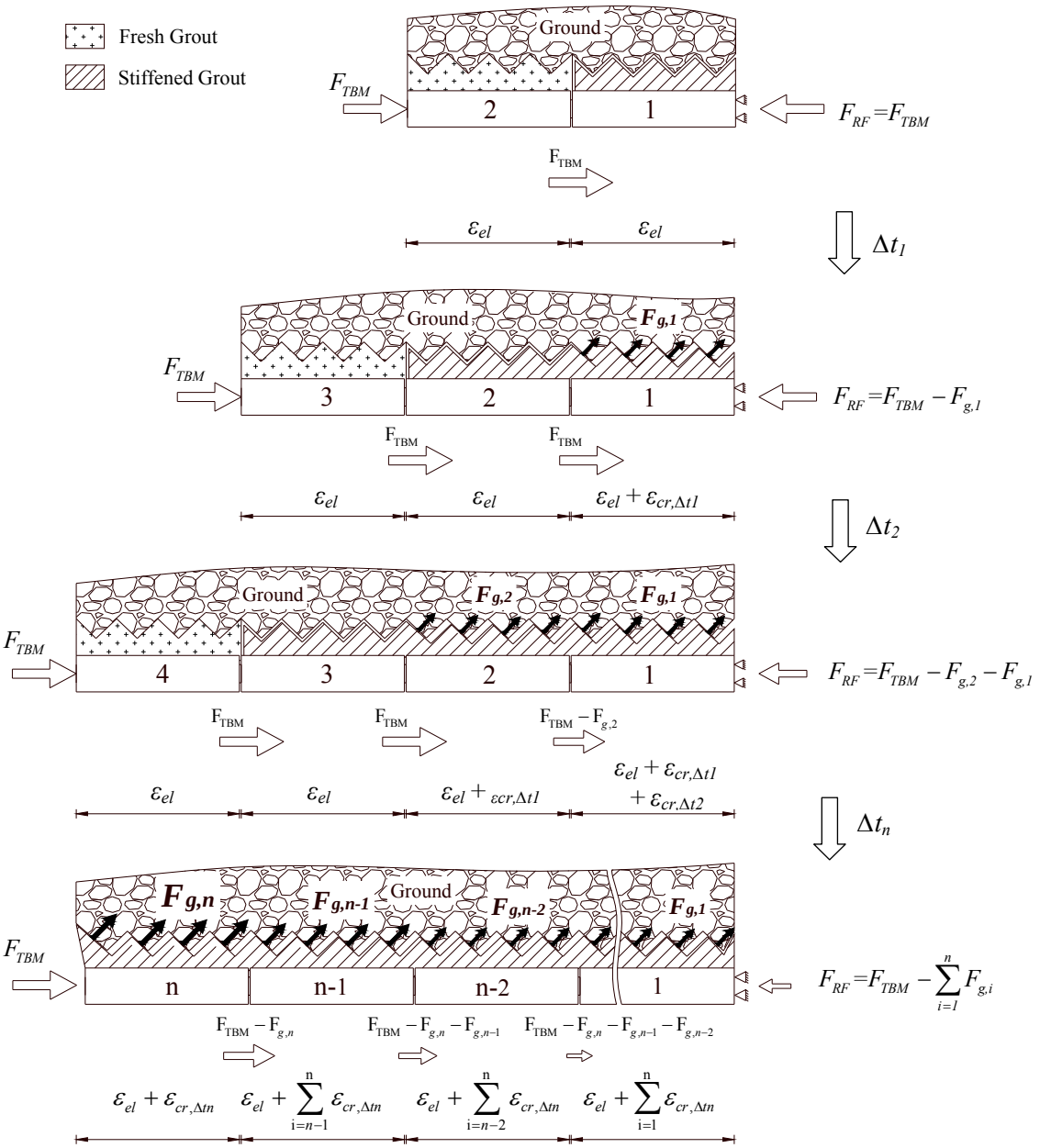

Figure 4.4. Schematization of force transmission due to lining creep.

The strain of concrete segments (ε_c) is composed by the elastic strain (ε_{el}) and the creep strain ($\varepsilon_{cr,\Delta t}$). Creep is the increase in strain caused by a sustained load in a time period Δt (Nawy, 2008). As described in section 2.1, the rings are initially fixed to the ground according to their elastic strain. As time goes by, creep phenomenon produces a reduction of the ring size due to the described strain increase. As a consequence, the concrete lining undergoes longitudinal displacements that activate the ground-structure interaction. Whilst the ground tangential behavior remains linear, a larger movement results in a larger force transmitted to the ground. As can be observed in figure 4.4, the transmission of the force to the ground (F_g) implies that the force in the previous ring decreases, also diminishing its stress and its elastic strain (ε_{el}). Consequently, a stress/strain redistribution occurs in order to achieve a new equilibrium of forces.

As it was previously explained, as long as the maximum tangential stress of the ground (or the ground-grout interface) has not been exceeded, the length of the force transmission zone (L_{an}) is independent of the magnitude of the force. This means that outside the anchorage zone, the force transmission from the lining to the ground should be zero. This assumption implies that, once the surrounding grout has hardened, the displacement of each ring should be zero as well. The only possibility to accomplish this requirement is that the total strain of a ring at a certain time t, $\varepsilon_c(t)$ is equal to its initial strain $\varepsilon_c(t_0)$ (Eq. 4.6). This phenomenon occurs when the values of the positive relative strains caused by creep are equal to the negative relative strains caused by the decrease of the compression stress. Therefore, the lining is subjected to a pure relaxation mechanism caused by its longitudinal creep that causes a reduction of its compressive stress in time.

$$\varepsilon_c(t) = \varepsilon_c(t_0) \qquad \text{(Eq. 4.6)}$$

$$\varepsilon_c(t) = \frac{\sigma_c(t_0)}{E_c}[1+\varphi(t,t_0)] + \frac{\Delta\sigma_c(t,t_0)}{E_c}[1+\chi(t,t_0)\cdot\varphi(t,t_0)] \qquad \text{(Eq. 4.7)}$$

The strain of the concrete at a certain time t is commonly evaluated by Eq. 4.7 (Bazant and Wittmann, 1988), where $\sigma_c(t_0)$ is the initial concrete stress, $\Delta\sigma_c(t,t_0)$ is the stress variation from the load time t_0 to t whilst $\varphi(t,t_0)$ and $\chi(t,t_0)$ are the creep coefficient and the aging coefficient related to the same time period respectively. The combination of Eq. 4.6 and Eq. 4.7 directly allows the derivation of a *Remaining Compression Factor* (RCF) (Eq. 4.8) which describes the proportion of the initial longitudinal lining stress that remains in the concrete lining after a certain time t (Eq. 4.9).

$$RCF(t) = 1 - \frac{\varphi(t,t_0)}{[1+\chi(t,t_0)\cdot\varphi(t,t_0)]} \quad \text{(Eq. 4.8)}$$

$$\sigma_c(t) = \sigma_c(t_0)\cdot RCF(t) \quad \text{(Eq. 4.9)}$$

During the construction process of the segmental lining, the concrete is loaded at a relatively advanced age (generally more than 60 days). As a consequence the value of the aging coefficient $\chi(t,t_0)$ is always near to 1 and can be considered constant for time periods longer than one year (Ghali et al., 2002). Figure 4.5 shows the evolution of the RCF as a function of the creep coefficient $\varphi(t,t_0)$, assuming a constant value $\chi(t,t_0)$=0.9. For small values of the creep coefficient (short time after loading) the RCF decreases relatively fast, achieving a value under 0.5 for a creep coefficient of 1.

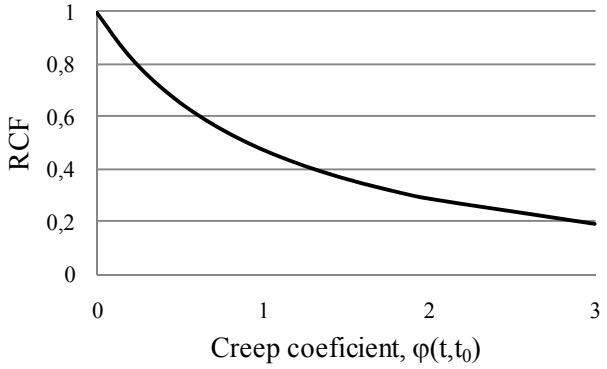

Figure 4.5. RCF evolution as a function of the concrete creep coefficient, $\chi(t,t_0)$=0.9.

4.3 NUMERICAL SIMULATION

A complete set of numerical analyses are employed to determine the validity of the proposed analytical formulations and the limitations imposed by the performed hypotheses. An advanced FE model that considers the longitudinal creep during the tunnel construction process is developed for such purpose. The analyses comprise a total number of nine simulations, reproducing three different concrete scenarios and three surrounding ground stiffnesses. To simplify the problem and to determine its minimum effect, only the concrete creep is considered (the effect of packers is not yet taken into account).

4.3.1 Case study and model description

The selected case study is a 900 m long tunnel with an external diameter of 10m and a thickness of 0.35 m. Its construction process is composed by the following steps: (1)- The lining starts at a reaction frame which is modeled by means of longitudinal rigid supports

at the first ring, (2)- the tunnel segments are placed according to a construction speed of 9 m per day, (3)- at the end of construction, the TBM force is not further applied and the initial reaction frame is disassembled, and (4)- time proceeds until 10000 days (27 years), which can reasonably be considered as the time of stabilization for the time-dependant properties of concrete.

Due to the symmetry of the circular tunnels and assuming a uniform distribution of the longitudinal stresses at every ring, it is possible to model the whole lining longitudinal behavior as a tunnel sector. Therefore, a rectangular cross section of 1x0.35 m is adopted. The longitudinal force applied by the TBM to the lining (F_{TBM}) is considered constant and permanent during the whole construction process. The selected value of F_{TBM} is 1750 kN, determined to produce a uniform compressive stress of -5 N/mm^2.

A bar elements model is proposed for the case study. The ground-structure interaction is modeled by means of distributed longitudinal springs (Fig. 4.3). Three different values of the ground-structure stiffness (K_l) are applied in order to cover a significant range of ground characteristics (Table 4.1). There is no generally accepted relation to determine the ground-structure longitudinal stiffness (K_l) from a certain tunnel and ground properties. In the numerical analyses carried out, K_l was assumed to be equal to the tunnel tangential stiffness (K_t), which is commonly accepted to be one third of the radial stiffness (K_r) (Eq. 4.10 and 4.11). These relations are obtained from the resolution of the ground distortion response and can be particularly adjusted to certain tunnel and ground conditions by means of finite element software as shown by Koek (2004).

Table 4.1. Ground types and characteristics employed in the numerical analyses.

Property	*Hard / Rock mass*	*Medium / Gravel*	*Soft / Soft Clay*
Longitudinal stiffness, K_l (N/mm^3)	0.1	0.01	0.001
Deformation modulus, E_s (N/mm^2)	1950	195	19.5
Poisson ratio (ν)	0.3	0.3	0.3
Rock strength, q_u (N/mm^2)	10		
Friction angle, Ø (º)		30	
Density, γ (kN/m^3)		24	
Cohesion, c (kN/m^2)		50	
Undrained shear strength, c_u (kN/m^2)			50
Tangential strength, τ_{sl} (kN/m^2)	500	179	25

$$K_r = \frac{E_s}{R \times (1+\nu)} \qquad \text{(Eq. 4.10)}$$

$$K_l = K_t = \frac{K_r}{3} \qquad \text{(Eq. 4.11)}$$

The ground-structure interaction failure is considered using elastic-plastic behavior to define the response of the longitudinal springs (Fig. 4.6). The determination of the maximum tangential stress for each ground type (τ_{sl} in Table 4.1) is performed according to the formulations and recommendations described by Fleming et al. (1994), assimilating the tunnel lining to a single pile foundation and assuming the ground properties given in Table 4.1. The reduced tunnel pressure of Terzaghi (JSCE, 1996) was used to determine the effective ground pressure on the tunnel. The spring displacement that produces the start of the plastic response (u_{sl}) is determined by the expression of the ground-structure longitudinal stiffness (Eq. 4.12).

$$u_{sl} = \frac{\tau_{sl}}{K_l} \qquad \text{(Eq. 4.12)}$$

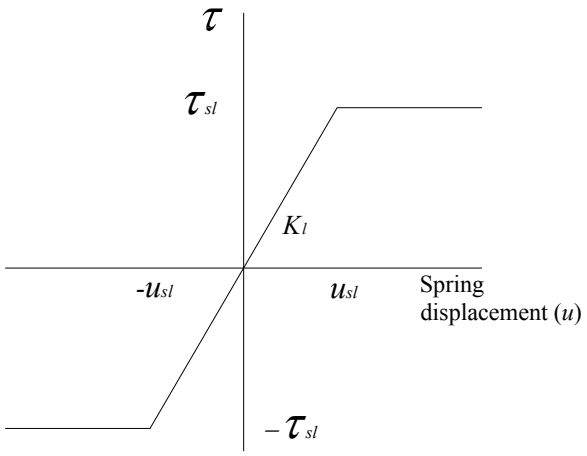

Figure 4.6. Model for ground-structure interaction springs response.

Diana 9 software is employed for the resolution of these staged construction analyses. This software includes the creep formulation proposed in the CEB-FIP Model Code (1993), which is adopted for the numerical analyses. Equation 4.13 shows the stress dependent strain ($\varepsilon_{c\sigma}$) proposed by CEB-FIP Model Code (1993). Creep coefficient φ_c mainly depends on the compressive strength of concrete, the dimensions of the member, the relative humidity to which the member is exposed and the age of loading. Table 4.2 shows the properties and parameters of the concrete scenarios analyzed, which provide the evolution of the creep coefficient $\varphi_c(t,t_0)$ shown in figure 4.7, and determine values of $\varphi_c(t,t_0)$ at 10.000 days from 1 to 2.

$$\varepsilon_{c\sigma}(t,t_0) = \sigma_c(t_0)\left[\frac{1}{E_c(t_0)} + \frac{\varphi_c(t,t_0)}{E_{c,28}}\right] \qquad \text{(Eq. 4.13)}$$

Table 4.2. Properties and parameters of the concrete scenarios analyzed.

Concrete Properties / Parameters	*Model A*	*Model B*	*Model C*
Concrete compressive strength, f_{cm} (N/mm^2)	50	40	30
Deformation modulus, E_c (N/mm^2)	38606	36246	33550
Concrete age of loading, t_0 (days)	100	60	30
Concrete area, A_c (m^2)	0.35	0.35	0.35
Perimeter in contact with the atmosphere, u_p (m)	1	1	1
Notational size of the member, $h = 2A_c / u_p$ (mm)	700	700	700
Relative Humidity, *HR* (%)	75	54	48
Resulting creep coefficient at 10000 days, $\varphi_c(t,t_0)$	1	1.5	2

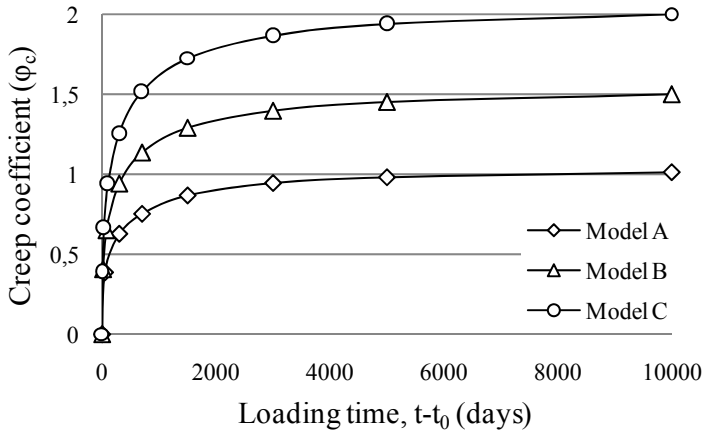

Figure 4.7. Concrete creep coefficient evolution for the analyzed scenarios according to the CEB-FIP Model Code (1993).

4.3.2 Numerical model results

Figure 4.8 presents the longitudinal lining stress distributions for Model A and K_l=0.01 N/mm^3 at different times. As well known, the concrete creep effect is largest immediately after loading of the structural member, starting the loss of force during the construction process. When the last ring has been placed (just before the initial reaction frame disassembly, Cons End Pre-RFD in Fig. 4.8), the longitudinal stress at the start of the lining is -3.79 N/mm^2, representing a reduction of 24.2 % (2.69 % per 100 m of tunnel).

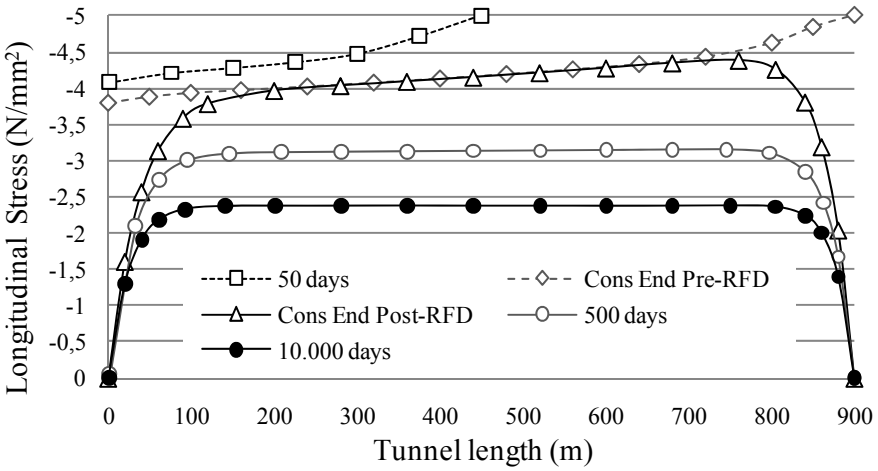

Figure 4.8. Evolution of longitudinal lining stress for Model A and K_l = 0.01 N/mm^3.

In 500 days after the start of construction, almost the whole lining sustains a stabilized stress of -3.13 N/mm^2, diminishing to a value of -2.37 N/mm^2 after 10000 days. As a consequence, 71.1 % of the total stress losses occur during the first 500 days.

At end of construction, when the TBM force stops and the initial reaction frame is disassembled (Fig. 4.8, Cons End Post-RFD), the length of the anchorage zones can be clearly appraised. The anchorage length does not present significant variations during the stress relaxation process.

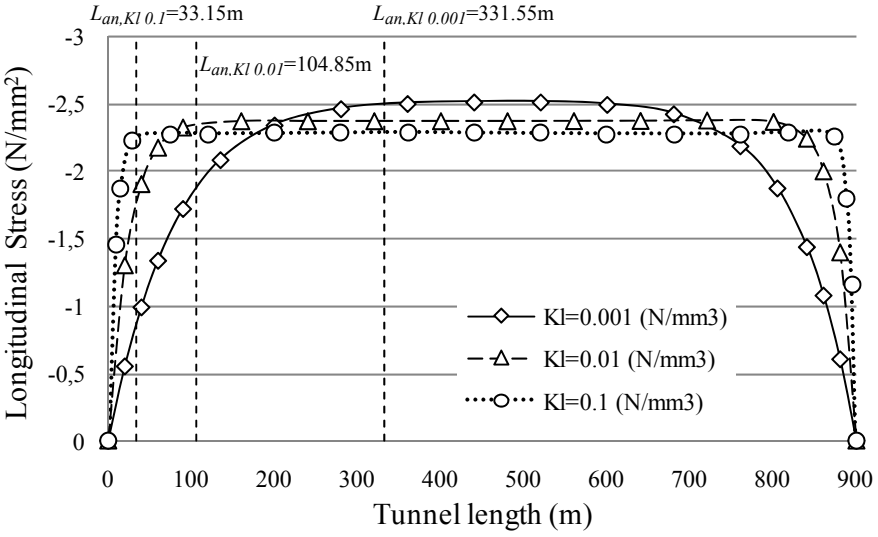

Figure 4.9. Longitudinal lining stress at 10000 days for Model A and different K_l values.

Figure 4.9 shows the longitudinal stresses obtained at 10000 days for Model A concrete and the different ground conditions. As explained in section 2.1, the surrounding ground stiffness does not show a significant influence on the remaining longitudinal compression of the lining. The small differences that can be appraised in figure 4.9 are related to the

sequential construction process. Depending on the ground stiffness, the stress-strain redistributions that constantly occur during the tunnel construction due to the lining creep slightly differ. Then, the lining stress distribution at construction end is also different (figure 4.10), conditioning the creep and stress evolution of the lining.

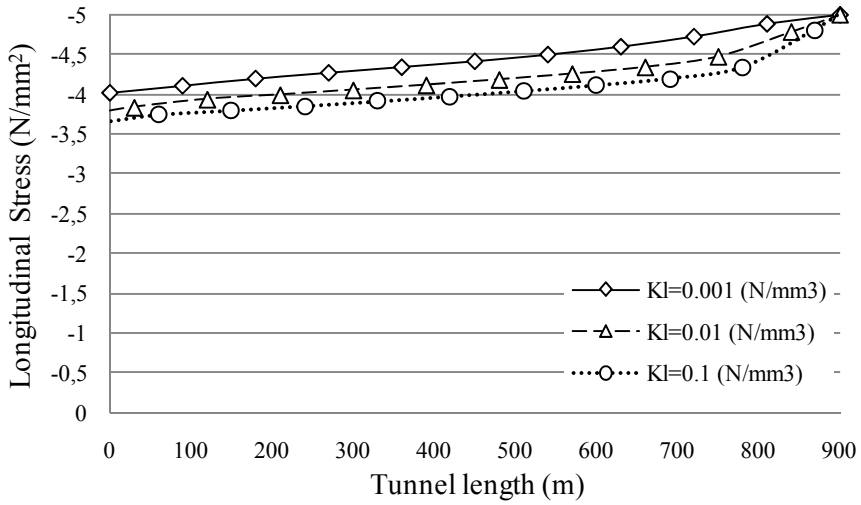

Figure 4.10. Distribution of the longitudinal stress for Model A and different K_l values at construction end just before the reaction frame disassembly.

The ground stress analysis reveals that the maximum tangential stress (τ_{sl}) is not achieved in any case. Consequently, the anchorage lengths (L_{an}) obtained with the proposed formulation (Eq. 4.5) should accurately fit the numerical results. As can be observed in figure 4.9, the analytical results of the anchorage lengths for the three different ground conditions (represented by the dotted lines in fig. 4.9) show excellent agreement with the lining response obtained with the numerical model.

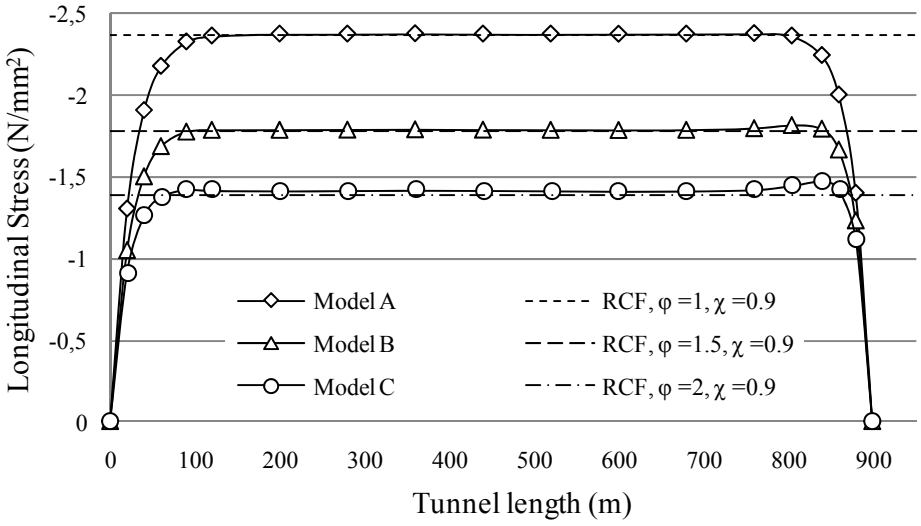

Figure 4.11. Longitudinal lining stress for different concrete models and the RCF prediction. K_l = 0.01N/mm^3.

Figure 4.11 presents the results of the three different concrete models after 10000 days for K_l = 0.01 N/mm^3 compared with the results obtained with the proposed formulation for the RCF (Eq. 4.8 and 4.9). It can be concluded that the accuracy achieved by the RCF approach for the prediction of the long term longitudinal stress is excellent. As the RCF formulation is obtained from the static analysis of the segmental tunnel lining, the time effects during the construction stages are not considered. As a consequence the accuracy for short times is low (Fig. 4.12). For the case study regarded (Model A with K_l=0.01 N/mm^3), the error of the RCF becomes lower than 10% after 750 days (2.05 years).

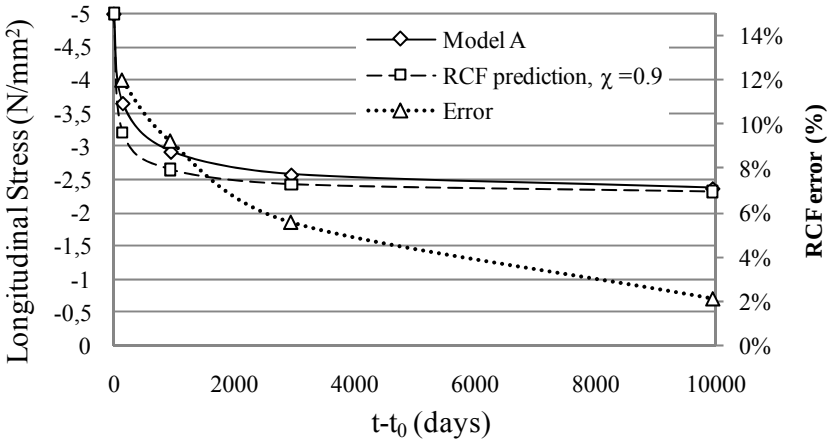

Figure 4.12. Evolution of longitudinal lining stress of Model A and K_l=0.01N/mm^3, RCF prediction and its error versus the numerical model.

4.3.3 Grout influence

Another set of analyses was carried out in order to study the backfill grout behavior and its influence on the longitudinal response of the lining. Three different grout modulus of elasticity were used in the analysis for each different ground condition described in section 3. An assessment of the influence of grout shrinkage was also performed by assuming a value of 0.05mm/m according to the favorable curing conditions. The previously described model was completed by means of the addition of plane strain elements between the bar elements (lining) and the springs (ground) to simulate the grout (Fig. 4.13).

The results showed that: (1) the grout modulus of elasticity does not present a significant influence on the lining axial stress, (2) along the anchorage zones the grout is mainly subjected to an axial stress that can cause its tensile cracking for very stiff grouts, and (3) the lining creep and the grout shrinkage do not significantly influence the grout tensile stress for general tunnel conditions. Backfill grout cracking should not have a significant effect on the radial structural capacity of the segmental tunnel lining, but it can diminish the watertightness of the lining.

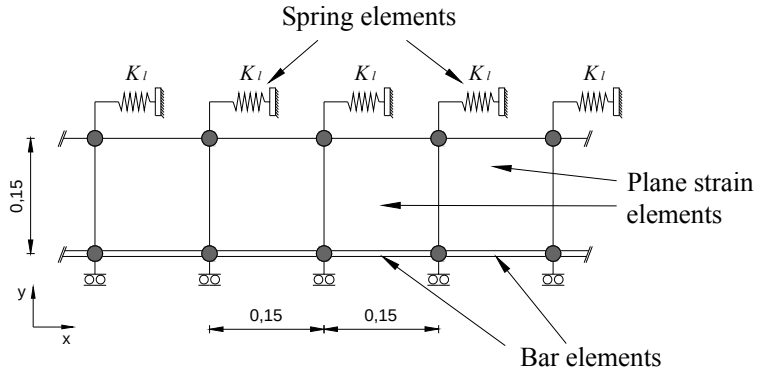

Figure 4.13. Modeling scheme adopted for grout analyses.

4.3.4 TBM force variations

The hypothesis of constant longitudinal force was assumed in order to simplify and clarify the study of the construction process and the time-dependant response of segmental tunnel linings. In real tunnel construction, the TBM force is not a constant value and can undergo significant variations mainly, caused by severe changes in ground conditions. Another set of numerical analyses of the tunnel construction process was carried out applying different TBM longitudinal forces at different lining sections. The analysis of the results led to two main conclusions: (1) when a TBM load variation occurs, a transmission zone is created around that point in order to transfer the force difference from the lining to the ground. This force transmission mechanism is the same as described in section 2.1 and, therefore, its length is independent of the magnitude of the force and can be accurately determined by means of Eq. 4.5. (2) Outside of the described anchorage or transmission zones, the RCF approach (Eq. 4.8 and 4.9) allows a correct prediction of the compression stress evolution of each tunnel section subjected to different longitudinal loads. It is only necessary to apply the proposed formulation to the initial compression stress and the creep properties of the section analyzed.

4.4 THE INFLUENCE OF CREEP OF THE PACKERS

Concrete segments are not the only structural members subjected to permanent compression in the longitudinal direction of segmental tunnel linings. A packing material is used to be placed at the circumferential joints (between adjacent rings) in order to control and regularize the longitudinal force transmission between the rings (Fig. 4.1). The lateral surface area covered by packers (S_{pl}) is always smaller than the concrete surface area (S_{cl}) and, as a consequence, they are subjected to higher stresses than the segments (aspect ratios $AR=S_{cl}/S_{pl}$ from 2 to 3 are common in current linings design). Despite their small thickness (around 2 mm) which is 1000 times smaller than common ring widths

(1500-2000 mm), their modulus of elasticity is around 150 times lower (about 30.000 versus 200 MPa). The combination of these factors with the higher compressive stress on the packers can lead to a situation that the packer creep represents a significant part of the total longitudinal creep of the lining.

Packers are usually made of plastic compounds or wood, where the first option is the most commonly used in current tunnel projects. Plywood packers can undergo some volume reductions in time due to the material rotting, especially if the tunnel is subjected to severe groundwater conditions (De Waal, 2000). This phenomenon is of another nature than creep but, in practice, it has a similar effect on the force in the lining.

The creep behavior of plastics is well known and is considered in the design of plastic components and pieces (Crowford, 1998; Brydson, 1999). Its characterization is commonly supplied by the main manufacturers of plastics for the original polymeric compound. Plastic packers are usually made of polyethylene, polyurethane or polypropylene and can be produced from recycled materials. Plastic's mechanical behavior is affected by multiple parameters (material properties, manufacturing process, temperature, stress type, etc) and, therefore, it is necessary to determine the particular creep of plastic packers if it has to be considered in the lining response.

4.4.1 Experimental program to determine the creep of plastic packers

In order to characterize the creep deformations of the plastic packers applied in segmental linings, an experimental program was carried out at the laboratory of structures technology (UPC, Barcelona). The plastic packers applied in three different Spanish tunnel projects were tested under compression stresses of 4 and 20 N/mm^2, representing a common stress range with regard to different TBM forces and lateral ring surface aspect ratios. Table 4.3 summarizes the main characteristics of the packers tested.

Table 4.3. Main characteristics of the packers subjected to creep testing.

Tunnel Project	*Thickness (L_p) (mm)*	*Measured modulus of elasticity (E_p) (N/mm^2)*
Metro of Line 9 (Barcelona)	2	202.1
Metro of La Cela (Madrid)	2	216.8
Road tunnel in M30 (Madrid)	2	188.7

The experimental set-up was based on columns of stapled specimens as commonly used in concrete creep testing (Fig. 4.14a). Five concrete cubic blocks of 150mm side were piled up in order to create four interfaces between the blocks; plastic packers were allocated in

three of them whilst the remaining joint represented a direct concrete contact to characterize its own time dependant deformations (Fig. 4.14b). The maximum planned stress exerted on the packers (20 N/mm^2) is large enough to generate concrete micro-cracking or non-linear creep. In order to avoid stress concentrations in the block corners and high concrete stress levels, the surface of the packer specimens was limited to 100x100 mm^2 (Fig. 4.14c). Table 4.4 presents the packer and concrete average compression stresses, the applied axial force and the necessary pressure at the ∅200mm hydraulic jack of columns for the two different test configurations.

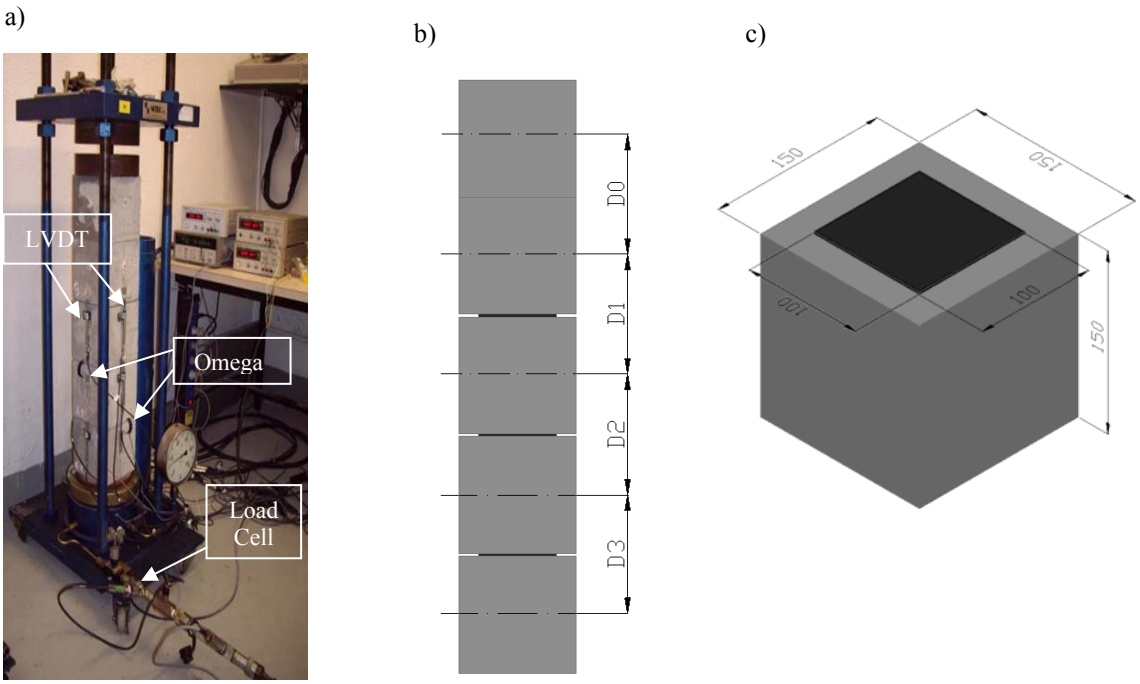

Figure 4.14. Packer creep test configuration.

Table 4.4. Stress, force and pressure applied on the test columns.

Packer stress (N/mm^2)	*Concrete stress (N/mm^2)*	*Axial force (kN)*	*Hydraulic Jack pressure (kPa)*
4	1,78	40	1273
20	8,89	200	6366

Concrete blocks were casted at the same laboratory applying a C30/37 concrete which strength was controlled by means of standard uniaxial compression tests carried out on a 100x100x100mm cubic specimens at 7 and 28 days.

The deformation of the packers was measured at three different faces of the concrete blocks in order to adequately determine the deformation planes. Initially, a continuous measurement was performed by means of 9 displacement transducers (6 LVDT and 3 OMEGA transducers) connected to a data acquisition system. Once the measurements achieved a high level of stabilization, the transducers were replaced by DEMEC points. The application of a mechanical strain gauge with digital display supplies the evolution of joints movements in a discrete manner.

With the experimental set-up chosen the real packer-concrete interface behavior can be measured. On the other hand, the measurement devices are fixed in the concrete blocks and, as a consequence, the influence of the concrete creep and shrinkage has to be adequately considered and subtracted from the total measurement.

The evaluation of the time-dependant deformations of the concrete was measured by means of DEMEC points bridging the concrete-to-concrete joints (Fig. 4.14). The results were compared with the analytical creep and shrinkage values according to the CEB-FIP Model Code (1993), in order to eliminate the influence of the surface contact. The calculations only include the drying component of shrinkage, because the blocks were loaded after finishing the curing process: a very good agreement with the experiments was observed.

4.4.2 Test results

Figures 4.15 and 4.16 show the test results for the packer creep coefficient (φ_p), which is evaluated as the relation between the creep strain ($\varepsilon_{p\text{-}cr}$) and the elastic strain ($\varepsilon_{p\text{-}el}$) (Eq. 4.14). For small compression stresses (4 N/mm^2), the creep evolution shows an almost linear behavior whilst for high compression (20 N/mm^2) the creep coefficient shows an early increase suggesting an exponential response (similar to those of concrete materials). At the end of the test (330 days), the La Cela packer presents a large creep coefficient of 1.34 at 20 MPa whilst 0.98 is obtained at 4MPa. On the contrary, Line 9 and M30 measurements do not present significant variations according to different stresses. At 330 days, Line 9 packer presents a creep coefficient around $\varphi_{p,\ L9}$ = 0.76-0.88 whilst M30 presents a value between $\varphi_{p,\ M30}$ = 0.42-0.44. The small negative values obtained for M30 packer at the start of the 4 MPa test may be caused by an adaptation phenomenon of the samples. This measurement dysfunction was not presented for the 20 MPa test, showing that higher stresses provide more reliable results.

$$\varphi_p = \frac{\varepsilon_{p-cr}}{\varepsilon_{p-el}} \qquad \text{(Eq. 4.14)}$$

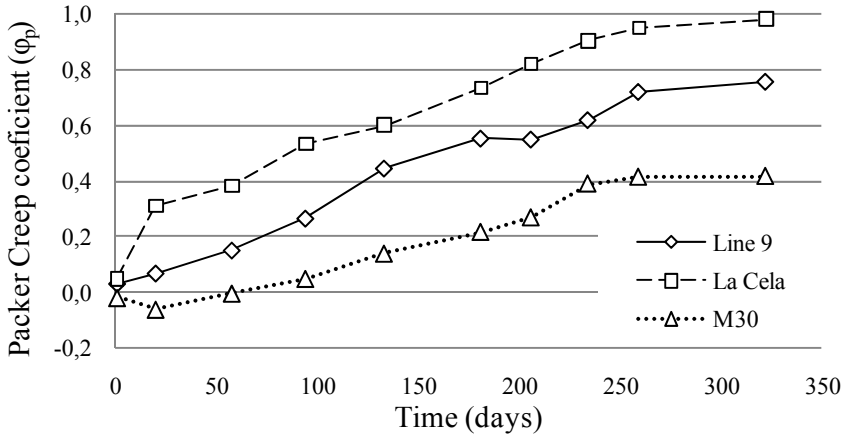

Figure 4.15. Measured packer creep coefficient (φ_p) at 4 N/mm^2.

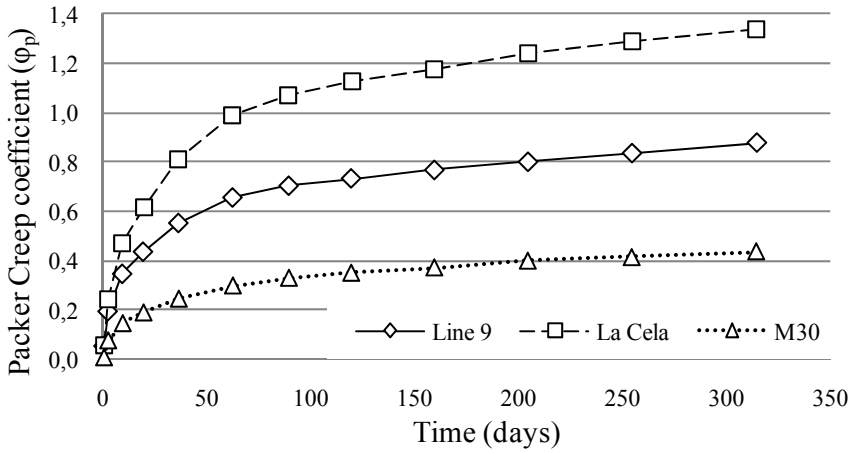

Figure 4.16. Measured packer creep coefficient (φ_p) at 20 N/mm^2.

The 20 MPa results are employed to perform a curve fitting based on Eq. 4.15, which corresponds to the usual formulation used in the definition of the concrete creep coefficient. Table 4.5 summarizes the obtained values for *A*, *B* and *C* parameters and its corresponding correlation factor r^2, showing the agreement of the packers response to the selected expression (Fig. 4.17). Assuming that packers creep evolves as expressed in Eq. 4.15, the expected creep coefficients for long term analysis (10000 days) are 1.50 for the La Cela packer, 1.05 for Line 9 packer and 0.53 for M30 packer.

$$\varphi_p(t-t_0) = A\cdot\left[\frac{(t-t_0)}{B+(t-t_0)}\right]^C \qquad \text{(Eq. 4.15)}$$

Table 4.5. Values obtained for packers creep coefficient curve fittings.

Packer	*Value of parameters:*			*Correlation coefficient* r^2
	A	*B*	*C*	
Metro of Line 9 (Barcelona)	1.0565	233	0.349	0.9874
Metro of La Cela (Madrid)	1.512	96.37	0.495	0.9963
Road tunnel in M30 (Madrid)	0.5355	210.2	0.4127	0.9932

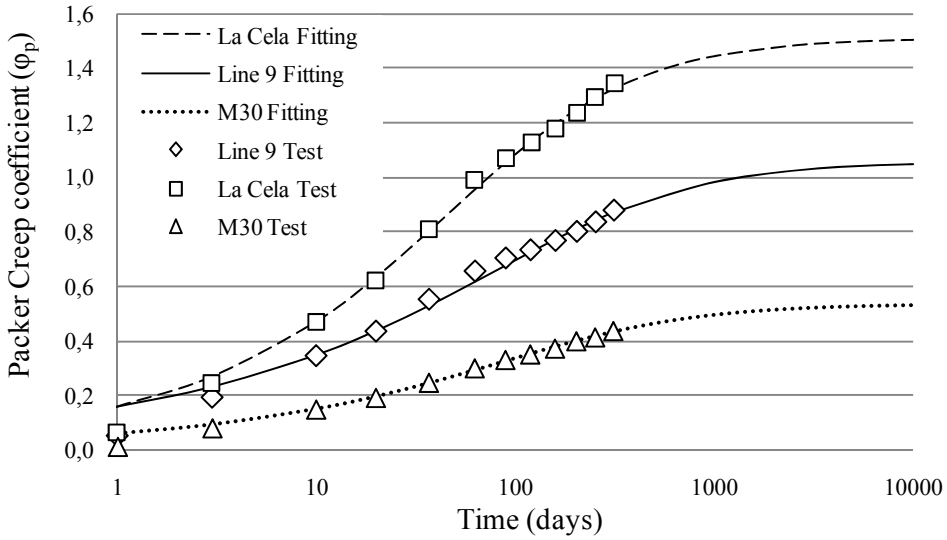

Figure 4.17. Curve fittings of packers creep coefficient.

4.4.3 Lining global creep coefficient

A formulation of a global creep coefficient (φ_G) is proposed in order to consider the long term deformation of packers in the longitudinal behavior of segmental tunnel linings. It is obtained by analyzing the total long term deformation of a set composed by the ring and the corresponding packer (Fig. 4.18). Its reference to the concrete elastic deformation (Eq. 4.16) will allow its direct use on the RCF formulation (Eq. 4.8) by replacing the concrete creep coefficient.

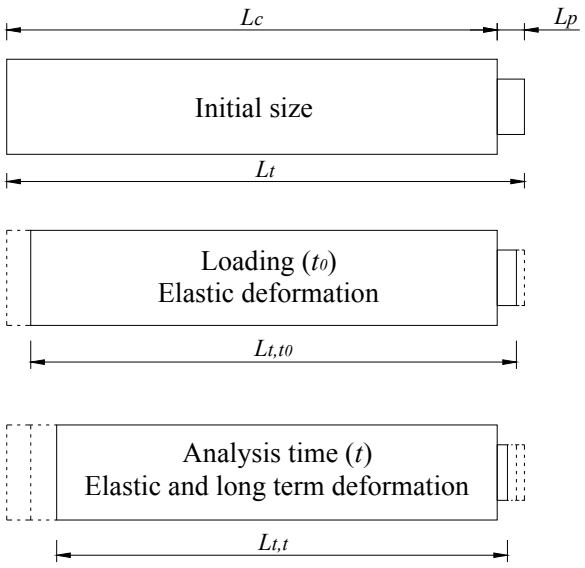

Figure 4.18. Deformation of a segment-packer pack at different stages.

$$L_{t,t} - L_{t,t0} = \varepsilon_{c,t0} \cdot L_t \cdot \varphi_G(t - t_0) \qquad \text{(Eq. 4.16)}$$

$$L_{t,t} - L_{t,t0} = \varepsilon_{c,t0} \cdot L_c \cdot \varphi_c(t - t_0) + \varepsilon_{p,t0} \cdot L_p \cdot \varphi_p(t - t_0) \qquad \text{(Eq. 4.17)}$$

The total long term deformation of a ring and packer set is described in equation 4.17. It is combined with equation 4.16 and the strain is expressed as function of the stress, providing equation 4.18. The use of the lateral surface aspect ratio (*AR*) allows determining the packer stress as a function of concrete stress. The final expression for the global creep coefficient of the lining $\varphi_G(t\text{-}t_0)$ is presented in equation 4.19.

$$\frac{\sigma_{c,t0}}{E_c} \cdot L_t \cdot \varphi_G(t - t_0) = \frac{\sigma_{c,t0}}{E_c} \cdot L_c \cdot \varphi_c(t - t_0) + \frac{\sigma_{c,t0} \cdot AR}{E_p} \cdot L_p \cdot \varphi_p(t - t_0) \qquad \text{(Eq. 4.18)}$$

$$\varphi_G(t - t_0) = \frac{E_c}{L_t} \cdot \left(\frac{L_c \cdot \varphi_c(t - t_0)}{E_c} + \frac{L_p \cdot AR \cdot \varphi_p(t - t_0)}{E_p} \right) \qquad \text{(Eq. 4.19)}$$

This expression (Eq. 4.19) can be simplified by assuming that the total ring width (L_t) is equal to the width of the concrete ring (L_c), giving a more compact formulation which allows an easier and faster comprehension of the involved parameters and their effect (Eq. 4.20).

$$\varphi_G(t - t_0) = \varphi_c(t - t_0) + \frac{L_p \cdot AR \cdot \varphi_p(t - t_0) \cdot E_c}{E_p \cdot L_c} \qquad \text{(Eq. 4.20)}$$

4.4.4 Influence of packer creep in a tunnel lining

In order to assess the influence of the packer creep on the remaining compression of the lining, the global creep coefficient of Model A tunnel (Table 4.2) with Line 9 packer is initially determined. The concrete creep (CEB-FIP Model Code, 1993), the packer creep (Eq. 4.15) and the tunnel properties listed in table 4.6 are applied to Eq. 4.19. The inclusion of the packer creep produces a significant increase of the global longitudinal creep of the lining (Fig. 4.19). For the long term analysis of the case study (10000 days), the global creep coefficient increases from 1 to 1.524 (52.4 %), producing the reduction of the RCF value from 0.474 to 0.357. This means that disregarding the packers creep in the case study would produce an overestimation of 32.7 % of the lining remaining compression.

Table 4.6. Parameters adopted for the global creep coefficient calculation of Model A with Line 9 packer.

Properties / Parameters	
Concrete deformation modulus, E_c (N/mm^2)	36246
Packer deformation modulus, E_p (N/mm^2)	202.1
Concrete ring width, L_c (mm)	1800
Packer thickness, L_p (mm)	2
Total ring width, L_t (mm)	1802
Concrete-Packer Aspect ratio, *AR*	2.5

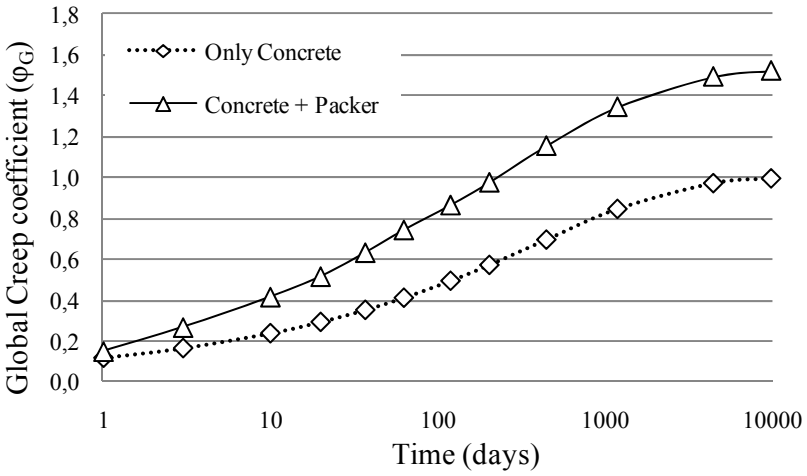

Figure 4.19. Global creep coefficient of Model A with and without Line 9 packer.

4.5 CONCLUSIONS

The particular configuration of segmental tunnel linings produces that their structural response depends on the existent longitudinal force. As a consequence, it is necessary to analyze the longitudinal ground-structure interaction in order to determine the longitudinal force remaining on the lining during its service life.

The theoretical and numerical studies carried out demonstrate that segmental tunnel linings present a longitudinal time-dependent behavior which depends on the combination of the particular construction process and the long term deformations of their constitutive materials, i.e. concrete and packers. The longitudinal creep deformations of the lining produce a stress relaxation process that involves a gradual loss of the longitudinal compressive force initially introduced by the TBM.

A formulation to predict the remaining compression stress (RCF approach) is proposed. It is based on the longitudinal creep coefficient of the lining, presenting an excellent agreement with numerical results for mid and long term analyses. Significant reductions of more than 50% of the initial stress are obtained after 10.000 days (27.39 years) for favorable tunnel conditions. Numerical simulation allows the complete determination of the tunnel longitudinal stress evolution, since the construction process until the long term stationary conditions.

Additionally, a formulation to determine the length of the anchorage zones (L_{an}) at the end of the lining or under substantial changes of the TBM force is given. This formulation shows excellent agreement with the numerical results, as long as the ground and its interface with the structure remain in the linear elastic stage.

The longitudinal long term deformation of a lining depends on the response of both the concrete and the packer. An experimental program was specifically designed to determine the creep of different plastic packers, obtaining significant long term strains which can be analytically described similar to concrete creep. The combination of concrete and packers creep in a global creep coefficient of the lining (φ_G) shows the significant influence of the packers despite their reduced thickness. The consideration of packers creep produces a further increase of the global lining creep, reducing the long term compression stress that remains in the tunnel lining.

The description of the time-dependent longitudinal response of segmental tunnel linings allows the determination of the mechanisms and the variables that cause the longitudinal force loose in segmental tunnel linings. As a consequence, it is possible to adapt the construction process, materials and designs if the force loose wants to be reduced. The proposed formulations to predict the remaining compression factor and the anchorage

lengths define an interesting tool for design engineers in order to predict the longitudinal stress state of the lining and, then, to assess the interaction capacity between adjacent rings and the consequent three dimensional response of the lining.

ACKNOWLEDGEMENTS

The authors want to thank the construction company FCC Construcción, S.A. for its involvement in the research of the behavior of the packers and their structural influence. The first author also wants to thank the support of the University and Research Commissioner of the DIUE of the Generalitat de Catalunya and also the European Social Fund (ESF).

Chapter 5

THREE DIMENSIONAL STRUCTURAL RESPONSE OF SEGMENTAL TUNNEL LININGS

ABSTRACT

The particular configuration of segmental tunnel linings produces that its structural response in front of usual design loads could present a significant three dimensionality due to the structural interaction between adjacent rings (coupling effects). The present paper studies the phenomena associated to coupling effects, determines the main involved parameters and analyzes their influence on a real lining structural response by means of a 3D numerical model. The comparison with the usual plane models currently employed in linings designs provide significant conclusions about the coupling effects implications and the conditions in which become more relevant.

***Keywords*:** Segmental tunnel linings, coupling effects, 3D response, numerical simulation, nonlinear analysis.

5.1. INTRODUCTION

The evolution and improvement of the modern tunnel boring machines (TBMs) allows the construction of tunnels at an increasing range of depths, dimensions and ground conditions. As the TBM advances, a segmental lining composed of multiple adjacent concrete rings is continuously placed (Fig. 5.1). This segmental lining provides both the structural capacity to resist the ground and water pressures and the necessary reaction frame to push the TBM ahead. Each ring comprises a certain number of concrete segments, creating a multiple-hinged structure that presents a complex structural behavior (Muir Wood, 1975; Blom, 2002; Teachavorasinskun and Chub-uppakarn, 2010). The staggered configuration of the joints (masonry layout, Fig. 5.1) is commonly employed with the main objective of minimizing the sealing problem when four corners of the segments coincide (cross joints) (Blom, 2002; Guglielmetti *et al.*, 2008).

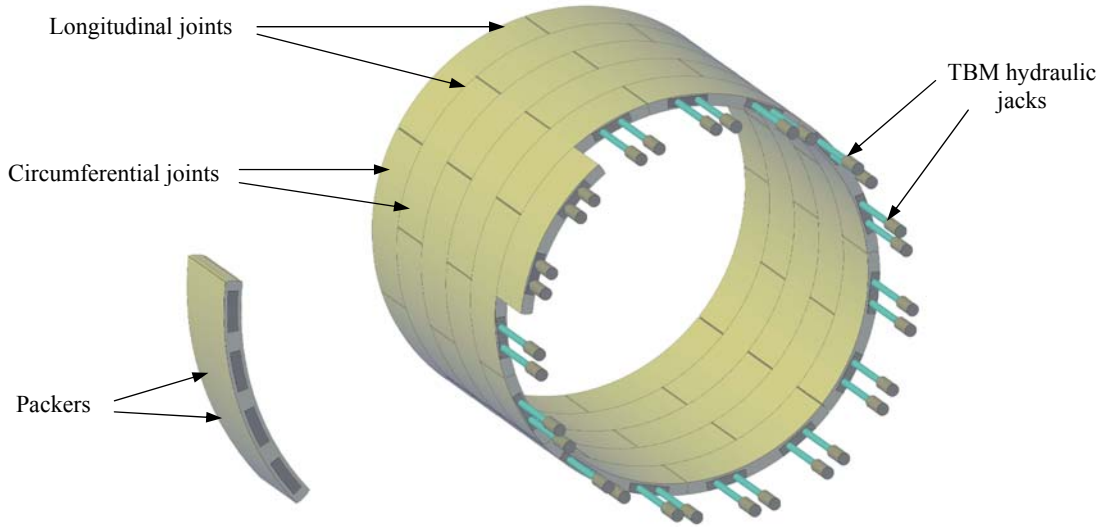

Figure 5.1. Segmental tunnel lining.

Usual tunnel conditions imply a nearly hydrostatic pressure that smoothly varies along the tunnel course. The longitudinal homogeneity of the ground produce that adjacent rings present the same load scheme and the consequent similar deformations that should not produce significant three dimensional responses. Despite that, the existence of coupling effects between adjacent rings is commonly accepted for linings with the staggered configuration of the joints. It is assumed that part of the bending force of a ring is transferred to the adjacent ones by means of the shear capacity of the circumferential joints (between adjacent rings) (Fig. 5.2). Initial attempts to consider this interaction were based on the inclusion of a transfer ratio of bending forces (ζ) in the analytical formulations employed to determine the member forces in segmental linings (JSCE, 1996; Koyama, 2003) (Fig. 5.2). The main handicap is the selection of its value according to the

particularities of the tunnel that is being designed. JSCE (1996) recommends a value of ζ between 0.3 and 0.5 based on the experience and the experimentation. Despite that, the usual design practice is based on the isolated ring models, maybe due to the lack of contrasted knowledge about the real coupling effects of rings.

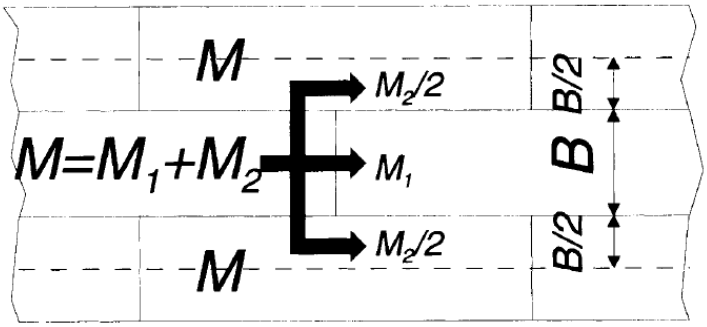

$$\zeta = M_2 / M$$

Figure 5.2. Conceptual scheme of the bending forces transference ratio, ζ. (Koyama, 2003)

The structural interaction between adjacent rings mainly depends on the joints configuration. Packing materials are placed in circumferential joints in order to properly transfer the longitudinal advance force of the TBM through the rings and to regularize the contact surface (Fig. 5.1). Packers are usually made of wood or plastic compounds and present a small thickness (around 2mm). The majority of the tunnel projects present a planar configuration of the circumferential joints and, therefore, the force transferences between rings are exclusively performed through the packers. The structural interaction in front of radial loads is therefore conditioned by the tangential force capacity of the packer-concrete pack, which response is clearly determined by a frictional mechanism. The normal stress presented at packers due to the applied longitudinal force, determines the tangential capacity of the circumferential joint before its slipping. As a consequence, the assessment of the three dimensional response requires the consideration of the longitudinal force present at the lining (Blom *et al.*, 1999; Mo and Chen, 2008). Additionally, part of this force is progressively lost as time goes by due to the longitudinal creep of the lining (Arnau *et al.*, 2012). Therefore, the structural interaction between adjacent rings can be modified with the aging of the structure.

A few tunnel projects, mainly subjected to bad soil conditions, include a dowel and socket system in order to limit the differences in deformation between adjacent rings (Blom, 2002). As a consequence, in dowel and socket joint, the packer only transfers tangential forces until the dimensional tolerance of the dowel and socket system is exhausted.

Some research programs have been developed in order to analyze the coupling effects on segmental tunnel linings subjected to longitudinally uniform design loads. Main

conclusions pointed out the increase of the lining stiffness caused by coupling effects, reducing the experienced deformation and increasing the internal bending forces. Blom (2002) developed an analytical model to study the effect of different circumferential joint stiffness for a certain tunnel case. He concluded that stiffer joints imply a significant increase of the ring internal bending forces (from 1.3 to 1.8 times the values obtained with the isolated ring) and a minor reduction on the movements, in comparison with those obtained by the isolated ring model. Klappers *et al.* (2006) studied a particular tunnel configuration under longitudinally uniform design loads by using two different models: a 2D spring coupled beam model and a 3D shell elements FE model. The influence of different longitudinal force levels from 40MN to 5MN are analyzed through assuming a packer-concrete friction coefficient of μ=0.5, average value obtained in the tests performed by Gijsbers and Hordijk (1997) on plywood packers. Klappers *et al.* (2006) concluded that the real behavior of the joints must be taken into account within the structural analyses of segmental lining and, also, that the value of longitudinal force does not significantly influence the lining response. For uniform design loads, it is not necessary to employ a 3D model due to the similar results provided by the simplest beam spring model with coupled rings.

Despite the agreement in the significance of properly considering the longitudinal joints response, both Klappers *et al.* (2006) and Blom (2002) models use rotational springs to simulate the segments connection and analyze a unique and particular case of tunnel subjected to a unique load conditions. In fact, some segmental linings are analyzed by employing a rigid ring model, which stiffness is commonly reduced by means of the Muir-Wood formulation (Muir Wood, 1975) in order to consider the longitudinal joints influence. Longitudinal joints present a complex non linear response caused by their incapacity of transferring tensile stresses, originating a gapping phenomenon from certain degree of rotation (Blom, 2002; Arnau and Molins, 2011). Their rotational response depends on the axial stress level, thus increasing the complexity of its appropriate consideration on the numerical models for structural analysis. As a consequence, it is necessary to employ advanced modeling procedures that include the accurate simulation of the joint behavior when the three dimensional response of a segmental tunnel lining is studied.

The present paper analyzes the influence of the interaction between adjacent rings in the structural response of segmental tunnel linings when they are subjected to typical design loads (longitudinally uniform). A theoretical analysis of the structural resistant mechanisms is carried out in order to establish the main parameters involved on the three dimensional response of the tunnel linings. A three dimensional finite elements model of a real tunnel section is performed, applying modeling techniques that allow the simulation of

both the joints responses and the material behavior. A sensitivity analysis is performed in order to assess the influence of some parameters such as: the ground stiffness, the actual load and the remaining longitudinal force, on the three dimensional response of the structure. The results obtained allow to conclude about the influence of the main involved parameters and to determine the conditions in which coupling effects are relevant by comparing with the isolated ring results. The comparison of the results of the 3D model with those provided by common design simplifications illustrates the advantages and drawbacks of the latter, providing useful information for the design process of segmental tunnel linings.

5.2. RINGS INTERACTION MECHANISMS

When an individual ring is loaded (Fig. 5.3a), it deforms according to its flexibility until the ground provides the necessary reaction (F_{GR}) to equilibrate the loads. The ground deformation to achieve such reaction depends on the surrounding ground stiffness and, therefore, it will play a decisive role on the radial displacements experienced by the ring (Fig. 5.3b).

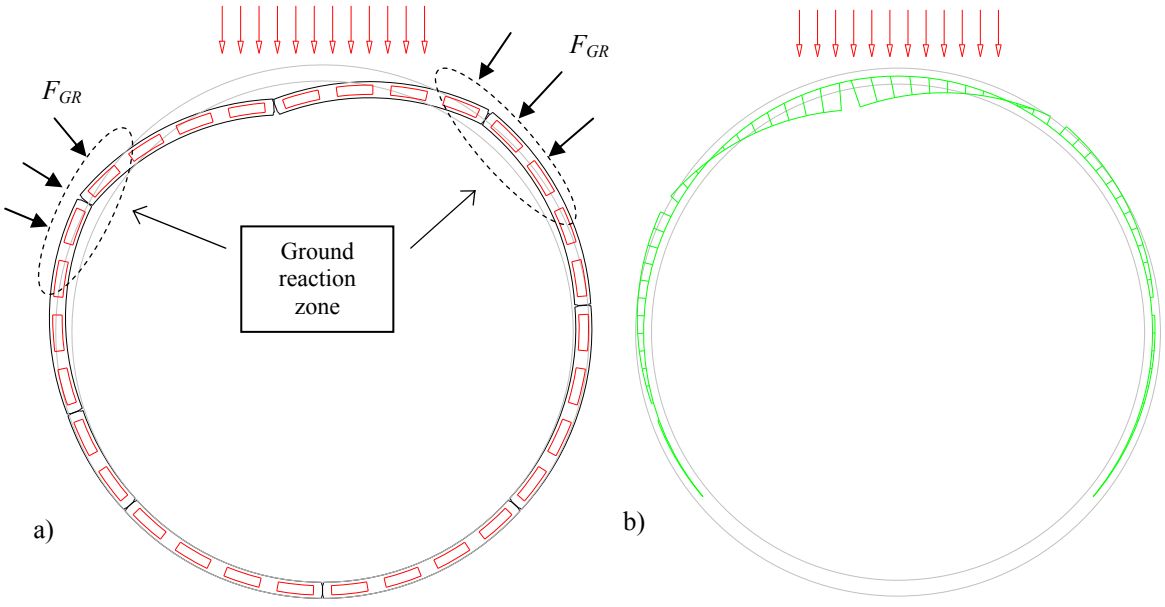

Figure 5.3. Ring radial response mechanism (a) and displacement (b) in front of a localized load.

Whilst concrete segments remain undamaged (with no cracks), the movements of the ring are mainly caused by concentrated rotations in longitudinal joints (Molins and Arnau, 2011). The contact zone of the longitudinal joints presents a smaller height than concrete segments, providing a lower mechanical inertia and hardly conditioning the flexibility of

the ring. Additionally, the rotational stiffness of the longitudinal joints became severally reduced since gapping phenomenon occurs.

Figure 5.3 shows the individual response of a ring in front of a localized load. In fact, the relative radial displacements between adjacent rings produce the shear deformation of the packers, originating the transference of tangential forces between them. The shear response of the circumferential joints determines the structural interaction between adjacent rings and, consequently, the degree of three-dimensionality of the lining behavior. Further reduction of the ground stiffness will result in higher differential radial displacements between adjacent rings, increasing the tangential force transferred and the influence of the structural interaction of rings.

Coupling effects can also influence the lining response when it is subjected to longitudinally uniform loads. The appliance of a perfectly hydrostatic pressure to a tunnel section (Fig. 5.4a) produces a pure compression state of the rings. Therefore, no movements are experienced in longitudinal joints and no interaction is expected between rings due to the same deformation of all of them. Commonly, the real pressure experienced by a tunnel is more similar to figure 5.4b, presenting differences between the vertical and the horizontal pressure due to the ground mechanical response. The resistance of this load unbalance requires the ovalization of the ring in order to find the necessary ground reaction to equilibrate the load. Different radial positions of the longitudinal joints between adjacent rings produce small differences in their deformations (Fig. 5.5a). As a consequence, relative radial displacements occur between adjacent rings (Fig. 5.5b), activating the tangential force transference mechanisms and modifying the expected structural response of an isolated ring.

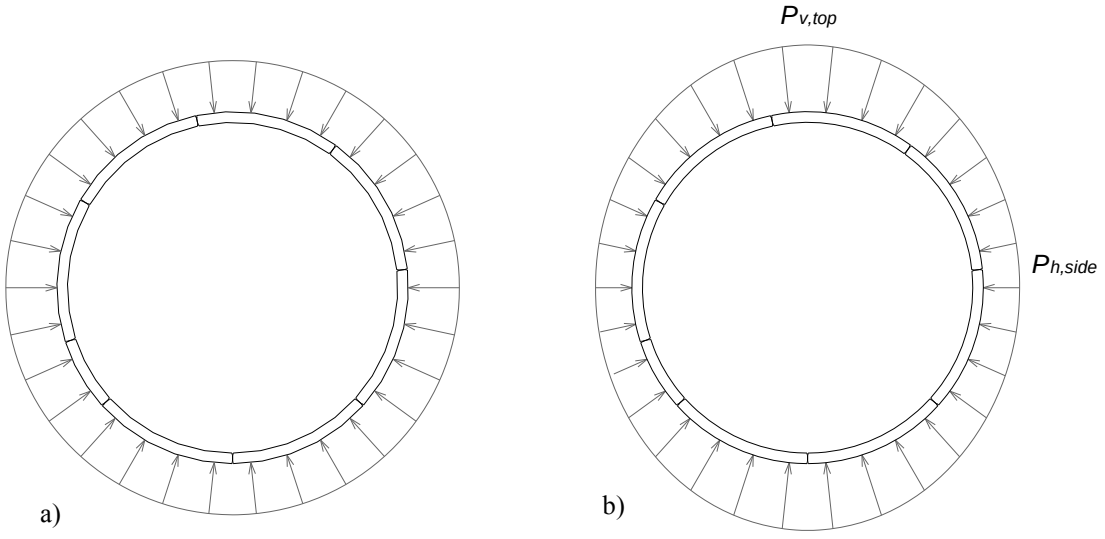

Figure 5.4. Perfectly hydrostatic pressure (a) and tunnel typical external pressure (b).

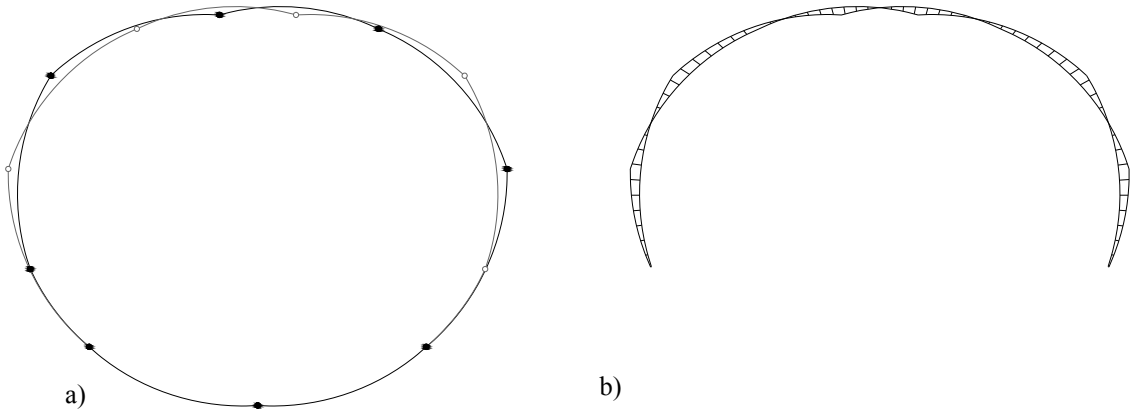

Figure 5.5. Different deformation of two adjacent rings subjected to the load pattern of Fig. 4b (a) and the resulting radial relative displacements (b)

Load unbalance cannot be directly analyzed as the difference between the maximum and the minimum pressures. The longitudinal joints response depends on the circumferential compression of the ring and, therefore, the load unbalance has to be related to the general magnitude of the load. In the present paper, the load unbalance is analyzed by means of equation 5.1 (ovalization load, *OVL*), which describes the difference between the mid tunnel horizontal pressure ($P_{h,side}$) and the crown vertical pressure ($P_{v,top}$) in respect to the last one (Fig. 5.4b).

$$OVL = \frac{P_{v,top} - P_{h,side}}{P_{v,top}} (\%) \qquad \text{(Eq. 5.1)}$$

In summary, the most influencing parameters on the coupling effect for a certain structure configuration would be the ground stiffness and the unbalance of the ground load. Additionally, the longitudinal force present at the lining has to be also considered due to its influence on the capacity of the circumferential joints to transfer shear loads between adjacent rings.

5.3. RINGS INTERACTION UNDER DESIGN LOADS

The present section analyzes the structural response of the lining when it is subjected to design loads (longitudinally uniform). The main objective is the analysis of the most important parameters involved in the coupling effects in order to determine its influence on the lining response. An advanced 3D FE model of a real section composed of eleven rings is developed to adequately reproduce the lateral interaction between adjacent rings. Results are compared with those obtained in an isolated ring model, showing the significance of the coupling effects on the segmental tunnel linings structural response.

5.3.1 Case study and model description

In order to perform the study on a real structure, a section of eleven rings of Line 9 (L9) subway tunnel of Barcelona is modeled (Fig. 5.6). These rings are composed by 7 conventional segments (A, B and C) plus 1 key segment (K), with an external diameter of 11.6m, 0.35m thickness, 1.80m width and 0.57º conicity (Molins and Arnau, 2011). The particular location of the K segment in each ring is reproduced in the model (view table 5.1).

Table 5.1. K segment positions of the modeled section of Line 9 Tunnel.

Modeled Ring number	*1*	*2*	*3*	*4*	*5*	*6*	*7*	*8*	*9*	*10*	*11*
K angular position (º)	138	114	234	354	18	306	66	210	90	282	210
Z initial	0	1802	3604	5406	7208	9010	10812	12614	14416	16218	18020
Z final	1800	3602	5404	7206	9008	10810	12612	14414	16216	18018	19820

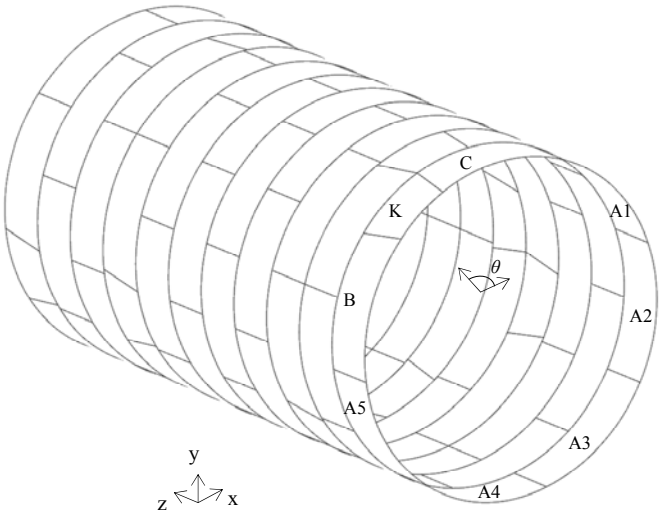

Figure 5.6. View of the 16 ring model of L9.

Every concrete segment is modeled by means of 216 4-node quadrilateral shell elements (and 108 in the k segments due to its reduced size). Initial model assumes a concrete linear behavior, presenting an elastic modulus of 38.700 N/mm^2 and a Poisson ratio of 0.2. In some of the analysis (section 5.3.3), a more realistic material behavior of reinforced concrete is considered, including both cracking in tension and crushing in compression for the concrete and yielding of the steel reinforcement bars.

The response of the longitudinal joints, which present a concrete to concrete contact surface of 204mm height, is modeled by means of nonlinear interface elements that present a rigid response in compression whilst gapping is produced in tension (Arnau and Molins,

2011). Each circumferential joint presents a total amount of 30 2mm thick plastic packers. All packers also present a height of 204mm and encompass an angle of 8º, defining the segment lateral configuration that is presented in figure 5.7 (except for K segment which only encompasses 2 packers).

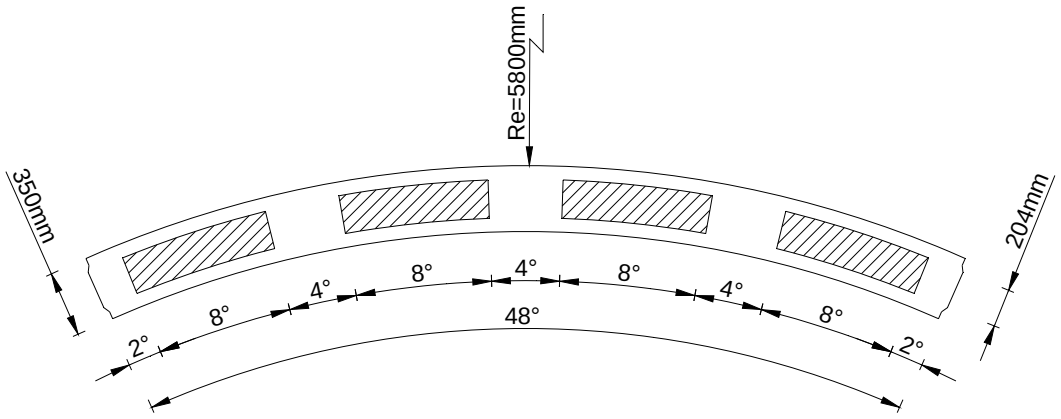

Figure 5.7. Packers configuration of L9 circumferential joint.

Every packer is modeled according to its actual position by means of interface elements connecting the shell one's of the segments. The frictional behavior of the plastic packer is modeled by means of a Mohr-Coulomb constitutive equation, which includes gapping. The elastic properties of the packer are an elastic modulus (E_p) of 202.1 N/mm^2 (Arnau *et al.*, 2012) and a shear modulus (G_p) 77.7 N/mm^2. The determination of the friction coefficient is based on the tangential resistance tests performed by Cavalaro (2009) on L9 packer at three different normal stresses. The linear regression of the tangential stress values that produce the slipping of the packer provide the friction coefficient to take into account in the model, μ=0.2076 (Fig. 5.8). A gap formation value of 0.278 N/mm^2 is assumed in order to consider the small joint prestressing originated by the tightening of the provisional steel bolts employed during the ring erection process. The influence of the waterproof gaskets is not considered.

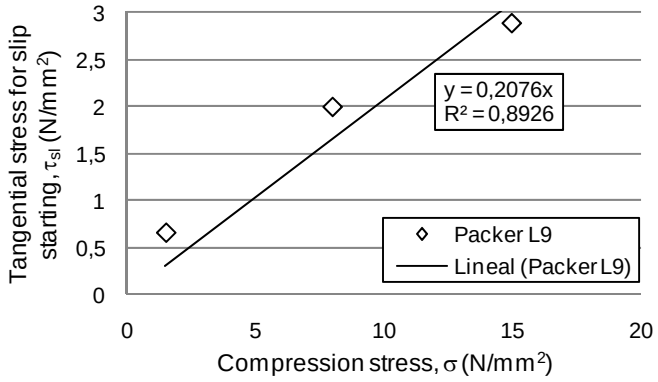

Figure 5.8. L9 packer-concrete friction coefficient obtained from the test performed by Cavalaro (2009).

The ground-structure interaction is modeled by means of spring elements placed in radial, tangential and longitudinal directions (Blom *et al.*, 1999; Arnau and Molins, 2011; Plizzari and Tiberti, 2006). Unilateral response is assigned to radial springs in order to allow the loose of contact with the ground, determining its stiffness (K_r) according to Eq. 5.2, which corresponds to the analytical solution of a circular tunnel in elastic ground (R define the tunnel radius and E_s the ground modulus of elasticity). Tangential (K_t) and longitudinal (K_l) stiffness (Eq. 5.3 an Eq. 5.4) are assumed as 1/3 of the radial one (Molins and Arnau, 2011), assuming a Poisson ratio of ν=0.3. The description and the amount of finite elements used in the three dimensional model are shown in Table 5.2.

$$K_r = \frac{E_s}{R \cdot (1+\nu)} \quad \text{(Eq. 5.2)} \qquad K_t = \frac{K_r}{3} \quad \text{(Eq. 5.3)} \qquad K_l = \frac{K_r}{3} \quad \text{(Eq. 5.4)}$$

Table 5.2. Finite elements types and characteristics employed in the numerical analyses.

	Description	*Quantity*
Nodes		20680
Segments Elements	Quadrilateral 4 nodes curved shell elements	17820
Packer Elements	Line interface shell elements, 2+2 nodes	1200
Segment joints elements	Line interface shell elements, 2+2 nodes	792
Spring elements	Translation spring element, 1 node	62040

The tunnel scenario presented in figure 5.9 is employed to determine the design loads of the case study according to equations 5.5 to 5.11. The tunnel crown presents an overburden of 25m whilst the groundwater table is located 15m below the surface. The ground presents a common density of γ_s = 18 kN/m^3 which is converted to γ_{sw} = 20 kN/m^3 when it becomes saturated of water (γ_w = 10 kN/m^3).

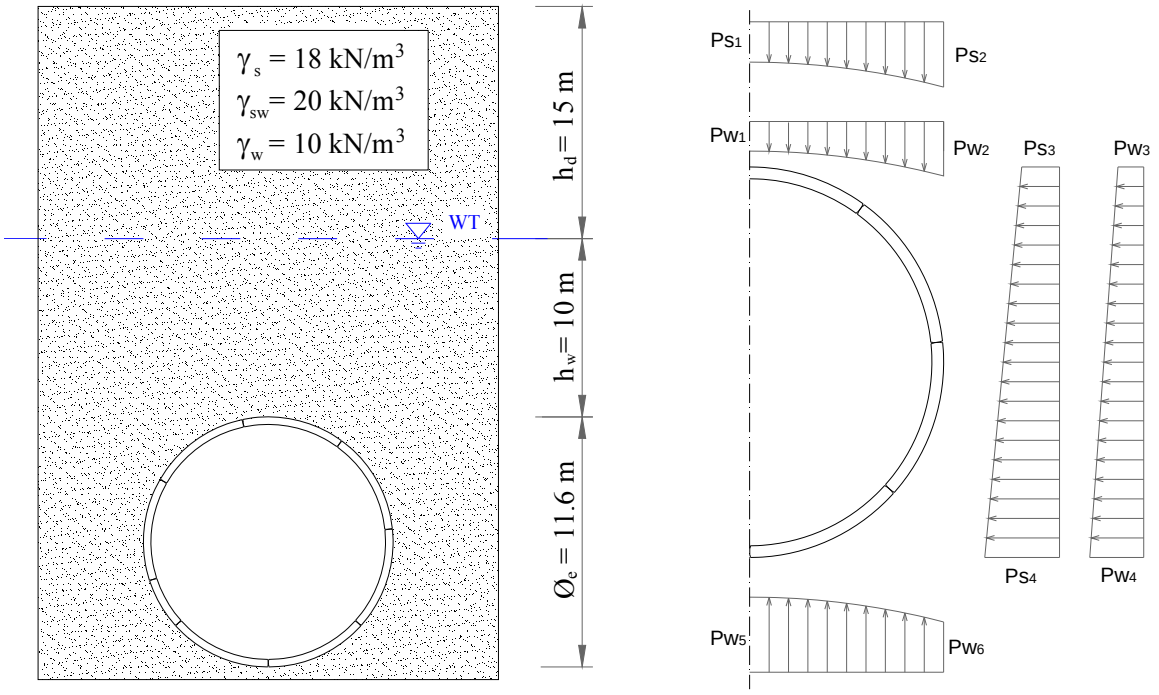

Figure 5.9. Selected tunnel scenario analyzed and the associated ground loads over L9 structure.

$$Ps_1 = h_d \cdot \gamma_s + h_w \cdot (\gamma_{sw} - \gamma_w) \quad \text{(Eq. 5.5)}$$

$$Ps_2 = h_d \cdot \gamma_s + (h_w + \varnothing_e / 2) \cdot (\gamma_{sw} - \gamma_w) \quad \text{(Eq. 5.6)}$$

$$Ps_3 = Ps_1 \cdot K_0 \quad \text{(Eq. 5.7)}$$

$$Ps_4 = \left[h_d \cdot \gamma_s + (h_w + \varnothing_e) \cdot (\gamma_{sw} - \gamma_w) \right] \cdot K_0 \quad \text{(Eq. 5.8)}$$

$$Pw_1 = Pw_3 = h_w \cdot \gamma_w \quad \text{(Eq. 5.9)}$$

$$Pw_2 = Pw_6 = (h_w + \varnothing_e / 2) \cdot \gamma_w \quad \text{(Eq. 5.10)}$$

$$Pw_4 = Pw_5 = (h_w + \varnothing_e) \cdot \gamma_w \quad \text{(Eq. 5.11)}$$

In order to analyze the influence of the load unbalance, the ground modulus of elasticity and the longitudinal force in the coupling effects, a comprehensive parametric analysis is performed using the three dimensional model. The ground lateral earth pressure (K_0) varies from 0.6 to 0.2 -to define the range of ovalization loads (Table 5.3)-, the ground modulus of elasticity (E_s) is varied from 25MPa to 150MPa -coupling effects are negligible for higher values of E_s-, and six different values of the longitudinal force (N) from 40 MN to 4 MN are considered (view Table 5.3). The combination of these parameters generates a total amount of 180 cases.

Table 5.3. Values for performing the parametric analysis.

Property	*Values*
Ground modulus of elasticity, E_s (N/mm^2)	25-50-75-100-125-150
Lateral earth pressure, K_0	0.2-0.3-0.4-0.5-0.6
Correspondent ovalization load, *OVL* (%)	48.2-39.1-30-20.8-11.7
Longitudinal force, *N* (MN)	40, 32, 24, 16, 8, 4
Total amount of cases	180

The adequate reproduction of the tunnel loading requires two different steps in the numerical model. Firstly, the longitudinal force is applied at both sides of the model, deactivating the ground-structure interaction in order to generate the initial longitudinal compression of the section, as occurs after assembling the rings inside the shield of the TBM. Then, the ground-structure is fully activated and the ground pressure is applied.

The lack of longitudinal force (0MN case) is considered as an isolated ring because coupling effects are then negligible. The central ring of the section (number 6 in Table 5.1) is employed to determine the structure response in such conditions.

The longitudinal force is a time dependant parameter due to its progressive reduction caused by lining creep. A comprehensive explanation of the phenomenon and a procedure to estimate the time evolution of the longitudinal force are presented in Arnau *et al*. (2012). In the present study, time is not considered as a varying parameter and all analysis are developed in stationary conditions.

Notice that the lining thickness of the case study could not be the optimal for some of the planned cases (i.e. for really soft grounds and high unbalanced loads it should be larger). However, it is necessary to assume a unique standard to properly contrast the results, and Line 9 provides all the data required for this application.

5.3.2 Results

Coupling effects produce that the radial displacement differences between adjacent rings originated by the staggered configuration of the joints is diminished, providing a stiffer response of the lining (Fig. 5.10). As a consequence, the global deformation of the lining is reduced whilst the internal bending forces increase.

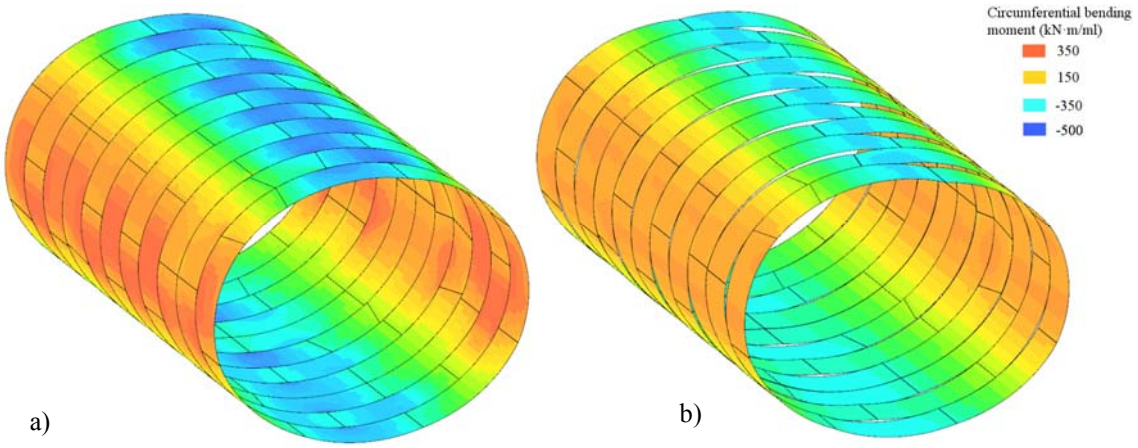

Figure 5.10. L9 Deformation and circumferential bending moment for E_s=25MPa, K_0=0.5 for the coupled system (N=40MN) (a) and uncoupled (b) (Deformation amplification factor = 18)

The study of the coupling effects influence on the lining deformation is carried out by analyzing the vertical ovalization of the central ring of the section (ring 6), defined as the difference between the vertical displacement on the top and the bottom of the ring. The effects on the internal forces are determined by analyzing the circumferential bending moments at the same central ring, which common response can be observed in figure 5.11.

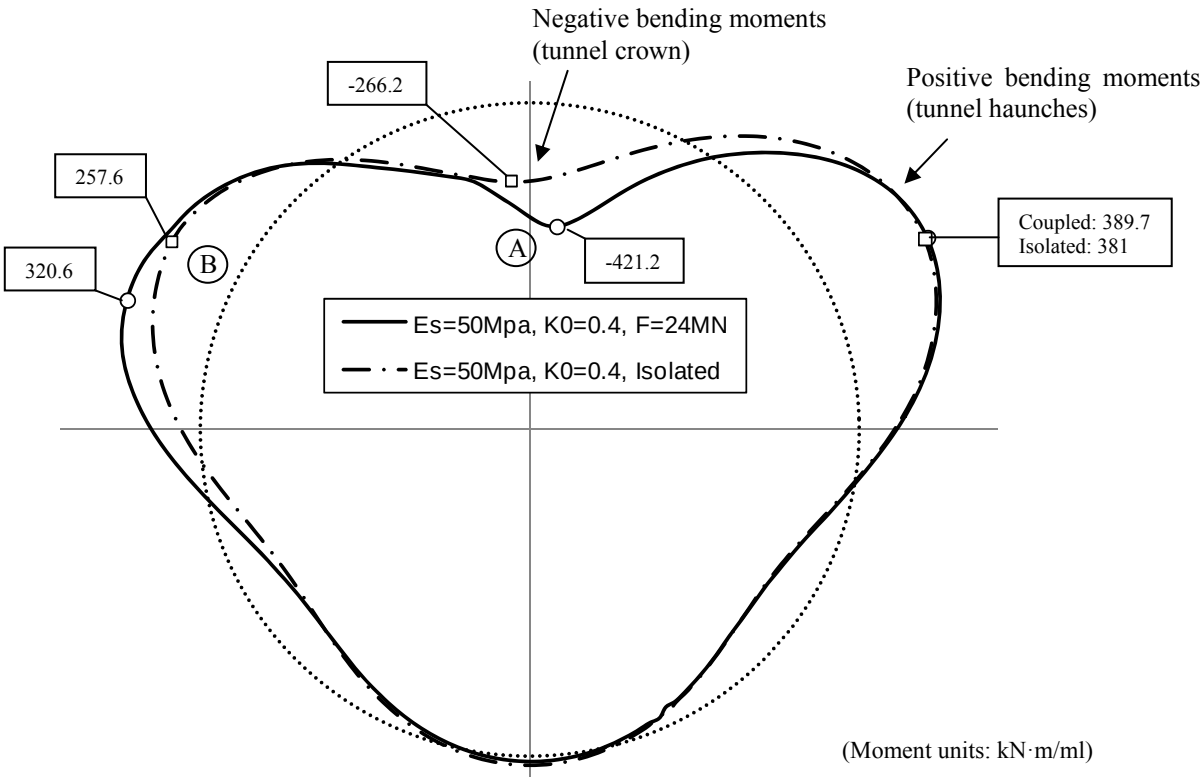

Figure 5.11. Representation of the circumferential bending moment of the central ring (6) for E_s=50MPa and K_0=0.4 in the coupled system (N=24MN) and in the isolated ring.

Maximum positive bending moments are produced in the haunches of the arch defined by the upper half of the ring whilst maximum negative bending forces are located close to the tunnel crown. Figure 5.11 clearly shows the local increase of the circumferential bending moments caused by the adjacent rings deformations. Points A and B correspond to the positions where the radial displacement difference and the consequent tangential force are maximum, clearly denoting the position of the adjacent rings longitudinal joints.

The numerical results of the maximum and minimum circumferential bending moments with a ground stiffness of 50MPa are presented in figure 5.12. As can be observed, the increase of the ovalization load (decrease of K_0) implies the production of higher bending forces at the tunnel crown zone with respect to the isolated ring results, achieving a maximum increase of 146% for K_0=0.2 and 59% for K_0=0.4. The presence of a small longitudinal force is enough to produce coupling effects, which appear to be independent of the force magnitude out of high ovalization loads. For low ovalization load, (E_s=50, K_0=0.6) the coupling effects are not presented, obtaining the same results than in the isolated ring for all longitudinal forces.

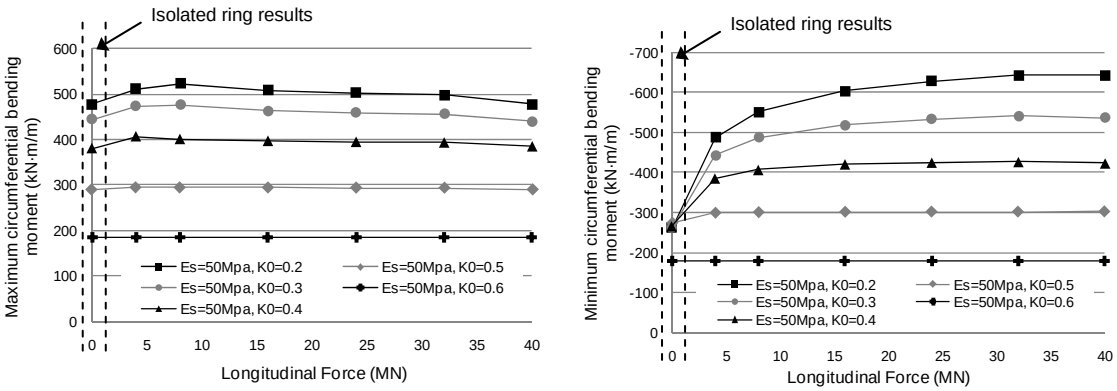

Figure 5.12. Maximum (positive) and minimum (negative) values of the internal bending forces for the central ring of the section (ring 6) for the case of E_s=50MPa.

Contrarily, the maximum positive bending forces produced at the upper haunches of the tunnel do not show significant differences in all cases. Despite the difference in shape shown in the left haunch of figure 5.11, maximum values do not present differences respect to the isolated ring model due to their allocation on the stiffer haunch depending on the longitudinal joints positions.

For E_s=50 MPa, the isolated ring analyses provide similar crown bending forces for the majority of ovalization loads. This fact is caused by the exhaustion of the upper longitudinal joints capacity, increasing the obtained movements and presenting larger differences respect to the coupled analysis as K_0 value decreases.

The analysis of the ground stiffness E_s=150 MPa (Fig. 5.13) reveals that coupling effects are only presented for K_0=0.2 and K_0=0.3, showing increases of the crown bending moment of 34% and 16% respectively. As a consequence, stiffer ground conditions reduce the influence of the coupling effects, increasing the necessary ovalization loads to produce it, and diminishing its influence on the lining internal forces.

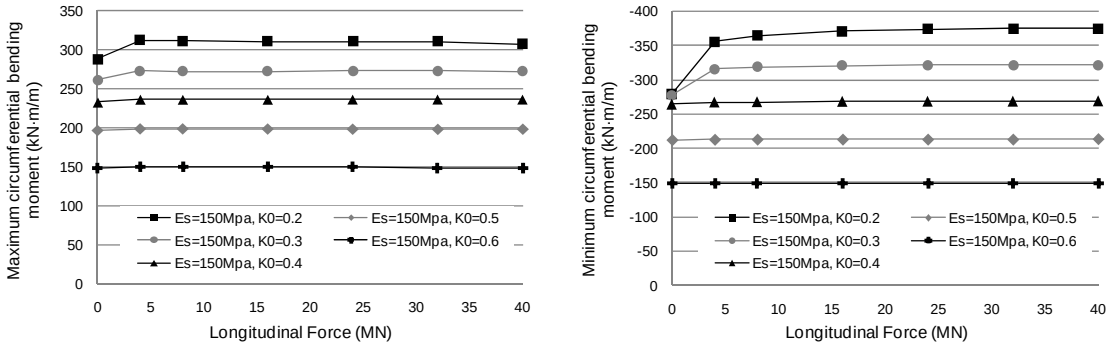

Figure 5.13. Maximum values of the internal bending forces for the central ring of the section (ring 6) for the case of E_s=150MPa.

The influence of the ground stiffness can be more accurately appraised in figure 5.14, where the increase of the tunnel crown bending forces and the reduction of the vertical ovalization respect to the isolated ring results are depicted. As can be observed, the consideration of the coupling effects only presents a significant influence on the obtained results when the segmental lining is analyzed in really soft ground conditions or for significant ovalization loads. For K_0=0.5, the coupling effect only influences the results for ground stiffness under 75 MPa, but for K_0=0.3, significant influences are obtained until E_s=150 MPa. The combination of both factors provides the highest coupled scenario, obtaining increments of bending forces up to 180% respect of the isolated ring for E_s=25 MPa and K_0=0.3.

Coupling effects also influence the deformations of segmental linings (Fig. 5.14). Reductions between 15% and 25% of the central ring vertical ovalization are obtained for really soft grounds, denoting the increase of the lining stiffness respect of the isolated ring consideration.

The diminution of the longitudinal force produces that the slipping of the packers starts for a lower tangential force. As a consequence, coupling effects are diminished, reducing the increase of the internal forces and providing larger lining deformations (Fig. 5.14). Despite that, significant influences of the longitudinal force magnitude are only presented for extremely soft ground and high ovalization pressures.

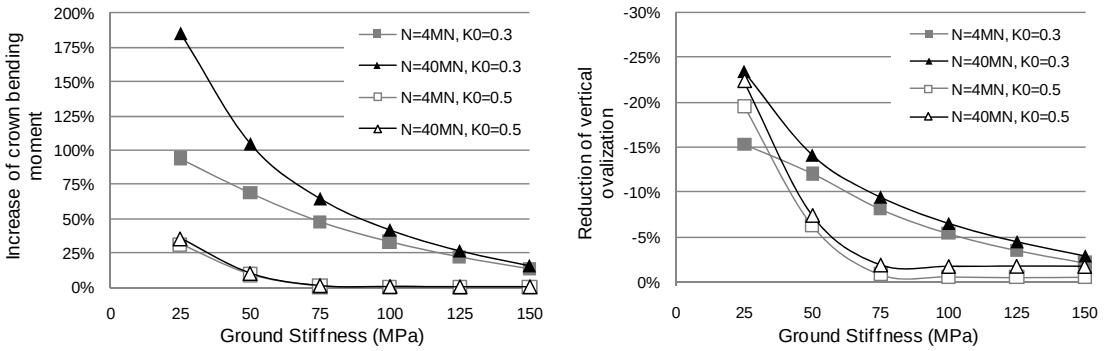

Figure 5.14. Influence of coupling effects respect to the isolated ring results.

The sensitivity analysis allows the determination of the ground stiffness and ovalization loads in which coupling effects play a significant role for the case study. The coupling influence zone (Fig. 5.15) determines the conditions where differences over 10% are obtained in vertical ovalization and bending moment respect to the isolated ring results. The longitudinal force value only presents influence when the reduction of vertical ovalization is considered.

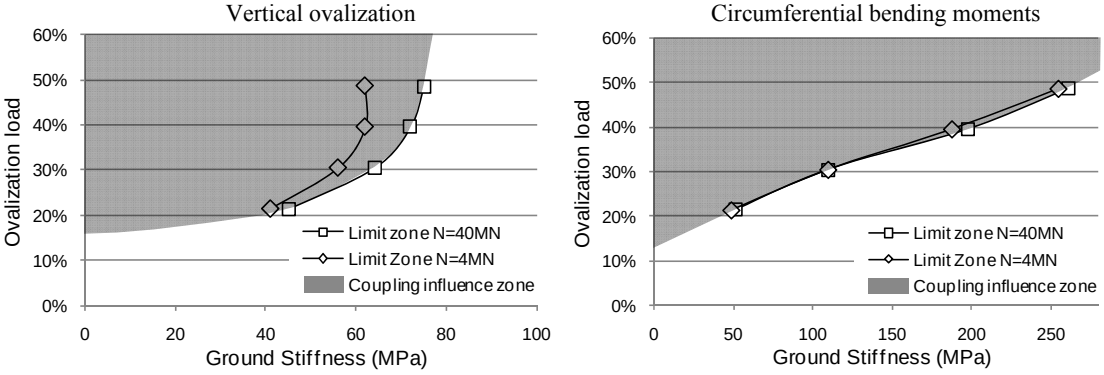

Figure 5.15. Coupling influence zones for deformation and circumferential bending moment.

These results are obtained for the rings configuration of table 5.1 compared with those provided by the isolated ring 6. Coupling effects produce that the lining behave more similar to a rigid pipe and, consequently, no significant differences are expected in respect to other sections of the same tunnel with different positions of the longitudinal joints caused by different rings configurations (K segment position, Fig. 5.6).

Segmental tunnel linings are confined in longitudinal direction by the surrounding ground. As a consequence, the radial loading of the rings can produce an increase of the longitudinal force of the lining due to the partial restraint of the transversal deformation (Poisson effect). For a certain ground load case, the circumferential axial stress should be similar for all longitudinal forces and, therefore, presenting similar increments. The performed analyses show that for usual cases, stiffer ground conditions provide higher increases of the longitudinal force despite the obtained values are small, achieving a

maximum of 0.42 MN for E_s=150 N/mm^2 (Fig. 5.16). Cases with reduced initial longitudinal force and significant rings deformations (combination of reduced ground stiffness and high ovalization loads), can present higher increments of the longitudinal force (Fig 5.16). This fact should be caused by movements of the rings that originate the dislocation of the segments, producing a small plane arch mechanism.

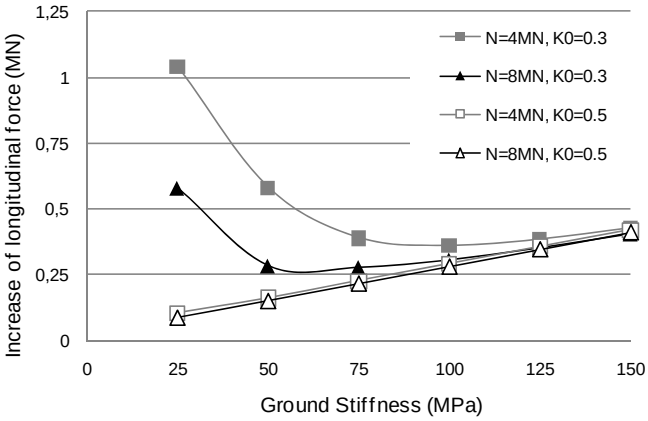

Figure 5.16. Increase of the longitudinal force caused by radial loading.

The magnitude of the displacements experienced by a certain ring also depends on its flexibility. More rigid rings imply lower deformations and, therefore, a reduced influence of the coupling effects is initially expected. Two additional analyses are performed in order to study the influence of the flexibility of the ring, and the relation between the segment thickness and the joint height. Firstly, the segment thickness is increased from 350 to 500mm while maintaining the same longitudinal joint height (Model A) and, later, the joint height is also increased in the same proportion as the segment (Model B) (Table 5.4). The vertical ovalization of the isolated ring results for E_s=50 K_0=0.5 presented in table 5.4 show the increase of rigidity for both cases respect to the original Line 9.

Table 5.4. Cases employed in the analysis of the influence of ring flexibility.

Case	*Segment thickness (mm)*	*Joint height (mm)*	*Isolated ring ovalization, E_s=50MPa, K_0=0.5 (mm)*
Line 9	350	204	20.45
Model A	500 (+42.9%)	204	16.33 (-20.1%)
Model B	500 (+42.9%)	291 (+42.9%)	10.88 (-46.8%)

Figure 5.17 presents the reduction of the vertical deflection and the increase of the bending moments respect to the isolated ring approach for K_0=0.5 and different ground stiffness. The general gains of rigidity of Model B, where both segments and joints are increased, produce a lower influence of coupling effects. On the other hand, the increase of the ratio

segment thickness- joint height (Model A) implies a significant increase of the coupling effects despite the reduction of the isolated ring flexibility. The exclusive increment of the segments stiffness (A) produces larger relative rotations in longitudinal joints to achieve the necessary ring deformation, increasing the radial displacement difference between adjacent rings. Additionally, the stiffness of the adjacent ring that tries to avoid the displacement difference is also higher, increasing the transferred force.

As a consequence, it can be concluded that coupling effects present a significant sensitivity to the relation between segments thickness and longitudinal joints response. This fact emphasizes the necessity of accurately reproduce the longitudinal joints response to achieve satisfactory results. In general, the global increase of the stiffness (both joints height and segment's thickness) produce a reduction of the coupling effects.

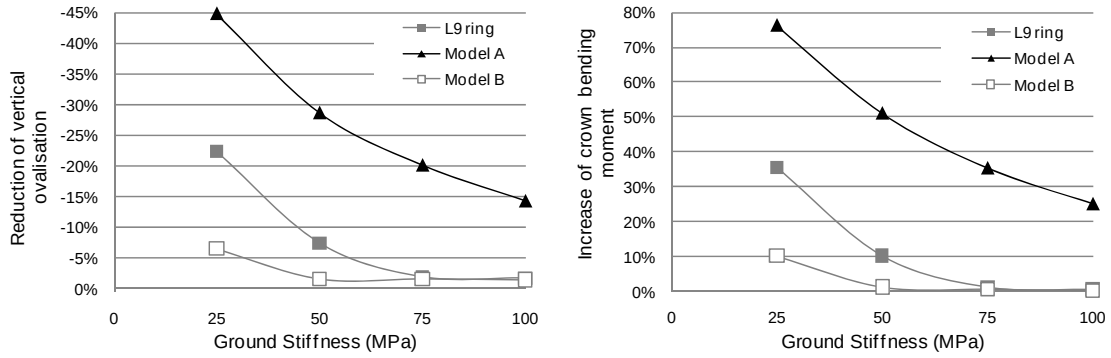

Figure 5.17. Influence of ring flexibility in coupling effects (K_0=0.5, N=40MN).

5.3.3 Neglecting coupling effects

In section 5.3.2 has been stated that bending forces obtained considering coupling effects can double the isolated ring approaches for soft ground conditions and high ovalization pressures. The structural design of segmental tunnel linings is commonly based on the isolated ring results and, therefore, it is necessary to determine the structural implications of neglecting coupling effects during the design process.

As can be expected, the increase of bending forces can achieve the cracking moment of the concrete section, producing changes in the stiffness of the structure and stress redistributions in this 3D system. In order to further analyze the structural response of the lining when cracking occurs, a non linear material version of the 3D model which properly considers the behavior of concrete and the reinforcement layout is developed. The Total Strain Rotate Crack model included in software Diana 9 is used, defining appropriate constitutive equations to simulate the reinforcement steel response, the concrete cracking in tension and its crushing in compression.

Two particular cases are analyzed; E_s=50MPa - K_0=0.4 and E_s=25MPa - K_0=0.4. The results of the isolated ring models were used to determine the design internal forces (table 5.5).The necessary amount of reinforcement for each case is determined by applying the Eurocode 2 regulations to the 350mm height section (Table 5.5), which is symmetrically adopted for both sides with a concrete cover of 50 mm.

Table 5.5. Design internal forces and obtained reinforcement for nonlinear material analyses.

Case	*Design Axial force, N_d (kN/m)*	*Design Bending force, M_d (kN·m/m)*	*Reinforcement (Both sides)*
E_s=50, K_0=0.4	3975	571.5	5Ø20 per meter
E_s=25, K_0=0.4	4035	664.05	5Ø25 per meter

The reinforcement of Table 5.5 is added to the 11 ring shell model by means of specific reinforcement elements, assigning them an elastic-plastic response with an elastic modulus of E_{steel}=200 GPa and a yield strength of f_y=500 N/mm^2. The concrete behavior is assumed as elastic-plastic in compression and brittle in tension, presenting an elastic modulus of E_c=38.7 GPa, a compressive strength of 50 N/mm^2 and a tensile strength of 4.1 N/mm^2. The analyses are performed progressively increasing the ground load for the maximum longitudinal force case (40MN).

Non linear material 3D model (NLM) results are compared with the ones obtained in the 3D linear material model and in the isolated ring model. In addition, to assess the influence of the coupling effects in front of usual design techniques, two different variants of a continuous ring are analyzed by suppressing the longitudinal joints in the isolated ring model. The first one adopt the thickness of the concrete segments (Rigid) whilst the second presents a smaller thickness (267.8mm) according to the equivalent inertia (I_e) proposed by Muir-Wood (1975) in order to consider the influence of the longitudinal joints (Eq. 5.12), where I and I_j are the segment and joint inertia respectively, whilst n define the number of joints of the ring.

$$I_e = I_j + I \cdot \left(\frac{4}{n}\right)^2 \qquad \text{(Eq. 5.12)}$$

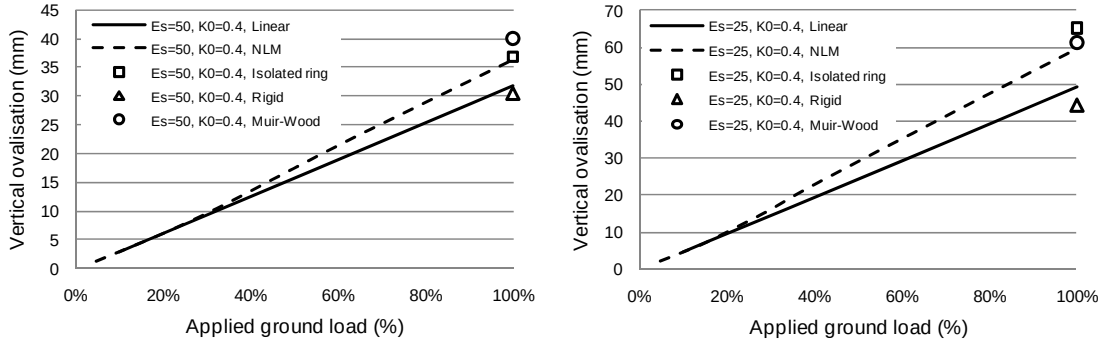

Figure 5.18. Vertical ovalization of central ring (6) obtained with different numerical approaches.

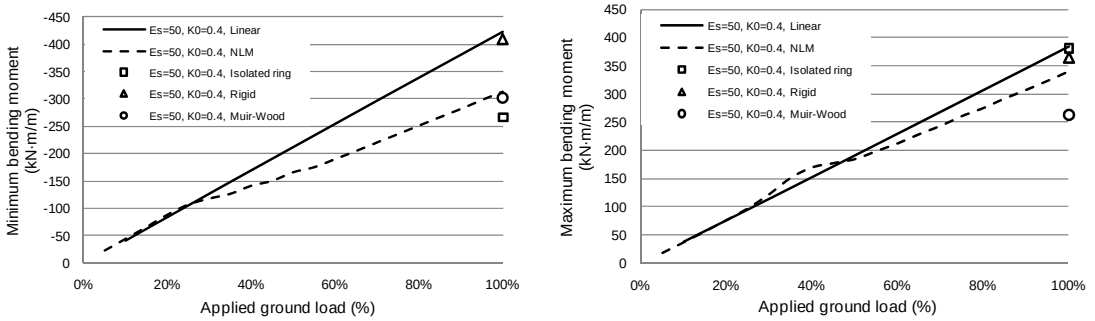

Figure 5.19. Central ring (6) maximum bending forces obtained with different numerical approaches (E_s=50 K_0=0.4).

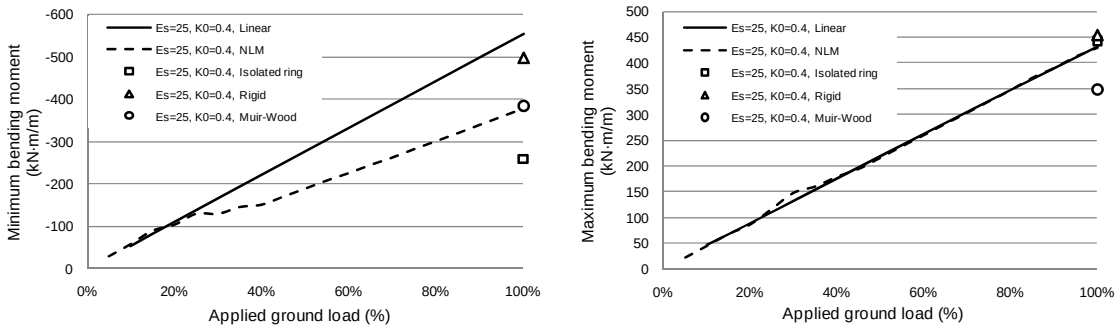

Figure 5.20. Central ring (6) maximum bending forces obtained with different numerical approaches (E_s=25 K_0=0.4).

The increase of the internal bending forces caused by coupling effects produces the concrete cracking on both cases, as can be clearly appraised in figures 5.18, 5.19 and 5.20 by the sudden separation of the linear response. This phenomenon implies a reduction of the lining stiffness, obtaining an increase of the central ring ovalization (Fig. 5.18). As a consequence, the isolated ring results and the Muir-Wood results present a good agreement with the expected deformation. The Rigid approach presents similar deformations than linear 3D model, according to the increase of the stiffness provided by the coupling effects.

Segments cracking produce redistributions of the bending moments, originating the diminution of the maximum and minimum values achieved (Fig. 5.19 and 5.20). The isolated ring results provide good general results with a slight underestimation of maximum negative bending moment, showing that certain degree of interaction remains in the structure despite segments cracking. According to that, favorable conditions for coupling effects (reduction of ground stiffness) imply an increase of the isolated ring approach deviation (Fig. 5.20). Muir-Wood results present an excellent agreement to the maximum negative bending moments for both cases but present significant differences for positive bending moments. This fact is caused by the assumption of a general diminished inertia, do not considering that joints close to the tunnel crown present more influence due to the applied load profile.

The analysis of the reinforcement tensile stress (Fig. 5.21) reveals that maximum values, and the consequent maximum crack widths, are presented in the laterals of the segments, where the tangential forces are transferred, diminishing with their advance to the center of the segments (Fig. 5.21).

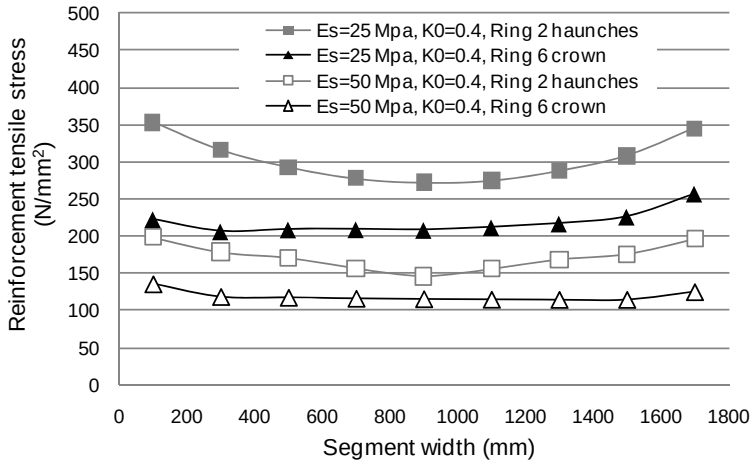

Figure 5.21. Reinforcement tension stress distribution across the section with the maximum crack opening (haunches of ring 2) and across the crown of the central ring (6).

The stress states of the segments and the reinforcements are employed to determine the maximum crack widths according to Eurocode 2 regulations (Table 5.6). Despite the significant influence that coupling effects present on the elastic internal forces of the lining, the sections designed from the isolated ring results present crack widths inside the limits established by concrete codes to accomplish the serviceability state. Therefore, despite the significant differences that coupling effects originate in lining stiffness and in linear bending forces, the consequences of employ an isolated ring model in the structural design of segmental tunnel linings should be acceptable out of extreme unfavorable conditions.

Table 5.6. Crack widths (w_m) obtained at the nonlinear material analyses of the lining section.

Case	*Central ring crown crack width (mm)*	*Maximum crack openings (mm)*		
		Position	*Center of the segment*	*Lateral of the segment*
E_s=50, K_0=0.4	0.08	Ring 2 haunches	0.11	0.15
E_s=25, K_0=0.4	0.12	Ring 2 haunches	0.15	0.2

In summary, the 3D nonlinear material analysis reveals that:

- The employment of an isolated ring model including longitudinal joints provides an underestimation of the internal bending forces, denoting that coupling effects still produce an increase of the lining stiffness despite the cracking of the segments. On the other hand, it was stated that the employment of the isolated ring results to design the lining reinforcement, should provide enough resistance to maintain crack widths inside the limits fixed by concrete codes for the serviceability state.

- The isolated rigid ring model, disregarding joints effects, presents a very good agreement in respect to the linear coupled analysis of the lining, clearly showing the inhibition of the longitudinal joints caused by coupling effects. As a consequence, the isolated rigid ring model could be useful to analyze cases affected by coupling effects but where segment's cracking is not achieved. In the case that loading produce cracking, rigid isolated ring provides an upper bound of the extreme bending forces, placing its employment for design purposes on the safety side.

- The reduction of rigid ring inertia proposed by Muir-Wood (1975) is uniformly applied to the whole ring, do not considering the fact that certain joints present more influence than others due to the load profile. As a consequence, very good agreement has been obtained in some results (displacements and negative bending moments) whilst a significant underestimation of the maximum bending moment is detected.

5.4 CONCLUSIONS

When a segmental tunnel lining is subjected to a longitudinally distributed design loads, the staggered configuration of its joints produces the activation of force interaction mechanisms between adjacent rings, originating the so called coupling effects. As a

consequence, the lining behaves as a 3D structure, presenting an increase of its stiffness and internal forces in respect to the isolated ring consideration.

The analysis of the lining radial response and the force transmission mechanisms between adjacent rings determines that, for certain segmental lining configuration (thickness, joints positions and height, packer materials, etc) ground stiffness, load unbalance and longitudinal force should be the most influence parameters in the coupling effects.

Results of the sensitivity analyses reveal that coupling effects are significant when the lining is embedded in soft ground conditions (below E_s=150MPa in the case study) or subjected to high unbalanced loads. Coupling effects produce a significant increase in lining radial bending forces respect to the isolated ring consideration, achieving on the case study increases over 150% for unfavorable conditions. The lining deformation is also reduced but in a minor significance, presenting maximum reductions of the vertical ovalization around 25%.

The necessary longitudinal force level to develop coupling effects is small compared with the usual forces exerted by the TBMs during the tunnel construction. As a consequence, the magnitude of the longitudinal force does not significantly influence the structural response of the lining out of the combination of really soft grounds and high unbalanced loads.

Coupling effects present a significant sensitivity to the relation segment thickness- joint height. Its increase implies greater influence of the coupling effects on the lining response. The general increase of certain ring stiffness (increasing both segment thickness and joint height) diminishes the significance of coupling effects. Then, the influence of the coupling effects increases with the slenderness of the lining.

The structural design of segmental tunnel linings is commonly tackled by means of isolated ring approaches and, therefore, it is necessary to determine the influence of neglecting the coupling effects. The increase of the internal forces generated by coupling effects can produce the segments cracking, reducing the lining stiffness and behaving in between a rigid pipe and an isolated ring. The employment of the isolated rigid ring model arises as a design option that provide an upper bond for the internal bending forces when coupling effects influences the segmental lining response.

ACKNOWLEDGEMENTS

The authors want to thank the construction company FCC Construcción, S.A. for its involvement in the research of the structural response of segmental tunnel linings through the research program *Túneles Urbanos*. The first author also wants to thank the support of the University and Research Commissioner of the DIUE of the Generalitat de Catalunya and also the European Social Fund (ESF).

Chapter 6

STRUCTURAL RESPONSE OF SEGMENTAL TUNNEL LININGS SUBJECTED TO LOCALIZED LOADS

6.1. INTRODUCTION

As it was previously explained in chapter 5, segmental tunnel linings are commonly subjected to nearly hydrostatic loads that smoothly vary along the tunnel track. However, there exist ground scenarios that can cause localized loads over a certain tunnel section or even a unique ring. These loads can present different origins like small faults in rocks, ground swelling phenomena or ground columns produced during the tunnel excavation due to the weakness of the surrounding ground.

Localized loads imply different loading of adjacent rings, obtaining the consequent different deformation. Therefore, significant radial relative displacements between adjacent rings are expected, producing a larger influence of coupling effects than in usual design load cases (chapter 5). Depending on the structural interaction presented by adjacent rings, the lining structural response in front of localized load will be more similar to an isolated ring or to a rigid pipe. In fact, all the tunnel situations that produce different structural responses of adjacent rings will be influenced by the same mechanism originated in localized loads. Therefore, coupling effects can present a significant influence on the structural response of the lining in tunnel openings, connections to shafts or between parallel tunnels, sudden changes in surrounding ground stiffness, etc.

Klappers *et al.* (2006) performed an analysis of a tunnel section with an opening (to build a cross passage between two tubes) by employing a 3D shell elements model (Fig. 6.1). Longitudinal joints were reproduced by nonlinear rotational springs whilst circumferential joints were approximated by means of lateral springs which consider the frictional response of the rings coupling. The structural response of the tunnel section is analyzed for a wide range of longitudinal forces, from 40 to 5MN. Contrarily to the observed for usual design loads, the numerical study concluded about the significant influence of the longitudinal force level on the deformation and the internal forces of the lining, indicating the necessity of using 3D models in the analysis of the situations that create different structural response of adjacent rings.

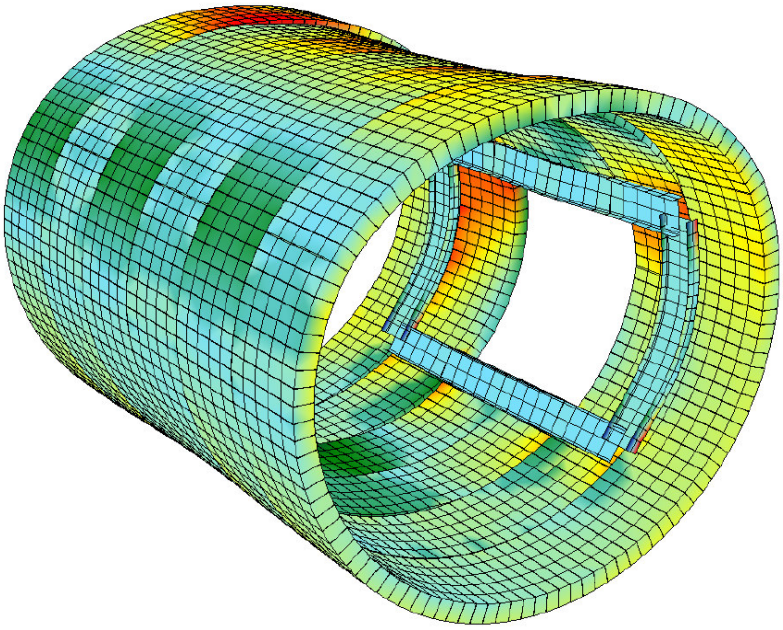

Figure 6.1.Analysis of a segmental tunnel lining opening performed by Klappers *et al.* (2006).

The accurate determination of the real degree of three-dimensionality presented by segmental tunnel linings in front of localized loads (or significant differences between adjacent ring responses), requires the assessment of the lateral rings interaction response in such situations. Present chapter studies the structural mechanisms involved in the transference of forces between adjacent rings when a localized load is applied on a tunnel section. A 3D numerical model which accurately considers all joints behaviors is employed to analyze the structural response of a real tunnel section in different scenarios of ground stiffness and longitudinal compression stress. The analysis of the results obtained provides significant conclusions about the main variables governing the interaction mechanisms between adjacent rings, and about the structural response of segmental tunnel inning subjected to localized loads.

6.2. ADJACENT RINGS INTERACTION MECHANISMS IN FRONT OF LOCALIZED LOADS

As it was previously exposed in chapter 5 (section 5.2), the main mechanism governing the structural interaction between adjacent rings is the transference of tangential forces caused by radial relative displacements (Fig. 5.2). The deformation experienced by a loaded ring strongly depends on the surrounding ground stiffness and, therefore, it plays a decisive role on the radial relative displacements produced between two adjacent rings. In section 5.2, the origin of the relative displacements is the different positions of the longitudinal joints, producing significant coupling effects only for soft ground conditions. When different structural responses of adjacent rings are expected, significant radial relative displacement can occur for a wider range of ground stiffness.

When a localized load is applied on the crown of a ring of a tunnel section, the lining should deform as it is shown in figure 6.2. For plane configurations of joints, the tangential forces between rings (F_R) are fully transmitted through the packing elements placed at circumferential joints, which experiments a tangential deformation and the associated tangential stress (τ_p) (Fig. 6.3). As it was previously discussed, packers present a frictional behavior and, therefore, the maximum tangential stress before slipping (τ_{sl}) depends on the existent compression stress (σ_p).

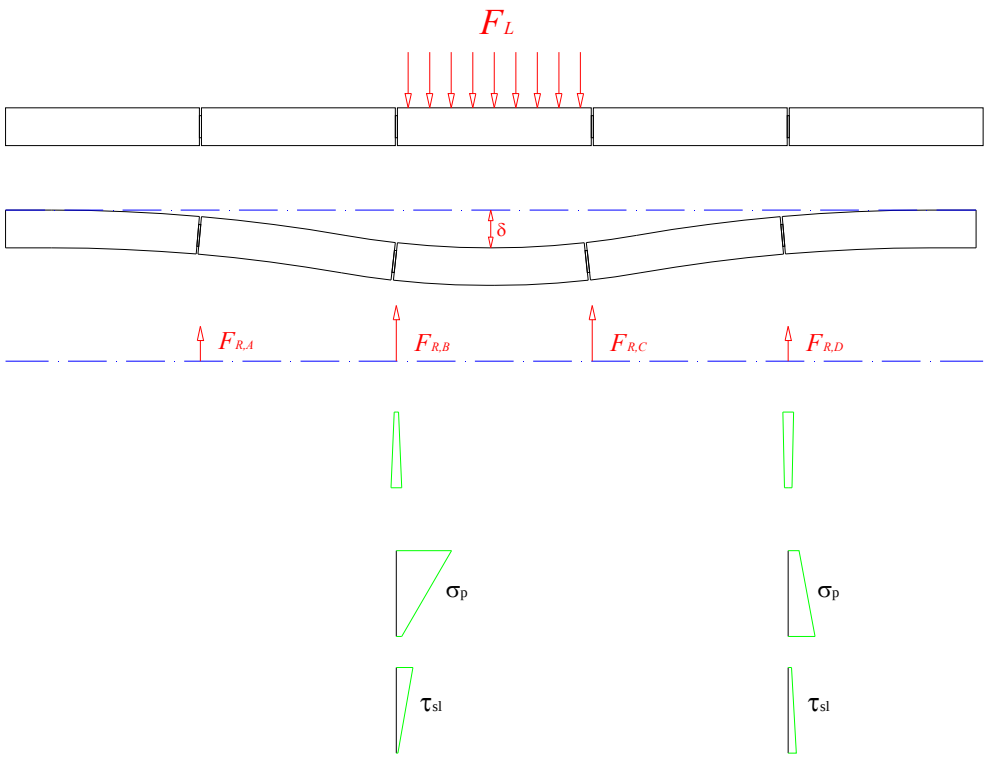

Figure 6.2. Segmental lining longitudinal resistant mechanism in front of localized loads.

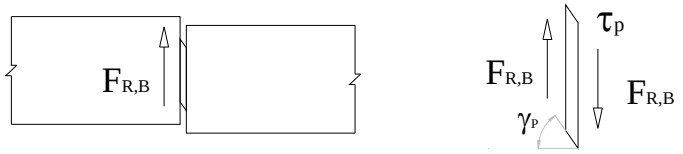

Figure 6.3. Tangential response presented by the packing material (packers).

Localized loads produce a longitudinal mechanism that locally modifies the stress distribution in the circumferential joints due to the rings deformations (Fig. 6.2). The compression stress at certain packer (σ_p) varies along its height and, therefore, the maximum tangential stress (τ_{sl}) is also modified, providing and additional complexity to the resistant mechanism. Moreover, the necessary compatibility between adjacent segments radial displacement produce a jack arch mechanism due to segments dislocation (Fig. 6.4). As a consequence, the compressive forces in the load influence zone increase with the lining deformation (δ in Fig. 6.2).

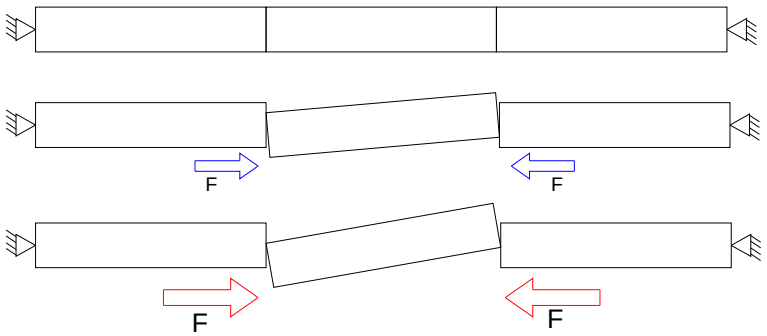

Figure 6.4. Schematization of the jack arch mechanism produced by the dislocation of the segments.

6.3. CASE STUDY AND NUMERICAL MODEL

The 11 rings tunnel model with linear elastic material properties presented on section 5.3 is employed in order to analyze the segmental linings response in front of localized loads. The reproduction of the frictional response of circumferential joints is carried out by means of interface elements and the Mohr-Coulomb material model described in section 5.3. In fact, the same material properties and joints configurations of Line 9 tunnel defined in chapter 5 are here also employed. The stiffness of the springs that simulate the ground structure interaction is updated according to the different ground conditions analyzed (Eq. 5.2, 5.3 and 5.4).

Localized loads can present different shapes, positions and magnitudes. As a consequence, it was decided to analyze the contribution mechanisms through the loading of the central ring of the modeled section (Fig. 6.5). According to that configuration, the structural response presented by the other rings is exclusively produced by the rings interaction mechanisms, thus facilitating its analysis and comprehension. Therefore, a vertical pressure ranging from 0 to 2 N/mm^2 is applied at the crown of the model central ring (vertically projected to ring 6), covering a 5m wide band and the entire ring width (Fig. 6.5).

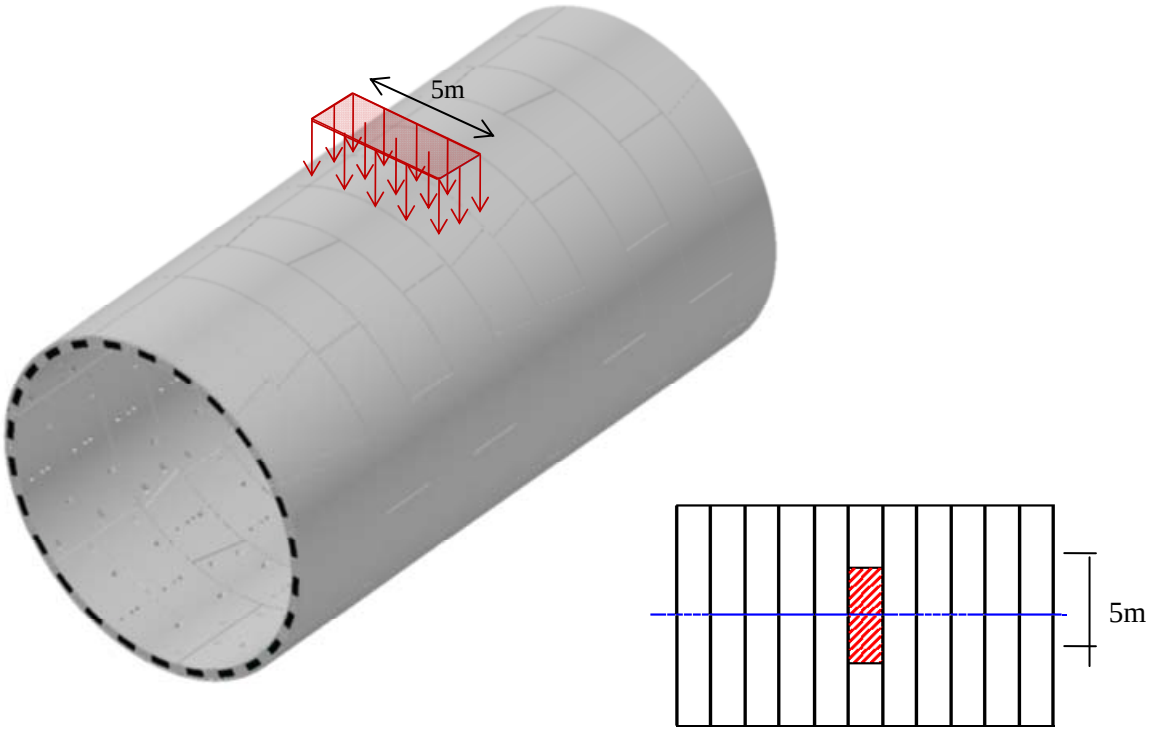

Figure 6.5. Localized loading scheme applied in the numerical study.

Four different levels of longitudinal force are applied in order to generate segmental lining pre-stresses of 5, 3.5, 2.5 and 1MPa (62, 43.4, 31 and 12 MN respectively) (Table 6.1). Localized loads can produce more significant relative radial displacements between adjacent rings than homogeneous loads. As a consequence, a wider range of ground stiffness is covered by means of three different hypotheses according to hard, medium and soft grounds (Table 6.1).

Table 6.1. Different scenarios applied to the localized load model.

Property	*Values*
Ground Stiffness, E_s (N/mm^2)	
Soft (SF)	100
Medium (ME)	1000
Hard (HD)	10000
Longitudinal Pre-compression, $\sigma_{c,l}$(MPa)	
	1
	2.5
	3.5
	5
Total amount of cases	12

Another set of isolated ring models without longitudinal pre-stress allows the evaluation of the influence of considering the lining three-dimensional response respect to the isolated ring approaches commonly employed in design practice.

The correct simulation of the tunnel real response requires the division of the loading procedure in two steps. The longitudinal force is initially applied, disabling the spring elements that reproduce the ground-structure interaction in order to adequately generate the lining pre-stress. The second step consists in the progressive appliance of the localized load once the ground-structure interaction has been enabled.

6.4. RESULTS

6.4.1. Lining structural response

According to the resistant mechanisms described in previous and current chapters (5 and 6), the reduction of the ground stiffness implies a higher interaction between adjacent rings. When the localized load is applied on hard ground conditions, significant bending forces are only produced at the loaded ring (Fig. 6.6). This quasi-individual response is fully consistent with the conclusions obtained in the “in situ” test (view chapter 2), where no significant contribution of the adjacent rings was measured for a rock tunnel subjected to a localized load.

On the other hand, the same load applied to the same structure embedded in soft ground, produces significant circumferential bending forces to adjacent rings (Fig. 6.6) clearly showing its structural contribution to resist the applied load. Therefore, the decrease in the surrounding ground stiffness should produce an increase in the three dimensional response of segmental tunnel lining.

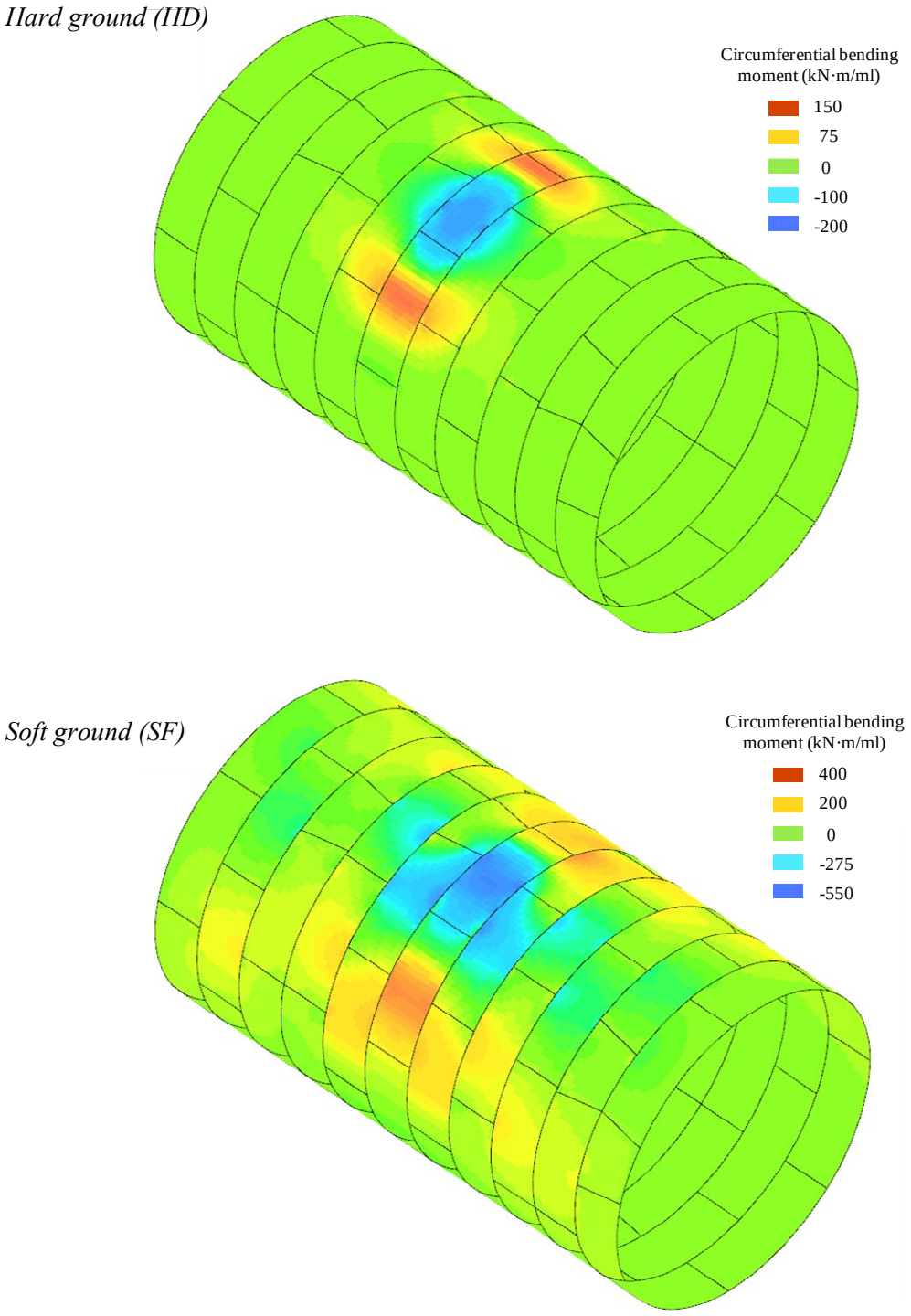

Figure 6.6. Circumferential bending forces for a localized pressure of 1N/mm^2 and longitudinal pre-compression of 5 MPa.

The evolution of the vertical ovalization of the loaded ring shows the influence of the longitudinal force on the lining stiffness (Fig. 6.7). Higher longitudinal compressions imply a reduction on the deformations obtained as the load pressure increases. This response is caused by the increase of the packer tangential capacity produced by a higher longitudinal compression. When a localized pressure of 1N/mm^2 is applied, the reduction of the longitudinal pre-stressing from 5 to 1Mpa implies an increase of the central ring deformation of 210% for soft ground (SF) and 44% for hard ground (HD). As it was expected, the three dimensional response of the lining presents a higher relevance with the decrease of the surrounding ground stiffness.

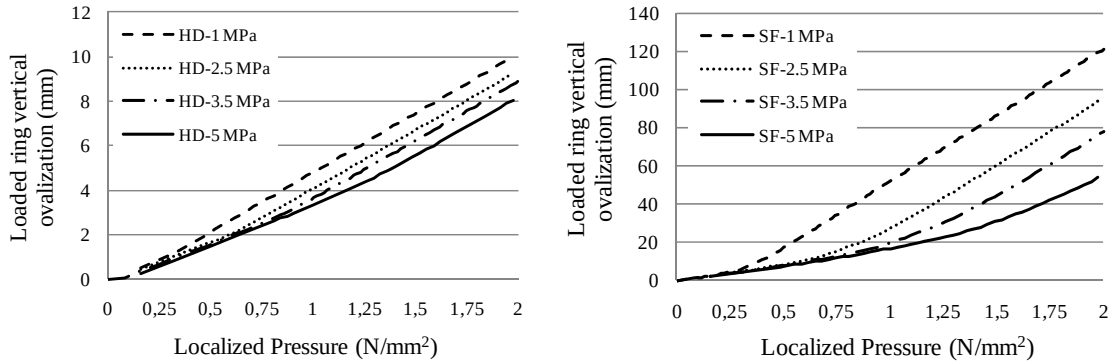

Figure 6.7. Evolution of the loaded ring vertical ovalization for hard (HD) and soft ground (SF) conditions depending on the longitudinal compression stress.

An effective and comprehensible way to appraise the structural interaction between rings consists in checking the vertical ovalization experienced by the rings directly adjacent to the locally loaded one. As can be observed in figure 6.8, the relative adjacent ring ovalization remains almost constant for small load values and independent of the lining pre-stress, achieving a value of 80% in soft ground conditions (SF) in front of the 40% obtained for hard ground (HD).

At certain load, the relative ovalization of the adjacent rings suddenly decreases, denoting the point where a significant number of packers start slipping (vertical dot lines in Fig. 6.8). Once the slipping starts, the structural collaboration tends to be established in a similar value around 20% for the analyzed cases. The value of the slipping load do not show dependency on the surrounding ground conditions, and remains only influenced by the longitudinal compressive stress of the lining. The results obtained show an almost perfect linearity between the longitudinal compression value and the necessary load to produce the significant slipping of packers (Fig. 6.9), presenting a relation coefficient of 0.255 which is close to the assumed packer-concrete friction coefficient (μ=0.2076, view section 5.3.1).

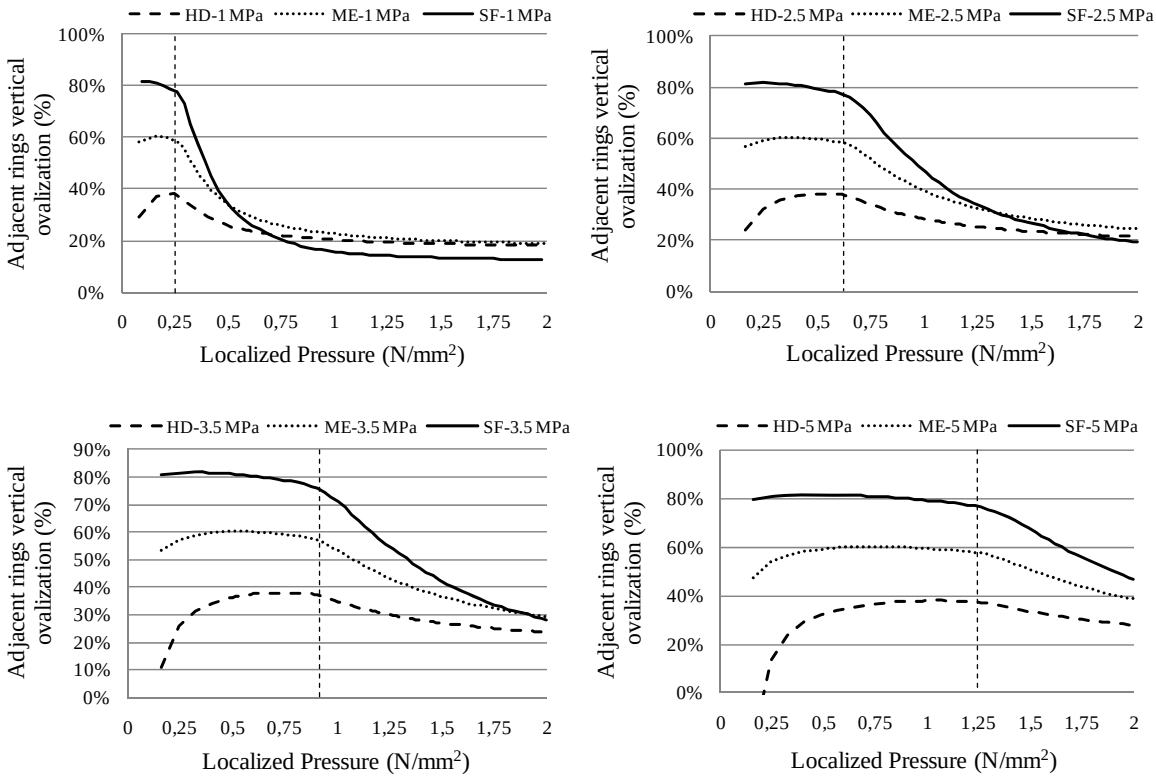

Figure 6.8. Relative vertical ovalization of the rings adjacent to the loaded one for different longitudinal pre-stress.

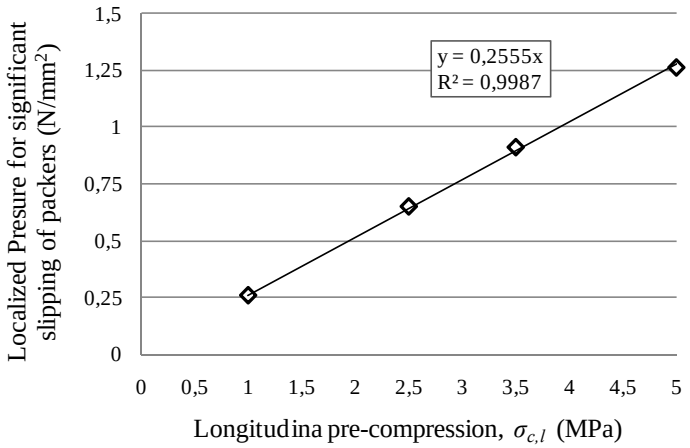

Figure 6.9. Relation between the localized pressure that produces the significant slipping of the packers and the longitudinal compression stress.

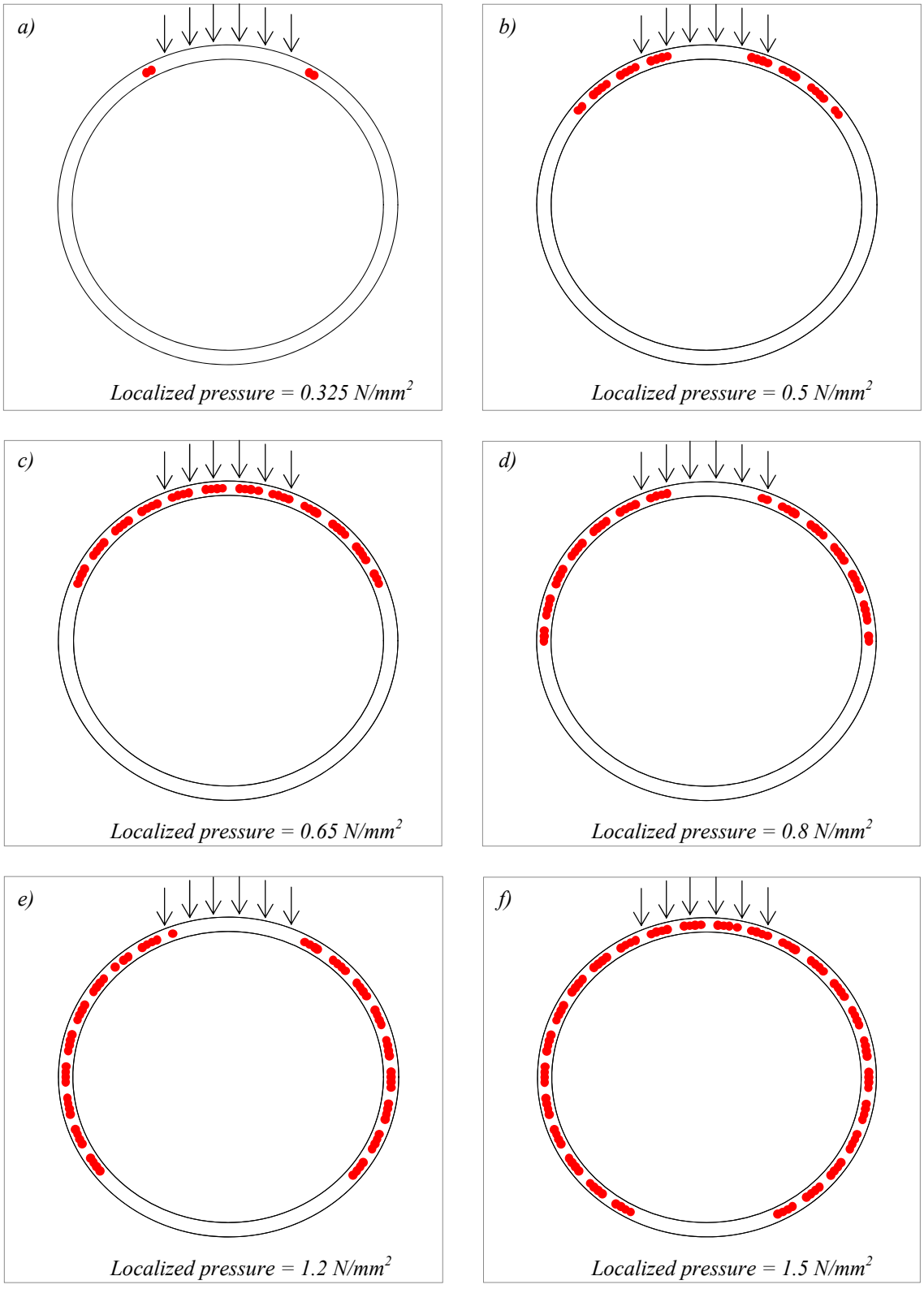

Figure 6.10. Central ring circumferential joint elements that present a complete slipping as load increases. Scenario: medium ground (ME) and longitudinal pre-stress of 2.5 MPa.

Figure 6.10 shows the evolution of the central ring packers slipping for a longitudinal pre-stress of 2.5MPa and medium ground conditions (ME). The points indicate the circumferential joint interface elements that present a complete slipping (each packer is simulated by means of four interface elements). The slipping of packers starts immediately out of the loaded zone (Fig. 6.10a), expanding mainly to the sides of the ring as the load increase (Fig. 6.10b). When the slipping of the tunnel crown packers is produced, almost the whole upper part of the ring presents sliding (Fig. 6.10c). This point coincides with the load that produces changes in the adjacent ring ovalization response, which was previously ascribed to the significant slippage of packers (vertical dot lines in Fig. 6.8).

The significant slipping of packers produces a faster increase of the loaded ring deformation. Therefore, the jack arch mechanism described in section 6.2 is enhanced, producing significant increments of the longitudinal compression stresses under the load appliance zone (Fig. 6.11). For the particular case analyzed in figures 6.10 and 6.11 (continue line), the fast increase of the crown compression provides higher tangential resistances to crown packers, stopping their slipping process for higher localized loads whilst the sliding extension continues to the lower part of the ring (Fig. 6.10.d and 6.10.e). Advanced load stages produce the restart of the crown packers slipping, presenting sliding at almost whole ring (Fig. 6.10f).

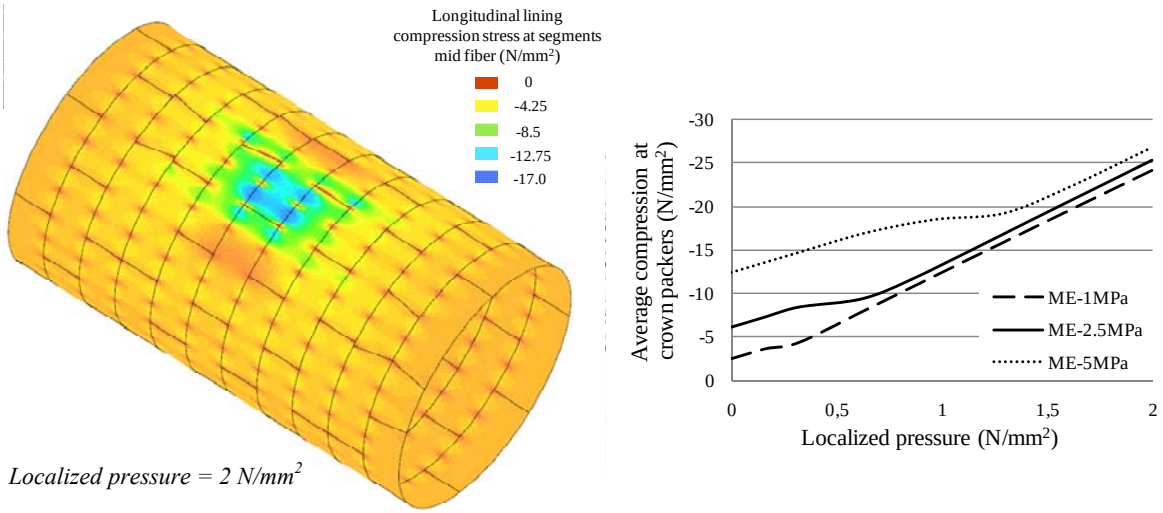

Figure 6.11. Local compression increase produced at the tunnel crown by the jack arch mechanism. Scenario: medium ground (ME) and longitudinal pre-stress of 2.5MPa.

Figure 6.12 shows the amount of elements per joint that present slipping for longitudinal pre-compressions of 1 and 2.5 MPa, previously and before the significant slipping observed in figure 6.8. The analysis of the whole tunnel reveals that significant slipping of packers is also produced out of the circumferential joints of the central ring (Fig. 6.12). In fact, for soft ground conditions, the central joints of the modeled section (5-6 and 6-7)

present a lower amount of packer elements slipping than others located farthest from the load (3-4 and 4-5 in Fig. 6.12). For medium ground conditions (ME) the amount of slipping elements are similar in the four central joints, whilst central ring joints present the maximum number for hard ground conditions (HD). The increase of the localized loads produces the presence of a significant slipping for more and further joints, showing that significant contribution of the adjacent rings remains when the significant slipping occurs. As it was stated along the present chapter, the softening of the ground stiffness implies a higher diffusion of the applied load (view Fig. 6.6), encompassing more rings and circumferential joints (Fig. 6.12).

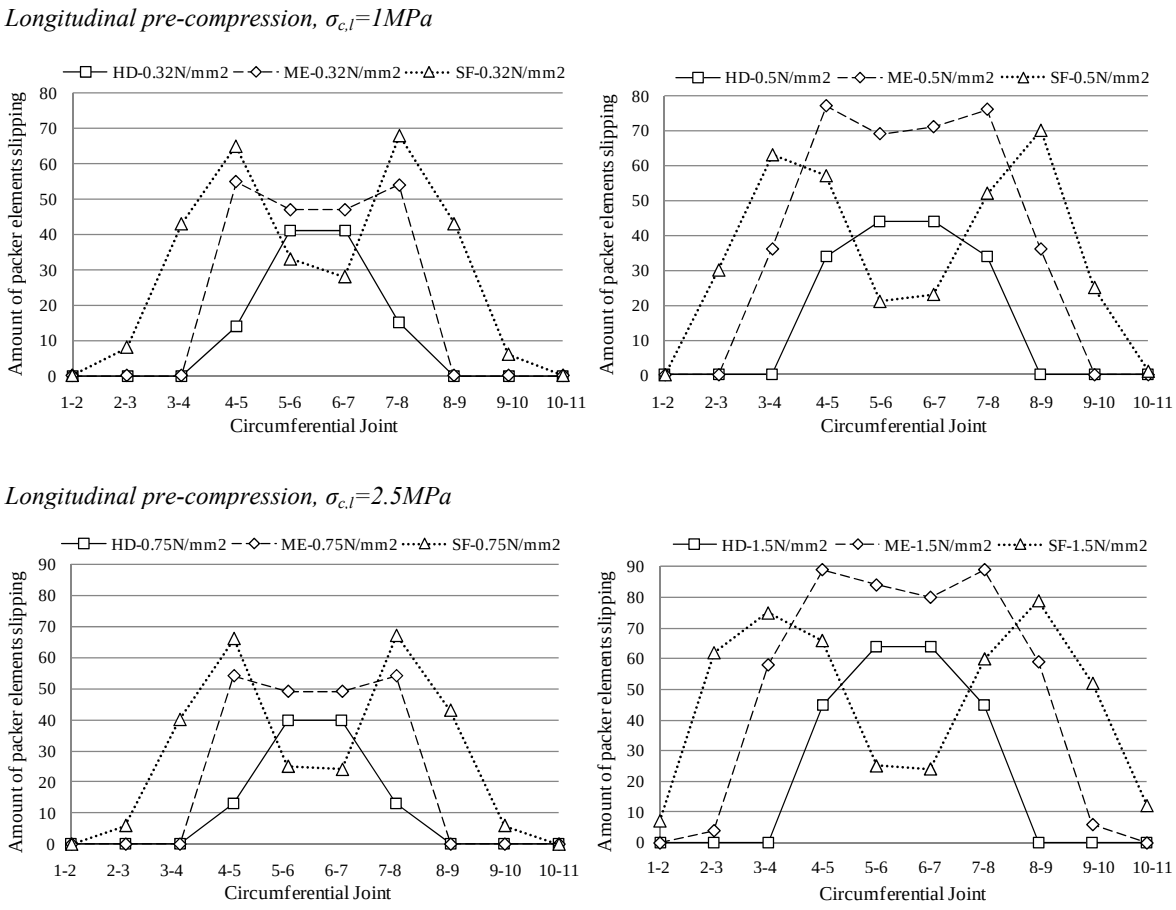

Figure 6.12. Amount of joint elements that present slipping for different scenarios.

On the other hand, the local compression zone caused by the jack arch mechanism does not show dependency with the surrounding ground stiffness, only affecting the three central rings (Fig. 6.13). According to the highest expected deformation, the compression increase produced in soft ground before and after the significant slipping of packers (localized loads of 0.5 and 1.5N/mm^2 respectively in figure 6.13) is higher than in hard ground conditions.

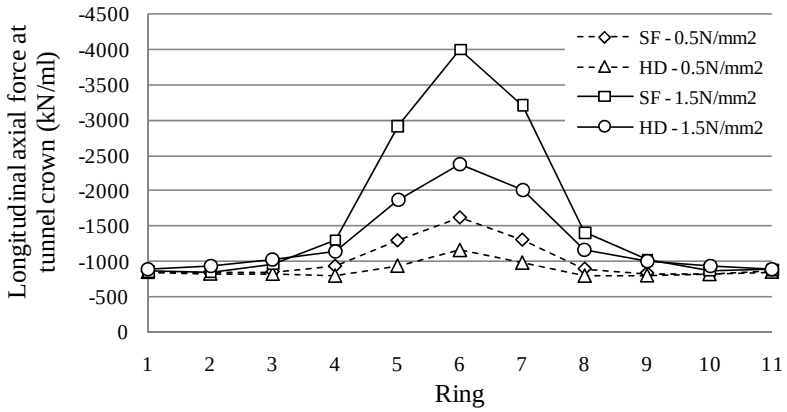

Figure 6.13. Longitudinal axial force at tunnel crown. Longitudinal pre-compression of 2.5MPa.

As it was previously explained, the jack arch mechanism is produced by the dislocation of the segments, modifying the stress distribution along the packers' height (Fig. 6.14). The increase of the applied load produce higher local stresses at one side of the packer whilst gapping phenomenon can appear at the opposite side for significant dislocations.

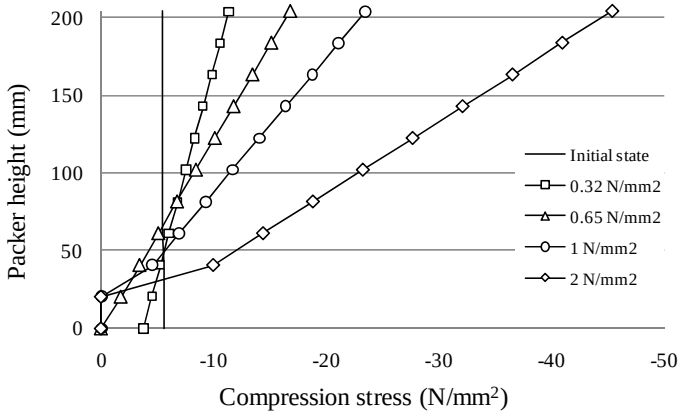

Figure 6.14. Stress distributions presented at midpoint of a central ring crown packer. Scenario: medium ground (ME) and longitudinal pre-stress of 2.5 MPa.

6.4.2. Influence of the three-dimensional effects

The structural analysis of segmental tunnel linings is commonly carried out by means of isolated ring models; do not considering the real three-dimensional response of the lining. In all cases, adjacent rings interaction produces a significant increase on the lining stiffness respect of the isolated ring analysis (Fig. 6.15). The vertical ovalization of the loaded ring is reduced close to 90% in soft ground and over 50% in hard ground conditions when the significant sliding of the packers has not been achieved. The decrease of the longitudinal force significantly diminishes the percentiles of deformation reduction in front of the isolated ring model, but a minimum value depending on the surrounding ground stiffness is maintained.

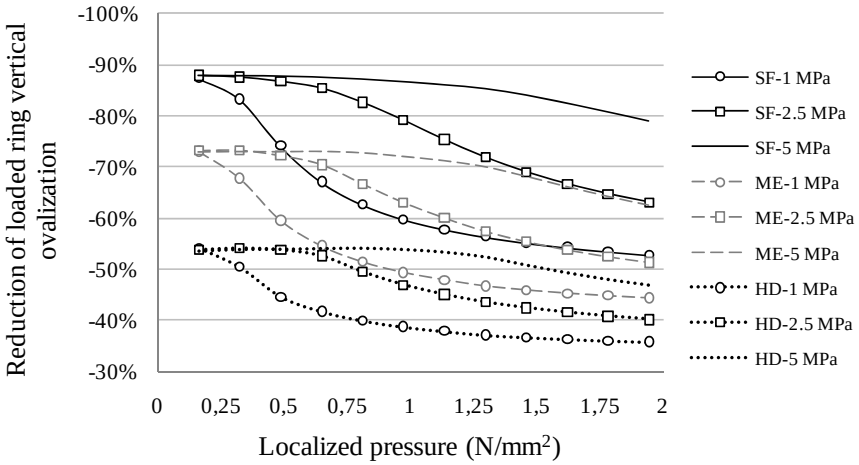

Figure 6.15. Reduction of loaded ring vertical ovalization respect to the isolated ring results.

The contribution of the adjacent rings also implies a significant reduction of the circumferential bending forces in front of the isolated ring analysis (Fig. 6.16). The circumferential bending forces present reductions between 48% and 62% before the packer slipping. Contrarily to the observed in lining stiffness, the reduction of the bending forces does not show proportionality with the surrounding ground stiffness.

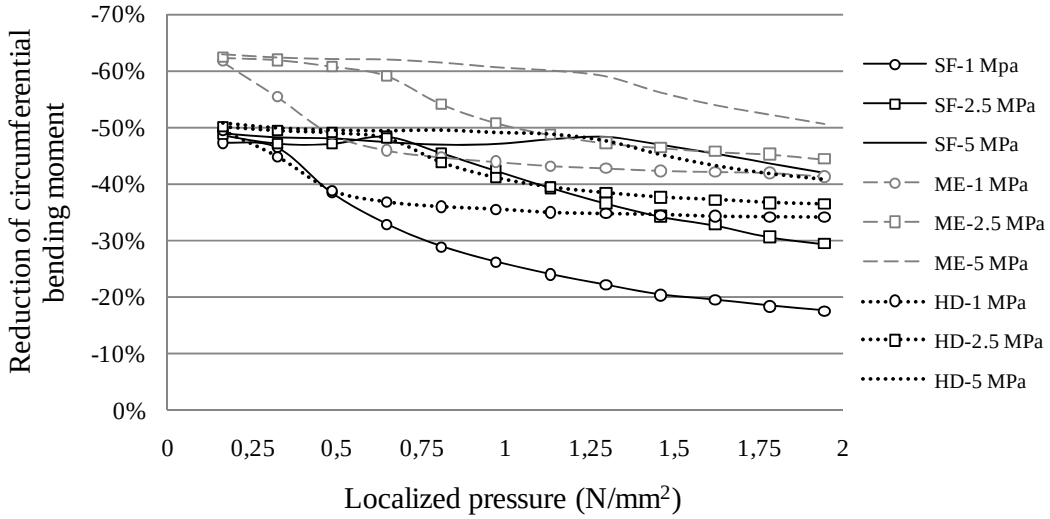

Figure 6.16. Reduction of loaded ring circumferential bending forces respect to the isolated ring results.

The reduction of the bending forces originated by the structural interaction between adjacent rings also produces a reduction on the tensile principal stress at the tunnel crown (Fig 6.17). As a consequence, the amount of localized load to achieve the maximum tensile strength of concrete (4.1N/mm^2, dot lines in figure 6.17) and produce the cracking of the segments significantly increases respect to the isolated ring approaches.

The longitudinal force level will also play a determining role on the cracking load. For medium ground conditions (ME), the increase of the longitudinal pre-stress from 1 to 2.5MPa implies a load increase of 52.2% to produce the cracking of the tunnel crown. On

the other hand, in the analyzed soft ground case (SF) the tensile principal stress increases really fast, achieving the concrete tensile strength close to the load that starts the slipping of packers for a longitudinal pre-stress of 1MPa. Therefore, for the analyzed soft ground conditions, the longitudinal force level only presents significant influence on the lining resistance for values under 1MPa (Fig. 6.17).

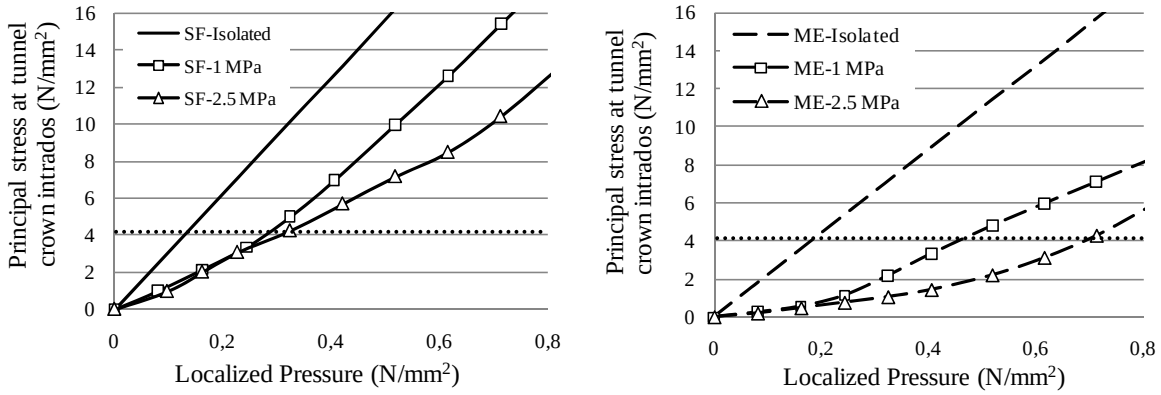

Figure 6.17. Evolution of the tensile principal stress at the tunnel crown.

In general, the obtained results show that the consideration of the longitudinal force and its magnitude implies an increase of the necessary localized load to produce the cracking of the tunnel crown (Fig. 6.18). For hard rock conditions, the structural mechanism that produces the tensile stresses in the tunnel crown differ respect to softer ground conditions, producing that the isolated ring model provides a higher resistance than the consideration of the real three dimensional effects. Localized loads produce internal bending forces in circumferential direction (originating the main deformation of the ring) but also in longitudinal direction (between circumferential joints). Usual conditions produce that bending forces in circumferential direction become more significant than in longitudinal direction (view medium ground results -ME- in Fig.6.19), emerging as the dominating phenomenon in segments cracking. For the analyzed hard rock conditions, bending forces in both directions takes similar values, but the compressive axial force is significantly higher in circumferential direction than in longitudinal (hard ground -HD- in Fig. 6.19). As a consequence, the tensile stress in longitudinal direction becomes higher (view Fig. 6.20), changing the usual mechanism of cracking of the ring.

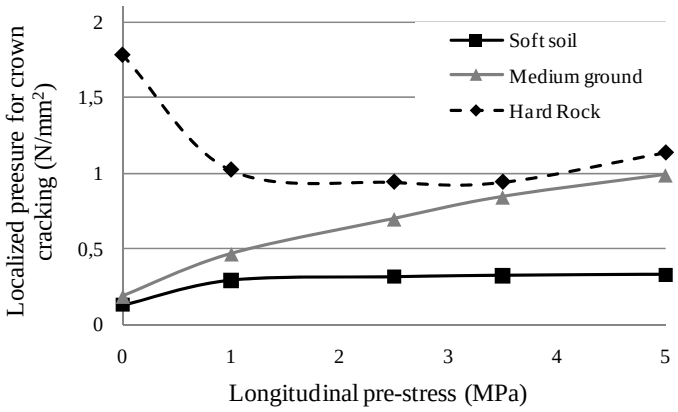

Figure 6.18. Influence of the longitudinal pre-stress on localized pressure for crown cracking.

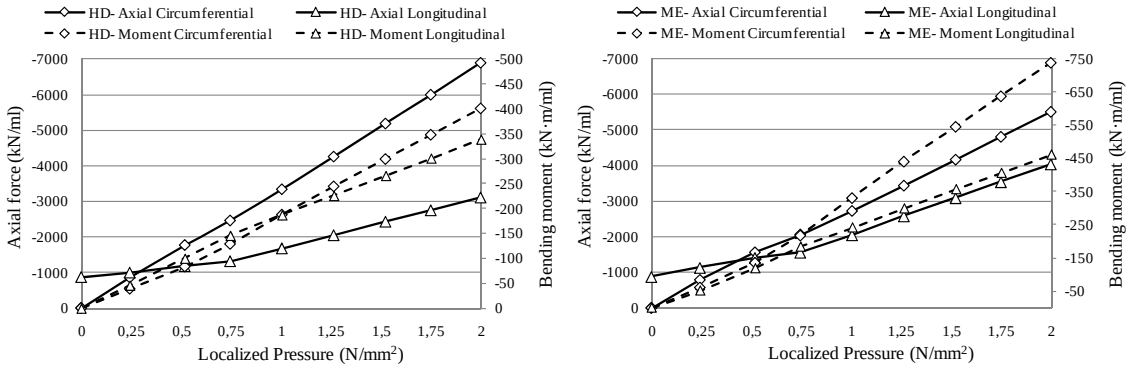

Figure 6.19. Axial and bending internal forces at the loaded ring crown in circumferential and longitudinal direction for hard (HD) and medium (ME) ground conditions. Longitudinal pre-compression of 2.5 MPa.

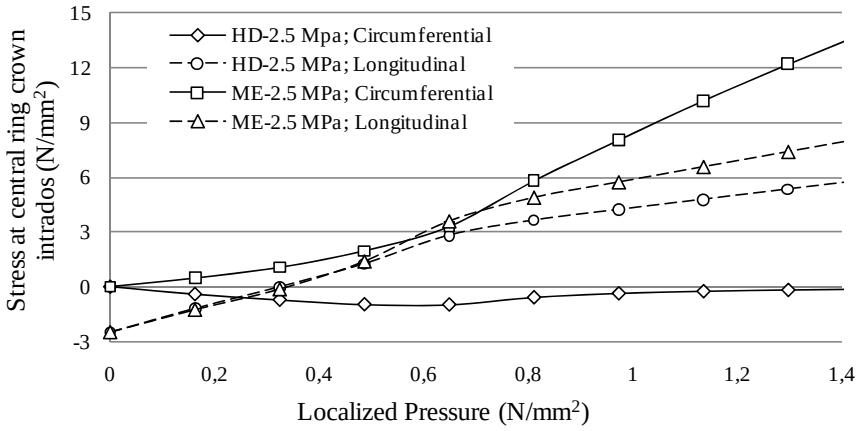

Figure 6.20. Tensile stresses produced at the loaded ring crown due to circumferential and longitudinal internal forces. Longitudinal pre-stress of 2.5 MPa.

6.5. CONCLUSIONS

When a localized load is applied to a segmental tunnel lining, adjacent rings present different radial deformation that activate the three dimensional response of the structure. The detailed theoretical study of the main involved phenomena reveals a significant complexity of the lining structural response due to the combination of circumferential and longitudinal mechanisms. Other situations that produce significant differences in the structural response of adjacent rings (tunnel openings, shaft connections, sudden ground changes, etc) should be governed by the same mechanisms than localized loads.

A sensitivity analysis is performed to analyze the segmental tunnel linings structural response in front of localized loads, using a contrasted 3D numerical model that properly considers the behavior of the joints. Unlike for uniformly distributed design loads (chapter 5), the results obtained show that significant three dimensional effects are produced for the majority of tunnel scenarios, covering all range of ground stiffness.

The structural contribution between adjacent rings produces a stiffer response of the lining and an increase of its resistance in front of localized loads. A higher degree of interaction implies an increase of the three dimensional response, thus increasing the reduction of the lining deformation and the necessary load to produce the cracking of the segments.

For a certain lining configuration (thickness, joints positions and height, packer materials, etc), the achieved level of interaction depends on the surrounding ground stiffness, increasing with the softening of the ground conditions. On the other hand, the longitudinal compression existent at the lining determines the load that produces the significant slipping of packers, without any influence of the surrounding ground conditions. Increase the lining longitudinal compression implies the assessment of the maximum rings interaction for higher loads, thus increasing the structural benefits of the three dimensional response of the lining in front of localized loads for a wider range of loads.

In general it can be concluded that segmental tunnel lining present a significant three-dimensional effects in front of localized loads or situations where significant radial displacements between adjacent rings are produced. As a consequence, the accurate prediction of segmental linings response requires an appropriate three dimensional consideration, taking into account the current longitudinal force level.

ACKNOWLEDGEMENTS

The authors want to thank the construction company FCC Construcción, S.A. for its involvement in the research project *Túneles Urbanos* focused on the structural response of precast concrete segmental tunnel linings. The first author also wants to thank the support of the University and Research Commissioner of the DIUE of the Generalitat de Catalunya and also the European Social Fund (ESF).

Chapter 7

CONCLUSIONS AND FUTURE WORK

7.1. GENERAL CONCLUSIONS

Present research has allowed the achievement of several conclusions that represent innovative contributions to the knowledge of the structural response of precast concrete segmental tunnel linings. Present section outlines the general conclusions achieved in this research whilst more detailed discussions can be found at the end of each chapter.

The performance of an “in situ” test provided experimental evidences of the real structural response of a steel fiber reinforced concrete (SFRC) segmental tunnel lining. The accurate treatment and analysis of the measurements allowed the identification, description and quantification of the main involved phenomena. It was pointed out that the deformation of the lining is mainly caused by concentrated rotations in the joints and in the cracked sections of the segments, whilst the tangential ground-structure interaction presents a major influence on the stress distribution across the ring.

It is now proved that the numerical simulation of the structural response of segmental tunnel linings can be successfully carried out by taking into account the main phenomena and properly integrating them in a unique analysis model. The numerical simulation of the “in situ” test demonstrates the excellent agreement obtained in terms of displacements, joints openings and crack patterns. The achievement of such precision levels required the accurate inclusion of the nonlinear behavior of the longitudinal joints, the complex plastic

response of the packing material, the adequate ground-structure interaction and the post-cracking behavior of the steel fiber reinforced concrete.

The study of the tunnel construction process and the longitudinal ground-structure interaction mechanisms pointed out that segmental tunnel linings present a longitudinal time-dependent behavior. Significant losses of the longitudinal force initially applied by the tunnel boring machine (TBM) occur due to the creep phenomenon experienced by both the concrete and the packing materials. Formulations to predict the remaining compression at certain time and the length of the anchorage zones produced at the ends of the linings are proposed, obtaining an excellent agreement with the numerical validation performed. The creep phenomenon of plastic packers is experimentally determined and a formulation to consider it on a global creep coefficient of the lining is presented.

When a segmental tunnel lining is subjected to the longitudinally distributed loads commonly used in design processes, the staggered configuration of the joints can activate the adjacent rings interaction mechanisms of the lining and behave as a three dimensional structure. The so called coupling effects arise for significant unbalanced loads or for soft ground conditions, increasing the lining stiffness. As a consequence, the deformation of the lining is reduced but the internal forces are significantly increased, producing the cracking of the segments if coupling effects have not been taken into account on the design. For design purposes, the isolated rigid ring models emerge as the approximation that provides an upper bond for the internal bending forces when the segmental lining response is conditioned by coupling effects.

The structural response of segmental tunnel linings subjected to localized loads or other situations that produce relative radial deformations between adjacent rings, significantly depends on the three dimensional effects. Higher interaction between adjacent rings implies a reduction of the lining deformations and an increase of the lining resistance in respect to the usual isolated ring consideration adopted in design processes. The surrounding ground stiffness determines the interaction degree achievable between adjacent rings whilst the longitudinal force level determines the range of loads for which the maximum interaction level is maintained.

7.2. FUTURE WORKS

The evolution of the present research has allowed the coverage of significant uncertainties about the structural response of precast concrete segmental tunnel linings, but arouses other topics that will contribute to a better comprehension and statement of the linings behavior.

Some of the described phenomena or responses have been obtained throughout the physical analysis or the numerical simulation. Therefore, the research works listed below are proposed in order to obtain experimental evidences that corroborate the described phenomena:

- Develop a new methodology to properly perform “in situ” tests on soft ground conditions. The significant influence of the ground stiffness on the structural response of the lining recommends the assessment of the exposed behavior with experimental evidences.

- Measure the relaxation process occurred in real linings in order to validate the formulations of the longitudinal force loss proposed in the present thesis.

Additionally, the systematic application of the developed modeling techniques could contribute to obtain a better understanding of relevant aspects of the structural response of segmental tunnel linings. Proposed works are:

- Analyze the influence of the relation segment/joint height in the coupling effects. Determine the optimal flexibility in order to avoid undesired increases of the internal bending forces.
- Simulate the construction process of the segmental tunnel linings, considering the TBM-structure interaction, in order to study the damages that frequently appear in segments during the TBM pushing phase.
- Analyze the structural implications of the high eccentric force applied by the TBM during the construction of the short radius curves used in urban tunnels.

References

Antunes, J.L.; Gettu, R.,2006. Determining the Tensile Stress-Crack Opening Curve of Concrete by Inverse Analysis. Journal of Engineering Mechanics. Vol. 132, Nº 2, 141-148.

Arnau, O., Molins, C., 2011. Experimental and analytical study of the structural response of segmental tunnel linings based on an *in situ* loading test. Part 2: Numerical Simulation. Tunnelling and Underground Space Technology, 26 (2011), 778-788.

Arnau, O., Molins, C., Blom, C.B.M., Walraven, J.C., 2012. Longitudinal-time dependent response of segmental tunnel linings. Tunnelling and Underground Space Technology, 28 (2012), 98-108.

Bazant, Z.P., Oh, B.H., 1983. Crack band theory for fracture of concrete. Materiaux et constructions, vol 16,Nº 93, 155-177.

Bazant, Z.P., Wittmann, F.H., 1988. Creep and shrinkage in Concrete Structures. John Wiley and Sons, New York.

Blom, C.B.M., van der Horst, E.J., Jovanovic, P.S., 1999. Three-dimensional Structural Analyses of the Shield-Driven "Green Heart" Tunnel of the High-Speed Line South. Tunnelling and Underground Space Technology, Vol 1, Nº 2, 217-224.

Blom, C.B.M., 2002. Design philosophy of concrete linings for tunnels in soft soils. PhD Thesis. Technische Universiteit Delft.

Bouma, A.L., 1989. Mechanica van constructies: elasto-statica van slanken structuren (in Dutch). Delft University Press, Delft.

Broere, W.; Brinkgreve, R.B.J., 2002. Phased Simulation of a Tunnel Boring Process in Soft Soil. Numerical Methods in Geotechnical Engineering. Presses de l'ENPC/LCPC, 529-536.

Brydson, J.A., 1999. Plastics Materials, 7th edition. Butterworth Heinemann.

Cavalaro, S.H:P., 2009. Aspectos tecnológicos de túneles construidos con tuneladora y dovelas prefabricadas de hormigón. PhD Thesis. Universitat Politècnica de Catalunya. (in spanish).

CEB-FIP, 1993. CEB-FIP Model Code 1990. Thomas Telford, London.

Crowford, R.J., 1998. Plastics Engineering, 3rd edition. Elsevier.

Ding, W.Q.; Yue, Q.Z.; Tham, G.L.; Zhu H.H.; Lee, C.F.; Hashimoto, T., 2004. Analysis of shield tunnel. International Journal for Numerical and Analytical Methods in Geomechanics, Nº58. 57-91.

Duddeck, H.; Erdmann, J., 1985. On Structural Design Models for Tunnels in Soft Soil. Underground Space, vol 9, 246-259.

Fleming, W.G.K., Weltman, A.J., Randolph, M.F., Elson W.K., 1994. Piling Engineering, 2nd edition. Blackie Academic and Professional, Glasgow.

Ghali, A., Favre, R., Eldbadry, M., 2002. Concrete Structures. Stresses and Deformation (third edition). Spon press, London.

Gijsberg, F.B.J., Hordijk, D.A., 1997, Experimenteel onderzoek naar het afschuifgedrag von ringvoegen, TNO-rapport COB K111 (in Dutch).

Guglielmetti, V., Grasso, P., Mahtab, A., Xu, S., 2008. Mechanized tunnelling in urban areas. Taylor & Francis. London.

Institut Belge de Normalisation (IBN), 1992. Essais des Bétons Renforcés de Fibres – Essai de flexion sur éprouvettes prismatiques', NBN B 15-238.(in French)

Japan Society of Civil Engineers (JSCE), 1996. Japanese Standard for Shield Tunneling.

Japan Society of Civil Engineers (JSCE), 2006. Standard specifications for Tunneling: Shield Tunnels. Tokio.

Kasper, T., Meschke, G., 2004. A 3D finite element simulation model for TBM tunnelling in soft ground. International Journal for Numerical and Analytical Methods in Geomechanics, Nº28. 1441-1460.

Kasper, T., Edvardsen, C., Wittneben, G., Neumann, D., 2007. Lining design for the district heating tunnel in Copenhagen with steel fibre reinforced concrete segments. Tunnelling and Underground Space Technology 23, 574-587.

Klappers, C., Grübl, F., Ostermeier, B., 2006. Structural analyses of segmental lining – coupled beam and spring analyses versus 3D-FEM calculations with shell elements. Proceedings of the ITA-AITES 2006 World Tunnel Congress, *Safety in the Underground Space*, 6 pp.

Koek, A.J., 2004. Axiale voorspanning in de lining van een geboorde tunnel (in Dutch). Master Thesis. TUDelft, The Netherlands.

Koyama, Y., 2003. Present status and technology of shield tunnelling method in Japan. Tunnelling and Underground Space Technology, Nº 18, 145-159.

Liao, S.M., Peng, F.L., Shen, S.L., 2008. Analysis of shearing effect on a tunnel induced by load transfer along longitudinal direction. Tunnelling and Underground Space Technology 23, 421-430.

Maidl, B., Herrenknecht, M., Anheuser, L., 1996. Mechanised Shield Tunnelling. Ernst and Sohn, Berlin.

Mo, H.H., Chen, J.S., 2008. Study on inner force and dislocation of segments caused by shield machine attitude. Tunnelling and Underground Space Technology 23, 281-291.

Molins, C., Marí, A.R., Aguado, A., 2005. Design of the loading test of the segmental tunnel lining of L9 subway of Barcelona. Procedings of the *III ACHE - Congreso de Puentes y Estructuras de Edificación de la Asociación,* November 14 to 17, 2005, 893-905, Zaragoza, Spain. (in Spanish)

Molins, C., Aguado, A., Saludes, S., 2009. Double Punch test to control the energy dissipation in tension of FRC (Barcelona test). Materials and Structures, 42, 415-425.

Molins, C., Arnau, O., 2011. Experimental and analytical study of the structural response of segmental tunnel linings based on an *In situ* loading test. Part 1: Test Configuration and Execution. Tunnelling and Underground Space Technology, 26 (2011), 764-777.

Mora, F., 2008. Distribution and orientation of fibers in tunnel segments, using the Barcelona test. PhD Thesis. Universitat Politècnica de Catalunya. (in Spanish)

Morgan, H. D., 1961. A contribution to the analysis of stress in a circular tunnel. Géotechnique, 11(1), 37-46.

Muir Wood, A.M., 1975. The circular tunnel in elastic ground. Géotechnique, 25(1), 115-127.

Nawy, E.G., 2008. Concrete Construction Engineering Handbook. CRC press.

Peila, D., Borio, L. Pelizza, S., 2011. The behaviour of a two-component back-filling grout used in a tunnel-boring machine. Acta Geotechnica Slovenica, 2011/1, 5-15.

Pelizza, S., Peila, D., Borio, L., Dal Negro, E., Schulkins, R., Boscaro, A., 2010. Analysis of the performance of two component back-filling grout in tunnel boring machines operating under face pressure. ITA-AITES World Tunnel Congress 2010, Tunnel Vision Towards 2020. Vancouver.

Plizzari, G.A., Tiberti, G., 2006. Steel Fibers as Reinforcement for Precast Tunnel Segments. Proceedings of the ITA-AITES 2006 World Tunnel Congress and 32nd ITA General Assembly. 6 pp.

Rilem TC 162-TDF, 2003. Test and design methods for steel fibre reinforced concrete. σ-ε Design method. Final recommendation. Materials and Structures, V. 36, 560-567.

Roelfstra, P.E., Wittmann, F.H., 1986. Numerical Method to link Strain Softening with failure of Concrete. Fracture Toughness and Fracture Energy of Concrete. Ed. F.H.Wittmann, Elsevier Science, 163-175.

Schulze, H., Duddeck, H., 1964. Statische Berechnung Schieldvorgetriebener Tunnel (Structural analysis of tunnels excavated with shield support). Beton und Monierbau AG 1889-1964, 87–114.

Teachavorasinskun, S., Chub-uppakarn, T., 2010. Influence of segmental joints on tunnel lining. Tunnelling and Underground Space Technology, 25, 490-494.

Thewes, M., Budach, C., 2009. Grouting of the annular gap in shield tunnelling – An important factor for minimisation of settlements and production performance. ITA-AITES world Tunnel Congress 2009 “Safe Tunnelling for the City and Environment”. Budapest.

Tiberti, G., Plizzari, G.A., Walraven, J.C., Blom, C.B.M., 2008. Concrete tunnel segments with combined traditional and fiber reinforcement. Proceedings of the fib 2008 symposium, Tailor Made Concrete Structures, Amsterdam, 199-205.

TNO, 2005. *Diana user's manual. Release 9*. www.tnodiana.com.

Van Empel, W.H.N.C.; Kaalberg, F.J., 2002. Advanced modeling of innovative bored tunnel design Amsterdam North-Southline. Procedings of the DIANA world conference, Tokyo, 439-448.

Vervuurt, A.H.J.M., Van del Veen, C., Gijsbers, F.B.J., Den Uijl, F.B.I., 2002. Numerical simulations of tests on a segmented tunnel lining. Procedings of the DIANA world conference, Tokyo, 429-437.

De Waal, R.G.A., 2000. Steel fibre reinforced tunnel segments for the application in shield driven tunnel linings. PhD Thesis. Technische Universiteit Delft.

Zhang, W., Koizumi, A., 2010. Behavior of composite segment for shield tunnel. Tunnelling and Underground Space Technology 25, 325-332.

Appendix 1

NOTATION

A_c	Concrete cross area
A_{el}	Finite element area
AR	Lateral surface aspect ratio
b	Segment's width
c_r	Rotational stiffness of a joint
e	Lining thickness
E_c	Concrete deformation modulus
E_c	Packing material deformation modulus
$E_{c,28}$	Concrete deformation modulus at 28 days
E_s	Ground deformation modulus
$F_{g,n}$	Force transmitted to the ground at ring n
F_{GR}	Ground radial reaction force
F_i	Initial force
F_L	Concentrated load
F_R	Tangential force between adjacent rings
F_{RF}	Force at tunnel initial reaction frame
F_t	Transferred force to the ground

F_{TBM} Longitudinal force applied by the TBM

f_{cm} Concrete compressive strength

f_{ct} Concrete elastic tensile strength

$f_{f,300}$ SFRC tensile strength at a vertical deflection of l/300 (NBN test)

f_r SFRC flexural tensile strength for the first crack (NBN test)

G_p Packing material shear modulus

h Notational size of the member

h_{ck} Crack bandwidth

h_d Groundwater table depth

h_w Groundwater table height over the tunnel crown

HR Relative humidity

I Segment inertia

I_e Equivalent inertia proposed by Muir Wood (1975)

I_j Longitudinal joint inertia

K_0 Lateral earth pressure coefficient

K_l Longitudinal ground-structure interaction stiffness

K_r Radial ground-structure interaction stiffness

K_t Tangential ground-structure interaction stiffness

L_{an} Anchorage length

L_c Concrete ring width

L_p Packer thickness

L_t Total ring width

l_h Height of the joint contact

N Longitudinal force

n Number of joints of a ring

OVL Ovalization load

P_e Tunnel external perimeter

$P_{h,side}$ Horizontal pressure at mid tunnel section

$P_{v,top}$ Vertical pressure at tunnel crown

Ps_i Soil pressure at certain point i

Pw_i Water pressure at certain point i

R Tunnel radius

r^2 Correlation coefficient of packers creep curve fitting

S_{cl} Lateral concrete surface of a ring

S_{pl} Lateral ring surface covered by packers

t Time of analysis

t_0 Age of loading

u Longitudinal displacement

u_p Perimeter in contact with the atmosphere

u_{sl} Ground spring displacement for plastic response

w_m Crack width

x Variable of position

γ_s Ground density

γ_{sw} Saturated ground density

γ_w Water density

δ Lining crown deflection

ε_c Concrete strain

ε_{ck} Crack strain

$\varepsilon_{c\sigma}$ Concrete stress dependant strain according to CEB-FIP Model Code

ε_{el} Concrete elastic strain

$\varepsilon_{cr,\Delta tn}$ Concrete creep strain at time period Δt_n

ε_g Grout strain

ε_p Packer strain

$\varepsilon_{p\text{-}el}$ Packer elastic strain

$\varepsilon_{p\text{-}cr}$ Packer creep strain

ζ Transfer ratio of bending forces

μ Friction coefficient

ν Poisson ratio

σ_c Concrete compressive stress

$\sigma_{c,l}$ Longitudinal pre-compression of the concrete lining

σ_p Packing material compression stress

σ_{rc} Tensile stress of SFRC

τ_p Packing material tangential stress

τ_{sl} Maximum tangential stress

$\varphi_c(t,t_0)$ Concrete creep coefficient for t_0 to t period

$\varphi_p(t,t_0)$ Packer creep coefficient for t_0 to t period

$\varphi_G(t,t_0)$ Lining global creep coefficient for t_0 to t period

ω Crack opening

$Ø_e$ Lining external diameter

$Ø_{int}$ Lining internal diameter

$Ø_f$ Steel fiber diameter

Appendix 2

RESUME OF EXTERNAL INSTRUMENTS MEASURES OF THE LINE 9 *IN SITU* TEST

Figures A2.1, A2.2, A2.3, A2.4, A2.5 and A2.6 show the measurements registered at the external instrumentation of the loaded ring during the different stages of the *in situ* test.

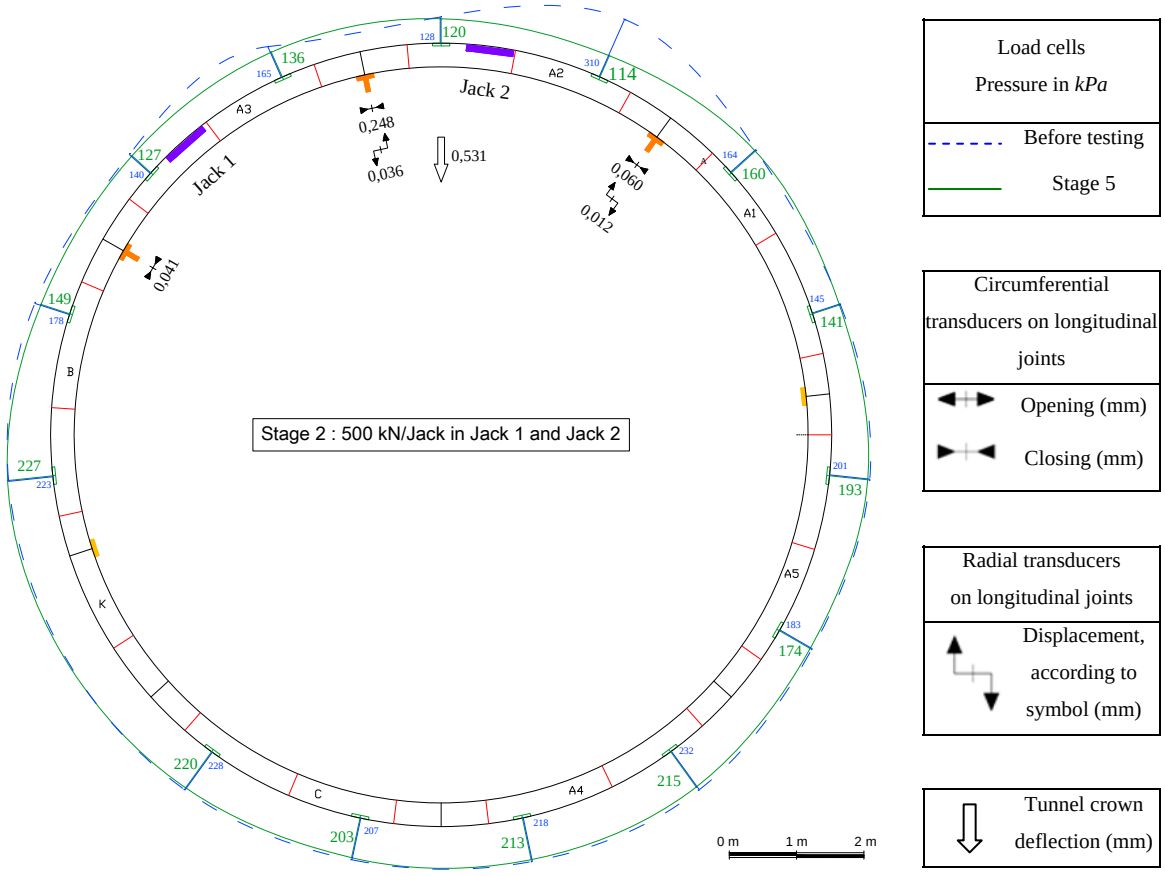

Figure A2.1. External instruments measures of the loaded ring at stage 2.

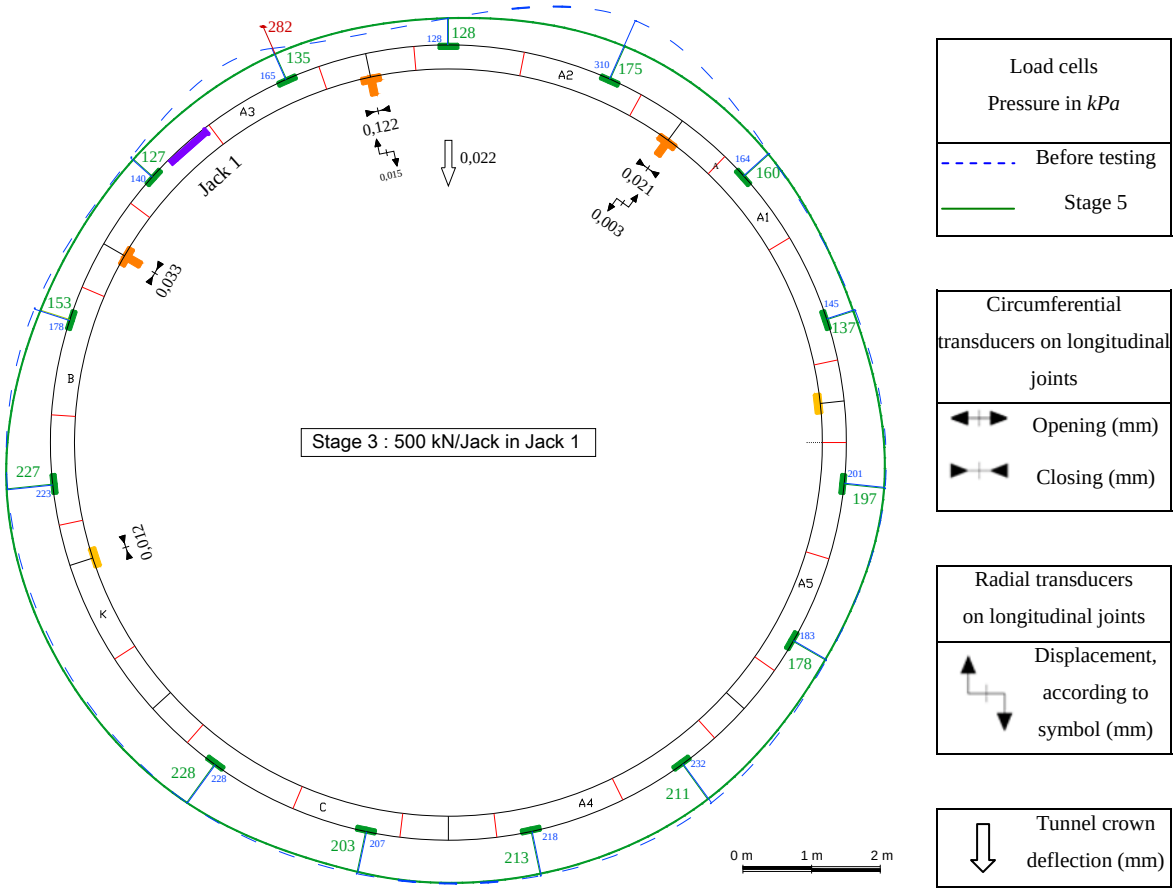

Figure A2.2. External instruments measures of the loaded ring at stage 3.

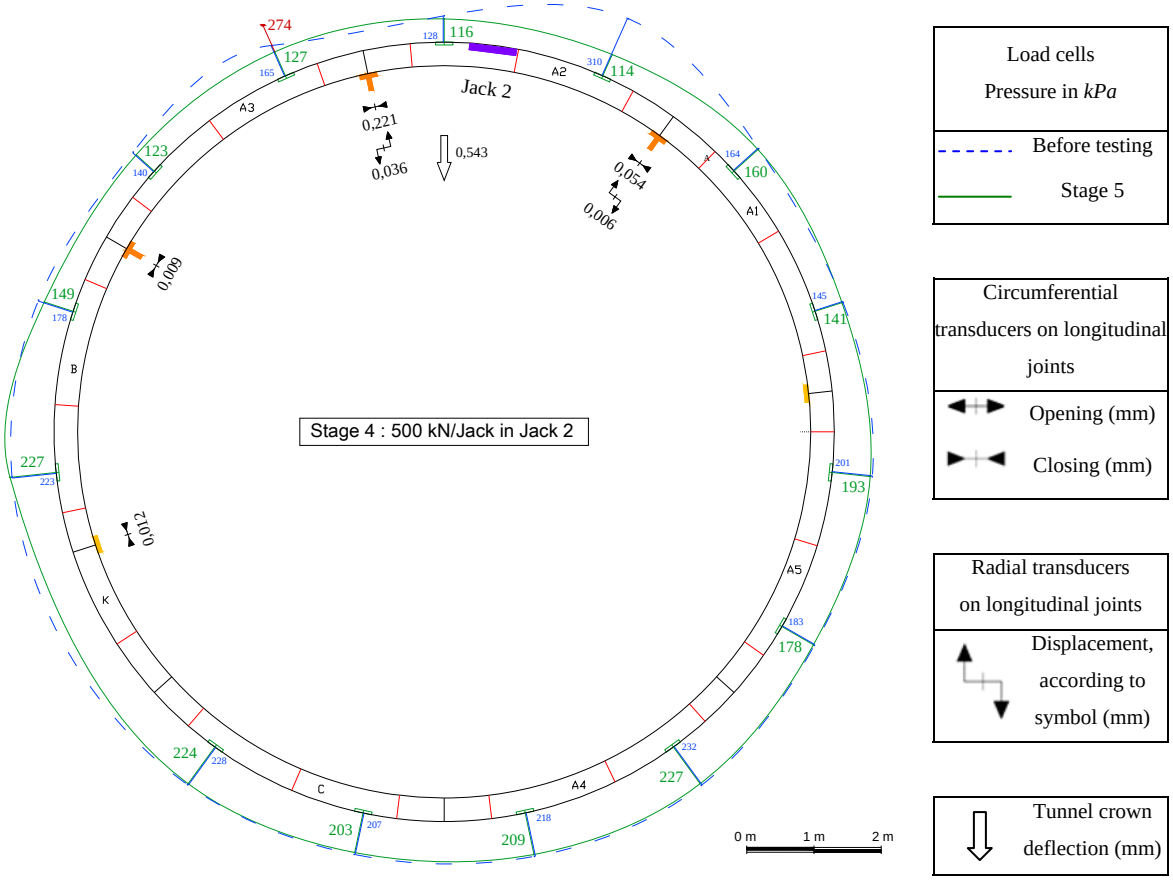

Figure A2.3. External instruments measures of the loaded ring at stage 4.

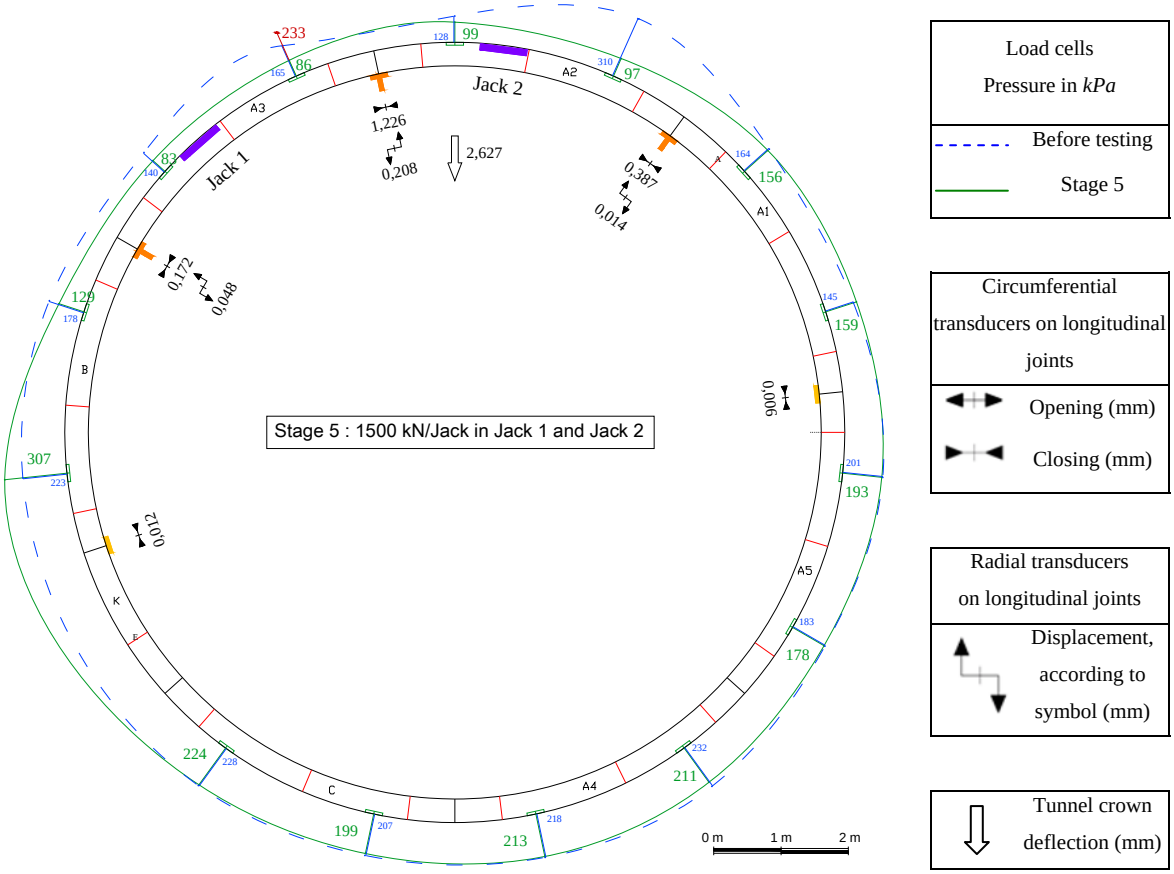

Figure A2.4. External instruments measures of the loaded ring at stage 5.

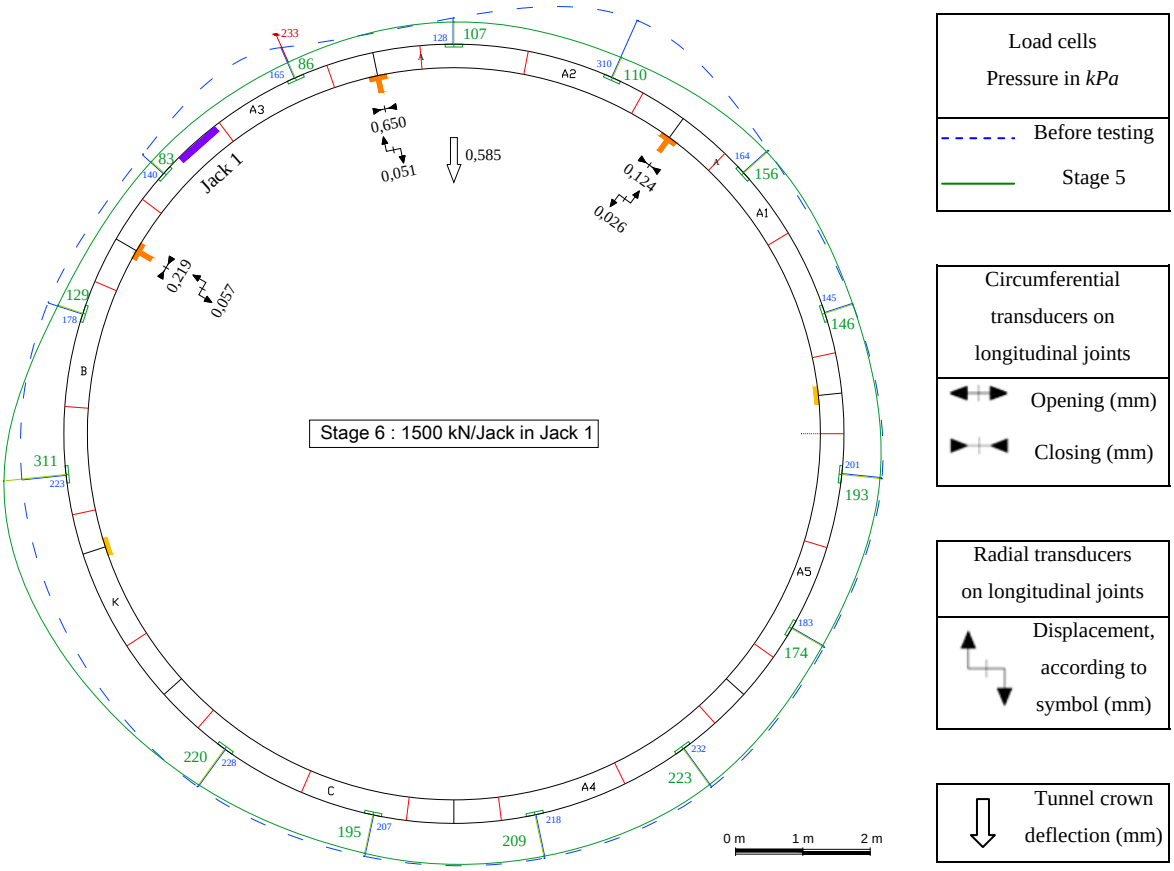

Figure A2.5. External instruments measures of the loaded ring at stage 6.

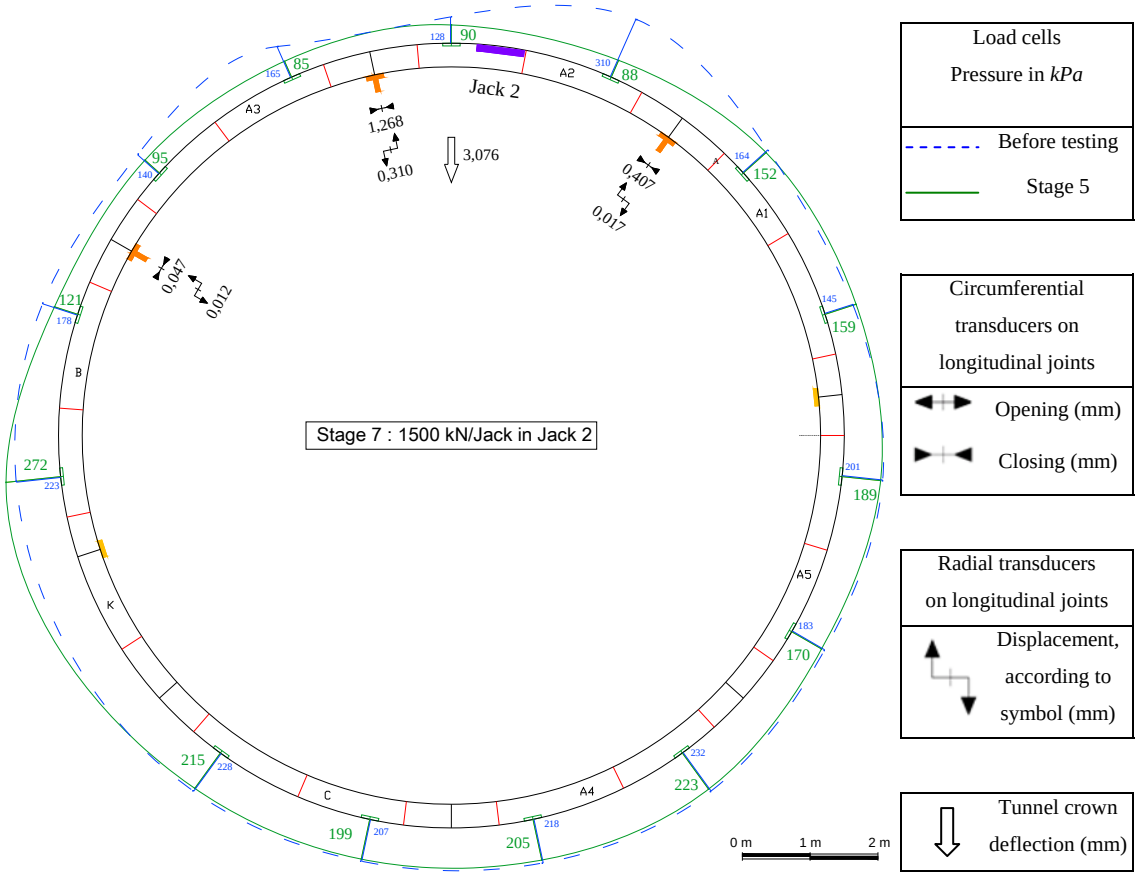

Figure A2.6. External instruments measures of the loaded ring at stage 7.